Publications

1. Agarwal M, Gupta SK, **Deshpande RD** and Yadava MG. (2006). Helium, radon and radiocarbon studies on a regional aquifer system of the North Gujarat–Cambay region, India. Chem. Geol., 228, 209–232.
2. Gupta SK and **Deshpande RD**, Agarwal M and Raval BR. (2005). Origin of high fluoride in groundwater in the North Gujarat-Cambay region, India. Hydrogeol. J., 13, 596–605.
3. Gupta SK and **Deshpande RD.** (2003). Origin of groundwater helium and temperature anomalies in the Cambay region of Gujarat, India. Chem. Geol., 198, 33–46.
4. Gupta SK and **Deshpande RD.** (2003). Dissolved helium and TDS in groundwater from Bhavnagar in Gujarat: Unrelated to seismic events between August 2000 and January 2001. Proc. Indian Acad. Sci. (Earth Planet. Sci.), 112(1), 51–60.
5. Gupta SK and **Deshpande RD.** (2003). High Fluoride in Groundwater of North Gujarat – Cambay Region: Origin, Community Perception and Remediation. *In* Proc. Int. Conf. on Water and Environment Vol. Ground Water Pollution (Eds. V.P. Singh & R.N. Yadav). Allied Publishers Pvt. Ltd. New Delhi. 368–388.

ELSEVIER

Chemical Geology 228 (2006) 209–232

CHEMICAL GEOLOGY
INCLUDING ISOTOPE GEOSCIENCE

www.elsevier.com/locate/chemgeo

Helium, radon and radiocarbon studies on a regional aquifer system of the North Gujarat–Cambay region, India

Meetu Agarwal, S.K. Gupta *, R.D. Deshpande, M.G. Yadava

Planetary and Geosciences Division, Physical Research Laboratory, Navrangpura, Ahmedabad 380 009, Gujarat, India

Received 22 July 2003; accepted 31 October 2005

Abstract

The study reports the age evolution of groundwater as it flows from the recharge area through a regional alluvial aquifer system in North Gujarat–Cambay region in western India. Radiocarbon (^{14}C), ^{4}He and $^{4}He/^{222}Rn$ dating methods have been employed. Sediments from a drill core in the Cambay Basin were also analysed for uranium (U) and thorium (Th) concentrations and the measured values have been used to estimate the ^{4}He and ^{222}Rn production rate for groundwater age calculations. Additionally, factors controlling the distribution of ^{222}Rn, ^{4}He and temperature anomalies in groundwater, vis-à-vis their relation to the tectonic framework and lithology of the study area, have also been examined.

The multi-isotope study indicated a reasonable correspondence in groundwater age estimates by the three methods employed. The groundwater ^{14}C ages increased, progressively, in the groundwater flow direction: from the foothills of Aravalli Mountains in the east, and reached a value of ~35 ka towards the region of lowest elevation, linking Little Rann of Kachchh (LRK)–Nalsarovar (NS)–Gulf of Khambhat (GK) in the western part of the study area. In this region, groundwater ages obtained for free flowing thermal wells and springs employing ^{4}He and $^{4}He/^{222}Rn$ systematics are in the order of million years. Such anomalous ages are possibly due to enhanced mobilisation and migration of 'excess helium' from hydrothermal circulation vents along deep-seated faults. Excluding such anomalous cases and considering all uncertainties, presently estimated ^{4}He and $^{4}He/^{222}Rn$ groundwater ages are in reasonable agreement with ^{14}C age estimates in the Cambay Basin for helium release factor (Λ_{He}) value of 0.4 ± 0.3. The ^{4}He method also indicated west-southwards progression of groundwater ages up to ~100 ka beyond the Cambay Basin.

Large 'excess helium' concentrations are also seen to be generally associated with anomalous groundwater temperatures (>35 °C) and found to overlie some of the basement faults in the study area, particularly along the east and the west flanks of the Cambay Basin. Groundwater ^{222}Rn activities in most of the study area are 800 ± 400 dpm/l. But, a thermal spring at Tuwa on the east flank of the Cambay Basin, having granitic basement at shallow depth, recorded the highest ^{222}Rn activity (~63,000 dpm/l).

Keywords: Helium; Radon; Radiocarbon; Groundwater age; Tectonics

1. Introduction

Determining the age evolution of groundwater as it moves in an aquifer from the recharge area to a distant discharge location is still a challenging task for hydrogeochemists. Sampling locations are often randomly scattered over an area where water from an aquifer is pumped from various depths or where springs bring

* Corresponding author. Tel.: +91 79 26314259; fax: +91 79 26301502.
E-mail addresses: meetu_agarwal20@yahoo.com (M. Agarwal), skgupta@prl.res.in (S.K. Gupta), deshpand@prl.res.in (R.D. Deshpande), myadava@prl.res.in (M.G. Yadava).

0009-2541/$ - see front matter © 2005 Elsevier B.V. All rights reserved.
doi:10.1016/j.chemgeo.2005.10.007

water to the surface. Several environmental tracers (including radio nuclides) find important and wide applications in determining direction and flow of groundwater, hydro-geological parameters of the aquifer and age of groundwater (Andrews et al., 1989; Cserepes and Lenkey, 1999).

In regional aquifer systems, groundwater ages may range up to 10^3 ka and beyond. Radiocarbon, with a half-life ($t_{1/2}$) of 5.73 ka can be used for groundwater dating up to ~35 ka (Geyh, 1990). The other available radionuclides such as ^{36}Cl ($t_{1/2}=3.01\times10^2$ ka; Andrews and Fontes, 1992), ^{81}Kr ($t_{1/2}=2.1\times10^3$ ka; Lehmann et al., 1991) and ^{234}U ($t_{1/2}=2.45\times10^2$ ka; Fröhlich and Gellermann, 1987) provide groundwater ages well beyond the radiocarbon dating range. On the other hand, the range of groundwater age estimation by radiogenic ^4He is 10^0 to 10^2 ka (Torgersen, 1980, 1992; Mazor and Bosch, 1992; Clark et al., 1998; Castro et al., 2000). When combined with ^{222}Rn activity measurements, the $^4He/^{222}Rn$ systematics also provide groundwater age estimation from 10^0 to 10^3 ka (Torgersen, 1980; Gupta et al., 2002). Another advantage of both ^4He and $^4He/^{222}Rn$ methods is that measurements of ^4He and ^{222}Rn are relatively simple. However, some complications also exist. (i) Recent studies (Stute et al., 1992; Imbach, 1997; Minissale et al., 2000; Gupta and Deshpande, 2003a,b) indicate that ^4He in deep groundwater often exceeds the accumulated in situ production by several orders of magnitude, particularly in regions of active tectonism and/or deep hydrothermal circulation. (ii) The possibility of a steady state whole crustal helium degassing flux affecting the dissolved helium in groundwater has been suggested (Torgersen and Clarke, 1985; Torgensen and Ivey, 1985). (iii) The possibility of enhanced release of geologically stored radiogenic helium in relatively young fine grained sediments derived from old protoliths was shown by Solomon et al. (1996). (iv) Ground waters carry small excesses of helium and radon along with dissolved air acquired during the recharge process, both in solubility equilibrium and as a supersaturation component of atmospheric air (Heaton and Vogel, 1981; Aeschbach-Hertig et al., 2000, 2002). Thus from a practical point, He in groundwater comprises, in addition to in situ radiogenic production, a mixture of atmospheric and terrigenic He. Use of ^4He for dating requires that components other than radiogenic production be small and /or accountable.

As part of a larger study aimed at understanding the recharge and flow in regional alluvial aquifer systems in arid environments and under exploitation stress, the applicability of ^{14}C, ^4He and $^4He/^{222}Rn$ groundwater dating methods was investigated in the regional aquifer system of the North Gujarat–Cambay region. The region is characterised by well defined recharge and discharge areas, presence of a few thermal springs (GSI, 2000) and neo-tectonic activity along major basement faults (Merh, 1995; Maurya et al., 1997; Srivastava et al., 2001).

The objectives of this investigation were to study (i) groundwater age progression from the recharge area towards the discharge area employing ^{14}C, ^4He and $^4He/^{222}Rn$ dating methods, and (ii) factors controlling the distribution of ^4He, ^{222}Rn and temperature in groundwater vis-à-vis their relation to the tectonic framework and hydrothermal venting in the North Gujarat–Cambay region.

2. Hydro-geological setting of the study area

The study area in the North Gujarat Cambay region (71.5–74°E and 22–24.5°N) has been divided into three main geographical units (i) the Cambay Basin (ii) West Flank, i.e., the region to the west of the West Cambay Basin Boundary Fault (WCBBF), and (iii) East Flank, i.e., the region to the east of the East Cambay Basin Boundary Fault (ECBBF); (Fig. 1).

The Cambay Basin, is a 'Graben' characterised by a NNW–SSE trending major fault system and successive down faulting along sympathetic faults that run parallel to the major trend line and many orthogonal faults cutting across (Merh, 1995). Geomorphologic studies have indicated recent movements along many faults in this region (Maurya et al., 1997; Srivastava et al., 2001). Several thermal springs also lie along some faults and fissures in this region (GSI, 2000) suggesting active hydrothermal circulation. The Deccan basalt of Late Cretaceous age forms the basement in most of the study area excepting the East Flank where Proterozoic granitic rocks are also exposed on the surface. Within the Cambay Basin, the Quaternary alluvial deposits are underlain by a succession of Tertiary sedimentary formations with productive oil and gas reservoirs. The thickness of the sedimentary cover varies from a few metres on the east and west flanks to >3 km towards the centre of Cambay Basin. Quaternary alluvial sediments with alternating sand and silty-clay layers constitute the regional aquifer system having its recharge area in the foothills of Aravalli Mountains and discharge area in the Little Rann of Kachchh–Nalsarovar–Gulf of Khambhat region (LRK–NS–GK). Deccan traps and Mesozoic sediments are exposed on the West Flank (Fig. 1). Parts of the East Flank lying along the foothills of Aravalli Mountains are mainly granitic.

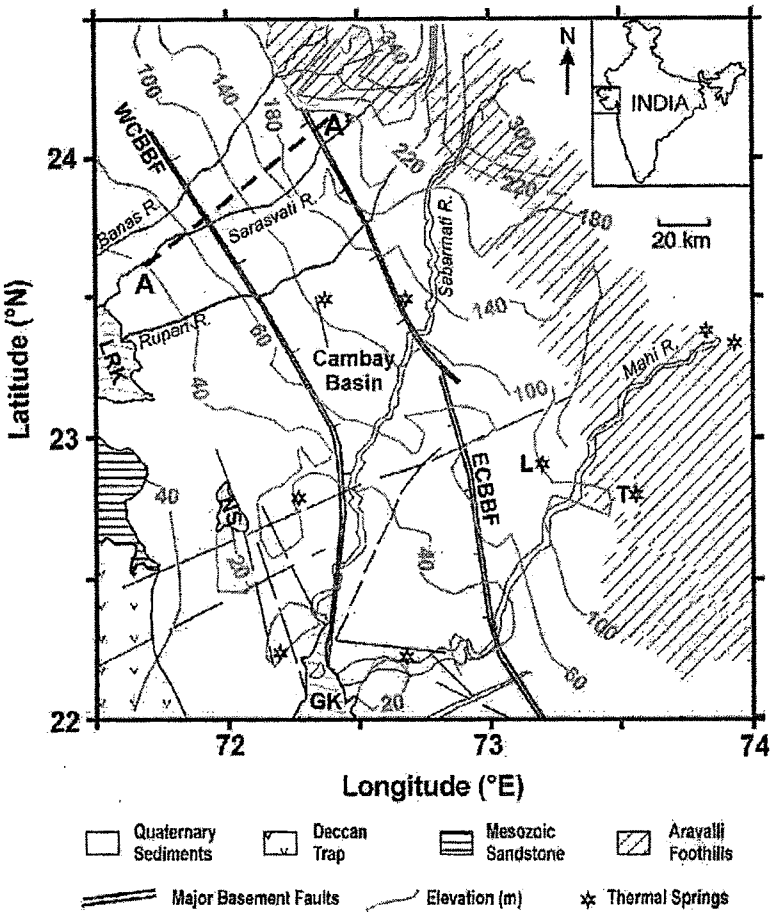

Fig. 1. Map of the North Gujarat–Cambay (NGC) region showing major geological formations, faults, surface elevations, major streams and locations of thermal springs. The Cambay basin (CB) is a Graben with a >3 km thick sedimentary succession. Several sympathetic faults, parallel and orthogonal to the two bounding faults, are also shown. A Quaternary regional aquifer system lies in the area between the Aravallis and the low lying track linking LRK–NS–GK. The foothills of the Aravallis act as the recharge zone. A section along AA' is shown in Fig. 2.

A subsurface section along AA' (Fig. 1), based on drilling logs obtained from Gujarat Water Resources Development Corporation Ltd (GWRDC) is shown in Fig. 2. It is seen that sand layers forming the major aquifer horizons are laterally continuous though vertically interspersed with silty-clay layers that may not have extensive lateral continuity. Approximate piezometric levels for two periods (1978–1983 and 1998–2003) recorded at the time of construction of new tubewells in the vicinity of the selected locations and obtained from the files of GWRDC are also shown in this diagram. The general groundwater flow direction is from the foothills of the Aravalli Mountains (elevations>300 m), towards the LRK–NS–GK region having the lowest ground elevations (~20 m). The ground elevation increases further west of LRK–NS–GK region. The deep tubewells in this part are free flowing artesian wells with their aquifer continuity in the east. In view of the very high artesian pressures recorded in the sixties (Exploratory Tubewells Organisation, Govt. of India, Unpublished data) and the continuity of deep aquifers with those in the Cambay Basin, it is considered that any significant recharge to the regional aquifer system from the west is not feasible. Farther west, only a thin cover of sediments cap the basaltic rocks exposed. The elevation gradient governs the surface drainage and major rivers, namely, the Banas, the Saraswati, the Rupen and the Sabarmati originate in the Aravalli hills and flow towards the south-west.

The rainfall in the study area is highly seasonal with >90% during south west monsoon in the months of June to September and decreases from ~90 cm a^{-1} in the east to ~65 cm a^{-1} in the region of the Cambay basin, further decreasing to <60 cm a^{-1} on the west flank (Gazetteer, 1975).

3. Theory

The theoretical background concerning the three groundwater dating methods employed in this study is summarised below.

3.1. ^{14}C dating

The method is based on measuring the residual activity of ^{14}C in the total dissolved inorganic carbon (TDIC) of a given groundwater sample. Two key assumptions made are: (i) the initial activity (A_0) in the TDIC in the recharge area is known and has remained constant in time; (ii) the system is closed to subsequent gain or loss of ^{14}C, except through the radioactive decay. In the case of radiocarbon dating of vegetal remains, A_0 can be taken as equal to 100% modern carbon (pmc) since the only source of ^{14}C is atmospheric CO_2. However, in case of ground waters A_0 in TDIC depends on the contribution from soil CO_2 and from soil carbonate which can have any value of ^{14}C activity between nil (dead carbon) to 100 pmc. Depending on the contribution from soil carbonate, A_0 can have any value between 50–100 pmc. This is because, of the two carbons in TDIC [$CaCO_3+H_2O+CO_2 \leftrightarrow Ca(HCO_3)_2$], one is derived from soil CO_2 and the other from soil carbonate. There is a further complication due to isotopic exchange between TDIC and the soil CO_2 and carbonate material. Various correction models exist, which principally attempt to estimate the contribution of soil carbonate to the TDIC and estimate the applicable value of A_0. This is done either through a

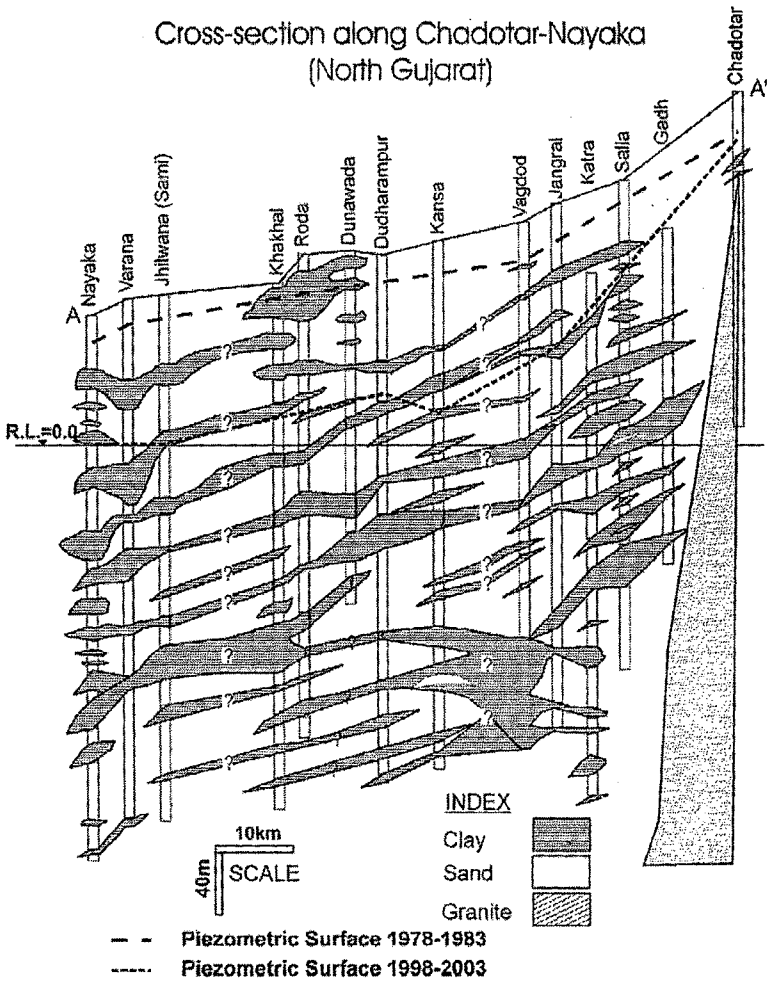

Fig. 2. Cross-section (along AA' in Fig. 1) depicting the lateral continuity of the major aquifer formed by sand layers interspersed by relatively thin silty-clay layers that may not have large lateral continuity. The uncertainty of continuity in view of large separation is indicated by question mark (?). Tubewells tap all water bearing horizons up to their maximum depth. The approximate positions of piezometric surfaces during 1978–1983 and 1998–2003 are also shown.

stoichiometry approach for the various chemical reactions involving carbon or by estimating dilution of active carbon using an isotope mixing approach based on the ^{13}C content of each species involved or a combination of the two approaches. Various methods for estimating A_0 can be found in Mook (1976) and Fontes and Garnier (1979). The error due to inappropriate estimation of A_0, however, is $<t_{1/2}$ of ^{14}C, except in some special cases of carbonate aquifers where continuous exchange between TDIC and the aquifer matrix may reduce A_0 to <50 pmc. Since most chemical and isotope exchanges occur in the unsaturated soil zone during the recharge process, and between TDIC and soil CO_2, the A_0 in several ground waters has been found to approach 85 ± 5 pmc (Vogel, 1967, 1970). However, in regional aquifers, the difference in groundwater ages between any two locations, after the confinement has become effective, depends little on the applicable value of A_0. Therefore, in the present investigation, the theoretical value of A_0 after equilibrium between soil CO_2, soil carbonate (at $^{14}C=0$ pmc; $\delta^{13}C=0‰$) and infiltrating water has been achieved, is estimated using the following equation (Münnich, 1957, 1968):

$$A_0 = \frac{\delta^{13}C_{TDIC}}{\delta^{13}C_{soil} - \varepsilon} 100 \quad (1)$$

where, $\delta^{13}C_{TDIC}$ is the $\delta^{13}C$ value of the groundwater TDIC, $\delta^{13}C_{soil}$ is the $\delta^{13}C$ of soil CO_2 (~−22‰) and ε is the equilibrium fractionation between the soil CO_2 and the TDIC of groundwater (~−9‰). This is done with the knowledge that application of any other model would give radiocarbon ages differing by $<\pm 2$ ka, that is much smaller than the errors inherent in the age estimation by ^4He and $^4He/^{222}Rn$ dating methods used in this investigation as discussed below.

3.2. ^4He dating

The method is based on estimating the amount and rate of accumulation of in situ produced radiogenic ^4He in groundwater (Andrews and Lee, 1979; Stute et al., 1992). If secular equilibrium and release of all the produced ^4He atoms into the interstitial water is assumed, the groundwater ages can be calculated as outlined in the following (Torgersen, 1980). The ^4He production rate in cm^3 STP g^{-1} rock a^{-1} is given by:

$$J'_{He} = 0.2355 \times 10^{-12}\ U^* \quad (2)$$

$$\text{where, } U^* = [U]\{1 + 0.123([Th]/[U] - 4)\} \quad (3)$$

[U] and [Th] are concentrations (ppm) of U and Th, respectively, in rock/sediment.

The accumulation rate of ^4He in cm^3 STP cm^{-3} water a^{-1} is therefore given by:

$$A'_{He} = J'_{He}\rho \cdot \Lambda_{He} \cdot (1 - n)/n \quad (4)$$

where, Λ_{He}=helium release factor; ρ=rock density (g cm^{-3}); n=rock porosity.

In the present study, the dissolved helium concentration is not given in cm^3 STP cm^{-3} water but is given in Air Equilibration Unit (AEU), which expresses the dissolved helium in terms of the corresponding equilibrium dry gas phase mixing ratio at 1 atm and 25 °C. As a result, water in equilibrium with air containing 5.3 ppmv helium is assigned a dissolved He concentration of 5.3 ppm AEU. Using a dimensionless Henry Coefficient (H_x) of 105.7 for helium at 25 °C (calculated from Weiss, 1971), this corresponds to a moist air equilibrium concentration of $4.45 \cdot 10^{-8}$ cm^3 STP He cm^{-3} water. Therefore,

$$A_{He} = A'_{He} 10^6 \cdot H_x \cdot (T/T_0) \cdot P_0/(P_0 - e) \quad (5)$$

where, A_{He}=accumulation rate of ^4He in ppm AEU a^{-1}; T_0=273.15 K; P_0=1 atm and e=saturation water vapour pressure (0.031 atm) at 25 °C, H_x=105.7.

For an average [U]=1 ppm for alluvial sedimentary formations and [Th]/[U]=4 (Ivanovich, 1992), n=20%; Λ_{He}=1; ρ=2.6 g cm^{-3}, an in situ ^4He accumulation rate (A_{He}) of 2.59×10^{-4} ppm AEU a^{-1} is obtained. Therefore, from the measured helium concentration of the sample (^4He_s), the age of groundwater can be obtained by using:

$$\text{Age (a)} = {}^4He_{ex}/A_{He} \quad (6)$$

where $^4He_{ex}$ is the 'excess He' (ppm AEU) and is obtained by subtracting dissolved helium in solubility equilibrium between water and atmosphere ($^4He_{eq}$= 5.3 ppm AEU at 25 °C and 1 atm pressure) from the measured concentration in the groundwater sample (^4He_s).

The above formulation, however, ignores 'excess air' helium ($^4He_{ea}$) due to supersaturation of atmospheric air as the groundwater infiltrates through the unsaturated zone. Various models have been proposed for estimating this component in groundwater studies (Aeschbach-Hertig et al., 2000; Kulongoski et al., 2003) based on measurement of other dissolved noble gases. Since measurements of dissolved noble gases have not been made in this study, it has not been possible to correct for this effect. However, from other studies (Holocher et al., 2002) it appears that $^4He_{ea}$ can

Table 1
Calculated ^{4}He ages along with geographical coordinates, well type and temperature, EC, pH and ^{4}He concentration of groundwater samples from the North Gujarat–Cambay Region, India

CBGW sample no.	Location name	Well type	Latitude (°N)	Longitude (°E)	Temp. (°C)	EC (mS)	pH	'Excess ^{4}He' ppm AEU	^{4}He ages (ka) (Λ_{He}=1)	^{4}He ages (ka) (Λ_{He}=0.4)
1	Gandhinagar	TW	23.24	72.68	–	0.5	–	0	0	0
2	Prantij	DCB	23.44	72.85	–	0.5	–	0	0	0
3	Prantij	TW	23.45	72.86	–	0.5	–	0	0	0
4	Shikha	DCB	23.39	73.23	–	0.6	–	0	0	0
5	Bayad	TW	23.22	73.21	–	4.8	–	0	0	0
6	Gundela	DW	23.12	73.36	–	0.8	–	0	0	0
7	Rojawa	TW	22.91	73.33	–	2.0	–	0	0	0
8	Lasundra	DW	22.91	73.14	52	7.4	–	186	547	1368
9	Lasundra	DW	22.91	73.14	–	7.6	–	55	162	404
10	Sinhuj	DCB	22.82	72.86	–	2.3	–	0	0	0
11	Dakore	TW	22.76	73.16	–	2.4	–	0	0	0
12	Ladvel	HP	22.91	73.12	–	0.7	–	0.2	1	1
13	Kapadvanj	DCB	23.04	73.10	–	0.9	–	0	0	0
14	Kunha	TW	23.01	72.77	–	1.0	–	0	0	0
15	Lasundra	TW	22.92	73.15	–	2.0	–	221	650	1625
16	Anghadi	DCB	22.81	73.30	–	0.7	–	0	0	0
17	Timba	HP	22.82	73.40	–	1.9	–	0	0	0
18	Tuwa	DW	22.80	73.46	61	3.4	–	137	403	1007
19	Tuwa	DW	22.80	73.46	47	6.2	–	96	282	706
20	Tuwa	DW	22.80	73.46	28	6.2	–	475	1397	3493
21	Tuwa	HP	22.80	73.46	51	4.7	–	1163	3421	8551
22	Tuwa	DW	22.80	73.46	–	0.7	–	0	0	0
23	Godhara	DW	22.78	73.60	–	0.8	–	0	0	0
24	Godhara	TW	22.76	73.61	–	0.5	–	0	0	0
25	Baska	HP	22.47	73.45	–	2.3	–	0	0	0
26	Baroda	TW	22.27	73.19	–	2.3	–	0	0	0
27	Jarod	HP	22.44	73.35	–	0.5	–	0	0	0
28	Khadki	HP	22.65	73.52	–	1.1	–	0	0	0
29	Dabhoi	HP	22.13	73.41	–	2.0	–	0	0	0
30	Sathod	TW	22.07	73.38	–	1.2	–	0	0	0
32	Adalaj	TW	23.17	72.58	–	2.1	–	0.1	0	1
33	Kalol	TW	23.26	72.47	–	2.3	–	0.1	0	1
34	Malharpur	HP	22.81	72.62	–	2.7	–	0.1	0	1
35	Marala	DCB	22.62	72.64	–	0.8	–	0.1	0	1
36	Khambhat	TW	22.33	72.62	–	2.8	–	0.8	2	6
37	Nadiad	TW	22.56	72.82	–	1.9	–	0.1	0	1
38	Bhadran	TW	22.37	72.90	–	2.2	–	0.4	1	3
39	Masar Rd.	TW	22.11	72.89	–	4.2	–	5.2	15	38
40	Kalak	DCB	22.02	72.76	–	2.2	–	0.1	0	1
43	Manglej	TW	22.09	73.17	–	1.6	–	0.1	0	1
44	Dholka	TW	22.69	72.43	–	3.1	–	0.5	1	4
45	Dholera	TA	22.25	72.19	43	6.9	–	109	321	801
50	Rampara	TW	22.11	71.89	–	1.3	–	2.7	8	20
51	Dhandhuka	DCB	22.38	71.98	–	3.1	–	0.2	1	1
52	Bawala	TW	22.83	72.36	33	1.6	–	6.3	19	46
53	Bagodra	TA	22.64	72.20	41	1.9	–	88	259	647
54	Bagodra	TA	22.64	72.20	41	1.4	–	190	559	1397
55	Gundi	TA	22.55	72.23	40	1.5	–	234	688	1721
56	Batod	HP	22.16	71.66	–	1.0	–	0.1	0	1
58	Vejalka	DCB	22.40	71.72	–	0.9	–	6.3	19	46
59	Wadhwan	TW	22.72	71.68	35	1.9	–	0.2	1	1
60	Bajana	TW	23.12	71.78	–	1.6	–	16	47	118
61	Dashada	TW	23.32	71.84	–	1.2	–	49	144	360
62	Sachana	TW	23.08	72.17	34	1.1	–	2.7	8	20
63	Vithalpur	TW	23.37	72.05	–	1.5	–	1	3	7

Table 1 (*continued*)

CBGW sample no.	Location name	Well type	Latitude (°N)	Longitude (°E)	Temp. (°C)	EC (mS)	pH	'Excess ^{4}He' ppm AEU	^{4}He ages (ka) (Λ_{He}=1)	^{4}He ages (ka) (Λ_{He}=0.4)
64	Umerkhaya	DW	22.90	72.02	–	7.6	–	0.2	1	1
65	Shiyala	TA	22.70	72.16	38	3.4	–	73	215	537
66	Ruhika	TA	22.66	72.23	41	3.0	–	157	462	1154
67	Sarala	TA	22.67	72.20	40	2.6	–	89	262	654
68	Vithalgadh	DW	22.99	71.97	–	5.9	–	0.2	1	1
69	Nardipur	TW	23.25	72.56	29	1.2	–	0	0	0
70	Santej	TW	23.11	72.47	29	1.2	–	0	0	0
71	Rancharda	TW	23.08	72.45	–	1.1	–	0	0	0
72	Nardipur	TW	23.25	72.56	29	1.2	–	0	0	0
73	Santej	TW	23.11	72.47	29	1.2	–	0	0	0
74	Rancharda	TW	23.08	72.45	–	1.1	–	0	0	0
75	Ananddham	TW	22.99	72.52	–	2.1	–	0	0	0
76	Sarkhej	TW	22.99	72.49	–	1.9	–	0	0	0
77	Sarkhej	TW	22.99	72.49	–	2.2	–	0	0	0
78	Collet	TW	22.97	72.43	33	1.6	–	1	3	7
79	Collet	TW	22.98	72.44	30	3.6	–	0	0	0
80	Sanand	TW	23.00	72.38	29	3.2	–	0.4	1	3
81	Thol	TW	23.13	72.38	32	3.2	–	0	0	0
82	Thol	HP	23.15	72.37	31	3.2	–	0	0	0
83	Rangpurda	TW	23.25	72.30	31	2.3	–	0.5	1	4
84	Kadi	TW	23.30	72.31	31	1.6	–	0	0	0
85	Bhoyani	TW	23.36	72.23	32	2.4	–	0.4	1	3
86	Katosan Road	TW	23.40	72.24	32	2.9	–	0.4	1	3
87	Navdeep Ind.	TW	23.01	72.34	30	2.4	–	0.8	2	6
88	Vansa	DCB	23.02	72.33	28	1.4	–	0.1	0	1
89	Sachana	TW	23.08	72.16	39	1.7	–	34	100	250
90	Hansalpur	TW	23.10	72.07	33	2.3	–	22	65	162
91	Viramgam	TW	23.10	72.06	34	1.8	–	66	194	485
92	Juna Padhar	TW	23.19	72.04	40	1.6	–	62	182	456
93	Endla	TW	23.29	72.04	38	1.6	–	23	68	169
94	Sitapur	TW	23.45	71.99	34	1.8	–	16	47	118
95	Sitapur	TW	23.44	71.98	38	1.5	–	21	62	154
96	Valevda	TW	23.46	71.94	32	4.3	–	2.8	8	21
97	Valevda	TW	23.45	71.94	40	1.8	–	17	50	125
98	Dhanap	TW	23.26	72.75	31	1.0	–	0.2	1	1
99	Majara	TW	23.36	72.80	29	1.2	–	0.1	0	1
100	Talod	TW	23.35	72.93	28	1.3	–	0	0	0
101	Tajpur Camp	HP	23.37	73.03	29	1.6	–	0.2	1	1
102	Vadagam	HP	23.33	73.17	29	0.5	–	0.2	1	1
103	Ramnagar	HP	23.39	73.23	28	0.6	–	0	0	0
104	Dhamanya	HP	23.34	73.25	29	0.7	–	0	0	0
105	Kamaliya	HP	23.33	73.31	28	1.5	–	0	0	0
106	Ranmalgadh	TW	22.98	72.34	33	1.5	–	0.7	2	5
107	Rethal	TW	22.88	72.19	34	1.5	–	12	35	87
108	Shahpur	HP	22.88	72.02	29	8.5	–	2	6	15
109	Vasvelia	TW	23.00	72.04	37	2.3	–	131	385	963
110	Bhojva	TW	23.15	72.03	31	3.0	–	2.3	7	17
111	Malanpur	TW	23.25	71.93	35	2.0	–	56	165	412
112	Zainabad	TW	23.26	71.68	34	2.3	–	112	329	824
113	Zainabad	HP	23.26	71.68	29	0.9	–	0	0	0
114	Zinzuvada	TW	23.35	71.65	35	2.6	–	31	91	228
115	Zinzuvada	HP	23.35	71.66	28	0.7	–	0	0	0
116	Changodar	HP	22.93	72.44	29	1.7	–	0.3	1	2
117	Kalayangdh	TW	22.72	72.27	27	5.2	–	1.4	4	10
118	Limbdi	HP	22.57	71.81	28	3.4	–	0	0	0
119	Vadod	TW	22.56	71.63	29	1.5	–	1.6	5	12
120	Zinzawadar	TW	22.45	71.69	34	3.5	–	2843	8362	20,904

(continued on next page)

Table 1 (*continued*)

CBGW sample no.	Location name	Well type	Latitude (°N)	Longitude (°E)	Temp. (°C)	EC (mS)	pH	'Excess ^{4}He' ppm AEU	^{4}He ages (ka) (Λ_{He}=1)	^{4}He ages (ka) (Λ_{He}=0.4)
121	Zinzawadar	HP	22.45	71.69	29	1.3	–	0	0	0
122	Chuda	TW	22.49	71.69	31	3.9	–	1290	3794	9485
123	Vekaria	HP	22.82	72.06	29	6.6	–	0.4	1	3
124	Fulgam	HP	22.54	71.54	31	1.1	–	0.2	1	1
125	Shekhpur–Rd.	TW	22.70	71.56	31	5.3	–	0.2	1	1
126	Vana	HP	22.87	71.71	–	6.0	–	0	0	0
127	Rangpur	DW	22.41	71.93	27	9.0	–	0.6	2	4
128	Vagad	DW	22.36	71.87	29	3.7	–	0	0	0
129	Nagnesh	TW	22.36	71.76	31	2.2	–	2	6	15
130	Nagnesh	HP	22.36	71.76	31	2.3	–	1.1	3	8
131	Alampur	DW	22.30	71.66	28	0.6	–	0	0	0
132	Paliyad	HP	22.25	71.56	30	2.3	–	0	0	0
133	Paliyad	TW	22.25	71.56	32	1.4	–	0.7	2	5
134	Botad	HP	22.17	71.66	–	0.9	–	0	0	0
135	Tatam	TW	22.06	71.62	31	1.1	–	0.8	2	6
137	Ahmedabad	TW	22.98	72.62	35	1.5	–	0	0	0
138	Hathijan	TW	22.94	72.64	35	1.1	–	0.5	1	4
139	Onthwari	DCB	22.82	72.80	35	2.0	–	0	0	0
140	Ran Na Muvada	DCB	22.84	72.95	35	1.5	–	3.6	11	26
141	Porda	DCB	22.92	73.00	33	0.8	–	0.2	1	1
147	Sarangpur	HP	22.16	71.77	34	2.2	–	0	0	0
149	Panavi	TW	22.08	71.89	41	6.0	–	1624	4776	11,941
150	Keriya Dhal	TW	22.11	71.89	35	0.8	–	0	0	0
151	Vaya	DW	22.20	71.87	30	1.0	–	0	0	0
152	Devthal	DCB	22.75	72.13	35	9.6	–	4.4	13	32
153	Devthal	TW	22.76	72.12	35	2.6	–	116	341	853
154	Kanera	TW	22.81	72.62	33	3.2	–	1.4	4	10
155	Sokhada	TW	22.74	72.68	34	5.7	–	0.3	1	2
156	Matar	TW	22.71	72.68	35	0.9	–	0.1	0	1
157	Nar	TW	22.48	72.71	35	2.5	–	0.7	2	5
158	Jogan	DCB	22.45	72.79	32	0.9	–	0.1	0	1
159	Bharel	TW	22.41	72.83	34	0.9	–	0.1	0	1
160	Dededa	DW	22.46	72.91	32	1.4	–	0.3	1	2
161	Anand	TW	22.53	72.96	32	0.8	–	0	0	0
162	Uttarsanda	TW	22.66	72.90	32	1.2	–	0	0	0
163	Sojitra	TW	22.55	72.74	35	1.5	–	1.8	5	13
164	Jedwapura	TW	22.55	72.83	34	2.3	–	0	0	0
165	Bedva	DCB	22.55	73.04	–	0.8	–	0	0	0
166	Ode	TW	22.62	73.11	32	0.8	–	0.7	2	5
167	Lingda	HP	22.69	73.08	31	0.7	–	0.5	1	4
168	Alindra	HP	22.70	72.97	34	0.6	–	0.5	1	4
169	Vaghasi	TW	22.54	73.00	–	0.9	–	0	0	0
170	Bhetasi	TW	22.43	73.02	33	1.2	–	0	0	0
171	Samiala	TW	22.26	73.12	33	0.9	–	0.1	0	1
172	Dabhasa	TW	22.25	73.05	34	1.0	–	0	0	0
173	Vadu	DCB	22.21	72.98	33	1.4	–	0.2	1	1
174	Vadu	TW	22.22	72.98	37	2.1	–	3.5	10	26
175	Gavasad	TW	22.19	72.97	35	0.9	–	0.1	0	1
176	Jambusar	TW	22.05	72.81	34	3.4	–	1	3	7
179	Karjan	TW	22.05	73.12	34	2.1	–	0	0	0
184	Kanara	TW	22.08	73.40	34	1.0	–	0	0	0
185	Mandwa	TW	22.01	73.43	35	0.7	–	0.1	0	1
186	Chandod	TW	22.99	73.46	34	0.8	–	0	0	0
187	Ankhi	TW	22.13	73.20	33	2.4	–	4.6	14	34
188	Kayvarohan	TW	22.08	73.24	33	1.2	–	0	0	0
189	Dantiwada	HP	24.17	72.48	34	0.5	–	0	0	0
190	Dantiwada	TW	24.16	72.48	31.5	0.6	–	0.4	1	3

Table 1 (*continued*)

CBGW sample no.	Location name	Well type	Latitude (°N)	Longitude (°E)	Temp. (°C)	EC (mS)	pH	'Excess ^{4}He' ppm AEU	^{4}He ages (ka) (Λ_{He}=1)	^{4}He ages (ka) (Λ_{He}=0.4)
191	Gola	DCB	24.19	72.78	28	0.7	–	0.2	1	1
192	Dharoi	HP	24.00	72.85	29	0.6	–	0.1	0	0
193	Mumanvas	DW	24.04	72.83	27	0.9	–	0.4	1	3
194	Mathasur	HP	23.80	73.01	30	1.2	–	0.2	1	1
195	Himmatnagar	HP	23.72	72.96	29	0.9	–	0.3	1	3
196	Dalpur	DCB	23.51	72.95	29	0.6	–	0	0	0
202	Math	HP	23.43	73.82	28	0.4	–	0.2	1	1
203	Aritha	HP	23.14	73.65	29	0.5	–	0.1	0	1
204	Limbodra	HP	23.19	73.60	29	0.7	–	0.3	1	2
205	Ghaliya Danti	HP	23.36	73.51	29	0.8	–	0.1	0	1
206	Shehra	HP	22.95	73.63	29	0.5	–	0.1	0	1
207	Popatpura	HP	22.79	73.45	29.5	0.6	–	0.2	1	1
208	Maniyor	TW	23.82	72.96	35	1.9	–	0.1	0	1
209	Dharewada	TW	23.98	72.39	35	3.5	–	2.0	6	15
210	Ganguva	TW	24.16	72.73	33	0.5	–	0	0	0
211	Chadotar	TW	24.21	72.39	32	1.0	–	0	0	0
212	Bhadath	TW	24.34	72.20	32	0.4	–	0.3	1	2
213	Kuwarava	TW	24.04	71.90	35	1.7	–	0.3	1	2
214	Kuwarava	TW	24.05	71.90	33	1.7	–	0.3	1	2
215	Tharad	TW	24.41	71.64	42	3.4	–	30	88	221
216	Jitoda	TW	23.74	72.15	35	2.3	–	0.6	2	4
217	Jitoda	TW	23.74	72.15	42	2.3	–	9.7	29	71
218	Sami	TW	23.70	71.78	44	3.9	–	64	188	471
219	Wavadi	TW	23.92	72.52	34	1.0	–	0	0	0
220	Pilwai	TW	23.53	72.69	39	1.6	–	17	50	125
221	Pilwai	TW	23.54	72.68	37	1.3	–	0.5	1	4
222	Hedwa	TW	23.57	72.34	37	2.3	–	1.8	5	13
223	Vaghpur	TW	23.68	73.42	33	1.4	–	23	68	169
224	Edla	TW	23.54	72.06	40	2.6	–	11	32	81
225	Sherisa	TW	23.20	72.48	35	1.7	–	0.3	1	2
312	Diyodar	TW	24.10	71.75	33	1.8	7.5	1.9	6	14
313	Diyodar	TW	24.10	71.75	33	4.1	7.2	1.2	4	9
314	Tharad	TW	24.41	71.64	39	2.3	7.4	30	88	221
316	Agathala	TW	24.29	71.88	31	1.8	7.6	0	0	0
317	Sujanipur	TW	23.89	72.11	31	9.5	7.1	0	0	0
318	Sujanipur	TW	23.90	72.12	37	3.6	7.1	16	47	118
319	Sujanipur	TW	23.91	72.12	29	5.3	7.6	0	0	0
320	Kuwarva	TW	24.04	71.90	32	1.9	7.6	0	0	0
321	Kharia	TW	23.94	71.83	30	1.0	7.8	0	0	0
322	Sami	TW	23.70	71.78	41	4.7	7.4	45	132	331
323	Hedwa	TW	23.57	72.34	33	3.1	7.1	1.5	4	11
324	Kuder	TW	23.70	71.87	34	2.5	7.3	1.5	4	11
325	Patan	TW	23.84	72.11	31	2.0	7.6	0	0	0
326	Patan	TW	23.84	72.11	32	1.8	7.8	0	0	0
327	Patan	TW	23.84	72.11	29	3.4	7.1	0	0	0
328	Jitoda	TW	23.74	72.15	33	3.3	7.1	0.3	1	2
329	Jitoda	TW	23.74	72.15	39	4.3	7.0	10	29	74
330	Kamboi	TW	23.67	72.02	32	2.8	7.1	6.4	19	47
331	Muthia	TW	23.09	72.69	31	1.4	7.5	0.3	1	2
332	Paliya	TW	23.18	72.83	31	1.6	7.1	0.3	1	2
333	Punsari	TW	23.39	73.10	30	0.7	7.4	0	0	0
334	Dalani Muwadi	TW	23.36	72.88	31	1.6	7.2	12	35	88
335	Rojad	HP	23.35	73.09	29	1.7	7.6	0	0	0
336	Vadrad	TW	23.42	72.89	31	1.6	7.1	0	0	0
337	Tejpur	TW	23.39	72.81	30	1.7	7.1	0	0	0
338	Navalpur	TW	23.60	72.90	32	1.5	6.9	0.6	2	4
339	Dhanap	TW	23.26	72.75	32	1.7	7.2	0	0	0

(continued on next page)

Table 1 (*continued*)

CBGW sample no.	Location name	Well type	Latitude (°N)	Longitude (°E)	Temp. (°C)	EC (mS)	pH	'Excess ^{4}He' ppm AEU	^{4}He ages (ka) (A_{He}=1)	^{4}He ages (ka) (A_{He}=0.4)
340	Indroda Park	TW	23.19	72.65	31	1.2	7.3	0.3	1	2
341	Rupawati	TW	23.00	72.30	37	2.1	7.8	0	0	0
342	Sokali	TW	23.10	72.11	32	4.6	7.4	0.6	2	4
343	Dudapur	TW	23.02	71.58	32	3.5	7.0	44	129	324
355	Salajada	TW	22.80	72.39	35	2.3	7.7	0.9	3	7
356	Salajada	TW	22.79	72.39	35	2.3	7.6	0.9	3	7
357	Salajada	TW	22.79	72.39	31	4.9	7.5	0	0	0
358	Gundi	TA	22.55	72.23	42	4.1	8.2	178	524	1309
359	Shiyal	TA	22.68	72.16	42	4.6	8.2	230	676	1691
360	Padgol	TW	22.59	72.84	32	1.8	7.6	1.4	4	10
361	Morad	TW	22.54	72.86	31	1.2	7.6	0	0	0
362	Gumadia	TW	22.76	73.23	31	1.3	7.7	0.3	1	2
363	Tuwa	HS	22.80	73.46	50	7.2	7.2	405	1191	2978
364	Tuwa	HS	22.80	73.46	43	7.4	7.5	229	674	1684
365	Tuwa	HS	22.80	73.46	36	7.1	7.4	265	779	1949
366	Tuwa	HS	22.80	73.46	33	8.0	7.6	253	744	1860
367	Dholera	TA	22.25	72.19	45	7.2	7.9	443	1303	3257

TW: tubewell; DCB: dug cum bore; DW: dug well; HP: handpump; TA: thermal artesian; HS: hot spring; 'Excess He'=measured − 5.3 ppm AEU; A_{He}=helium release factor; calculations of ^{4}He ages are based on Th=7.54±3.5; U=1.07±0.41; ρ=2.6 g cm^{-3}; n=20%.

be up to 10–30% of $^4He_{eq}$ resulting in a possible overestimation of groundwater age of up to ~6 ka.

Further, (^4He_s) can contain other terrigenic helium components (Stute et al., 1992) that can cause overestimation of groundwater age. These terrigenic components are: (1) flux from an external source, e.g., deep mantle or crust, adjacent aquifers etc. (Torgersen and Clarke, 1985); and (2) release of geologically stored ^{4}He from young sediments (Solomon et al., 1996). Depending upon the geological setting, particularly in regions of active tectonism and/or hydrothermal circulation, the contribution of these sources may exceed the in situ production by several orders of magnitude (Stute et al., 1992; Minissale et al., 2000; Gupta and Deshpande, 2003a,b). For recent reviews on terrigenic helium, reference is made to Ballentine and Burnard (2002) and Castro et al. (2000). Additional measurements/data (e.g., ^{3}He/^{4}He, other noble gases) are required to resolve these components. However, in many cases it seems possible to rule out major contribution from terrigenic He sources since the helium flux may be shielded by underlying aquifers that flush the Helium out of the system before it migrates across them (Torgensen and Ivey, 1985; Castro et al., 2000). According to Andrews and Lee (1979), with the exception of a few localised sites and for very old ground waters, 'excess He' in groundwater is due to in situ production only and is often used for quantitative age estimation within the aquifer if the U and Th concentrations of the aquifer material are known. But, in case there is evidence of deep crustal ^{4}He flux (J_0) entering the aquifer, Eq. (6) modifies to (Kulongoski et al., 2003):

$$\text{Age (a)} = {}^4\text{He}_{Ex}/[(J_0/nZ_0\rho_w) + A_{He}]/8.39 \times 10^{-9} \quad (7)$$

where, Z_0 is the depth (m) at which the ^{4}He flux enters the aquifer and ρ_w is the density of water (1 g cm^{-3}). In Eq. (7), the factor 8.39×10^{-9} results from expressing $^4He_{ex}$ in ppm AEU and A_{He} and J_0 terms in cm^3 STP/g.

3.3. $^4He/^{222}Rn$ dating

Since both ^{4}He and ^{222}Rn have a common origin in groundwater, being produced by the α decay of U and/or Th in the aquifer material, their simultaneous measurements in groundwater can also be utilized for calculating its age (Torgersen, 1980).

As in case of ^{4}He, the ^{222}Rn accumulation rate (cm^3 STP cm^{-3} water a^{-1}) is given by:

$$A_{Rn} = J'_{Rn}\rho \cdot A_{Rn} \cdot (1-n)/n \quad (8)$$

$$\text{where, } J'_{Rn} = 1.45 \times 10^{-14}[U] \quad (9)$$

and J'_{Rn}=production rate of ^{222}Rn in cm^3 STP g^{-1} rock a^{-1} and [U]=concentration (ppm) of U in rock/sediment.

Thus, computing the accumulation rate ratio of ^{4}He and ^{222}Rn ($=A_{He}/A_{Rn}$), the age of groundwater can be calculated as follows:

$$\text{Age (a)} = (A_{Rn}/A_{He})(A_{Rn}/A_{He})(C_4/A_{222}) \quad (10)$$

where, A_{Rn}/A_{He} is the release factor ratio for radon and helium from the aquifer material to groundwater; C_4 is concentration (atoms l^{-1}) of ^4He and A_{222} is activity (disintegration l^{-1} a^{-1}) of ^{222}Rn in groundwater. From Eqs. (2)–(4) and (8)–(10), it is seen that $^4He/^{222}Rn$ ages are independent of porosity, density and U concentration, but do require a measure of [Th]/[U] in the aquifer material. The ratio A_{Rn}/A_{He} depends upon grain size and recoil path length of both ^{222}Rn (~0.05 μm) and ^4He (30–100 μm) (Andrews, 1977). Release of ^{222}Rn by α-recoil from the outer surface (~0.05 μm) of a grain (~2–3 mm) has been estimated to ~0.005% (Krishnaswami and Seidemann, 1988). Apart from α-recoil, both ^{222}Rn and ^4He can diffuse out of rocks/minerals through a network of 100–200 Å wide nanopores throughout the rock or grain body (Rama and Moore, 1984). Radon release factors (A_{Rn}) ranging from 0.01–0.2 have been indicated from laboratory experiments for granites and common rock forming minerals (Krishnaswami and Seidemann, 1988; Rama and Moore, 1984). On the other hand, Torgersen and Clarke (1985), in agreement with numerous other authors have shown that the most likely value of A_{He} is ≈ 1. Converting C_4 (atoms l^{-1}) to ppm AEU units and A_{222} (disintegration $^{-1}$ a^{-1}) to dpm l^{-1} units, Eq. (10) can be rewritten as:

$$\text{Age (a)} = 4.3 \times 10^8 \cdot (A_{Rn}/A_{He}) \cdot (A_{Rn}/A_{He}) \cdot C_{He}(\text{ppmAEU})/A_{222}(\text{dpm } l^{-1}). \quad (11)$$

Here, 1 ppm AEU ^4He concentration corresponds to 2.26×10^{14} atoms of ^4He l^{-1} of water. Another inherent assumption of the $^4He/^{222}Rn$ dating method is that both ^4He and ^{222}Rn have originated from the same set of parent grains/rocks and their mobilization in groundwater is similarly affected.

Table 2
Results of groundwater radiocarbon dating from the North Gujarat–Cambay region, India

CBGW sample no.	Location name	Latitude (°N)	Longitude (°E)	$\delta^{13}C_{TDIC}$ (‰)	Percent modern carbon	^{14}C ages* (ka)	^{14}C ages**
208	Maniyor	23.82	72.96	−10.78	115 ± 1.1	Modern	Modern
209	Dharewada	23.98	72.39	−8.99	58 ± 0.7	4.45 ± 0.09	1.5 ± 0.14
210	Ganguva	24.16	72.73	−10.40	100 ± 0.9	Modern	Modern
211	Chadotar	24.21	72.40	−8.62	99 ± 0.9	Modern	Modern
212	Bhadath	24.34	72.20	−8.26	102 ± 1.0	Modern	Modern
215	Tharad	24.41	71.64	−8.47	2.3 ± 0.2	31.21 ± 0.68	27.6 ± 0.73
216	Jitoda	23.74	72.15	−7.26	35 ± 0.5	8.63 ± 0.12	3.9 ± 0.16
218	Sami	23.70	71.78	−11.74	0.61 ± 0.2	42.2 ± 2.6	41.3 ± 2.73
219	Wavadi	23.92	72.52	−9.56	90 ± 1.0	0.92 ± 0.09	Modern
220	Pilwai	23.53	72.69	−11.56	22 ± 0.4	12.53 ± 0.14	11.5 ± 0.17
222	Hedwa	23.57	72.34	−9.17	37 ± 0.5	8.19 ± 0.1	5.3 ± 0.14
223	Vaghpur	23.68	73.42	−11.34	81 ± 0.8	1.73 ± 0.08	0.6 ± 0.11
224	Edla	23.54	72.06	−10.12	1.7 ± 0.2	33.75 ± 0.88	31.6 ± 0.98
225	Sherisa	23.20	72.48	−9.47	50 ± 0.6	5.75 ± 0.1	3.1 ± 0.13
320	Kuwarava	24.04	71.90	−8.81	2.8 ± 0.3	29.64 ± 0.97	26.3 ± 0.90
331	Muthia	23.09	72.69	−8.60	68 ± 0.8	3.15 ± 0.1	Modern
333	Punsari	23.39	73.10	−9.11	89 ± 0.8	1.01 ± 0.07	Modern
336	Vadrad	23.42	72.89	−9.28	99 ± 0.9	Modern	Modern
337	Tajpur	23.39	72.81	−11.60	68 ± 0.7	3.25 ± 0.08	2.2 ± 0.11
341	Rupawati	23.00	72.30	−9.29	1.8 ± 0.2	33.29 ± 0.89	30.4 ± 0.93
344	Gajanav	22.92	71.36	−9.75	80 ± 0.7	1.82 ± 0.08	Modern
351	Navagam	22.62	71.18	−11.11	93 ± 0.8	0.61 ± 0.08	Modern
355	Salajada	22.80	72.39	−8.23	9.5 ± 0.2	19.5 ± 0.21	15.7 ± 0.20
358	Gundi	22.55	72.23	−21.36	b.d.l.	>45	>45
360	Padgol	22.59	72.84	−9.70	49 ± 0.5	5.87 ± 0.09	3.5 ± 0.12
362	Gumadia	22.76	73.23	−8.94	84 ± 0.8	1.47 ± 0.08	Modern
RC-1	PRL	23.04	72.54	−13.00	40 ± 0.6	7.58 ± 0.12	7.6 ± 0.14

b.d.l.: below detection limit; ^{14}C half life = 5730 ± 40 a.

* A_0 = 100% modern.

** $A_0(\text{corrected}) = \dfrac{\delta^{13}C_{TDIC}}{\delta^{13}C_{soil} - \varepsilon} 100$; $\delta^{13}C_{soil} = -22‰$ and $\varepsilon = -9‰$.

Andrews et al. (1982) used the following one-dimensional equation for calculating diffusive transport of ^{222}Rn in granites:

$$C_x = C_0 \exp\left(-\sqrt{\lambda/D}\cdot X\right) \quad (12)$$

where, C_0 and C_x are the concentrations of ^{222}Rn at the point $x=0$ and $x=X$; D is the diffusion coefficient in water ($\sim 10^{-5}$ cm^2 s^{-1}); and λ is the decay constant for ^{222}Rn. They calculated that $C_x/C_0=0.35$ at a distance equal to one diffusion length ($X=[D/\lambda]^{1/2}$, i.e., 2.18 cm). Therefore, even at high ^{222}Rn activity its diffusion beyond a few metres distance is not possible. The average radon diffusion coefficient in soils with low moisture content and composed of silty and clayey sand is even lower $\sim 2\times 10^{-6}$ cm^2 s^{-1} (Nazaroff et al., 1988). Therefore, ^{222}Rn measurements of groundwater depend essentially on U in the pumped aquifer horizons in the vicinity of the sampled tubewell. Further, measured ^{222}Rn because of

Table 3
Results of ^{4}He/^{222}Rn groundwater dating from the North Gujarat–Cambay region, India

CBGW sample no.	Location name	Latitude (°N)	Longitude (°E)	^{222}Rn activity (dpm/l)	'Excess ^{4}He' (ppm AEU)	^{4}He/^{222}Rn ages (ka)
312	Diyodar	24.10	71.74	945 ± 83	1.9	16
313	Diyodar	24.10	71.74	987 ± 91	1.2	10
314	Tharad	24.41	71.64	810 ± 65	33.7	330
316	Agathala	24.29	71.88	742 ± 67	0.6	6
317	Sujnipur	23.89	72.11	1077 ± 87	0.0	0
318	Sujnipur	23.90	72.12	1551 ± 124	5.5	28
319	Sujnipur	23.90	72.12	629 ± 57	0.0	0
320	Kuwarva	24.04	71.90	599 ± 57	0.0	0
321	Kharia	23.94	71.83	916 ± 83	0.0	0
322	Sami	23.70	71.78	137 ± 30	44.1	2553
323	Hedwa	23.57	72.34	469 ± 48	1.2	20
324	Kuder	23.73	72.19	462 ± 58	1.2	20
325	Patan	23.84	72.11	822 ± 72	0.0	0
326	Patan	23.84	72.11	673 ± 63	0.3	3
327	Patan	23.84	72.11	261 ± 36	0.0	0
328	Jitoda	23.74	72.15	1114 ± 106	0.6	4
329	Jitoda	23.74	72.15	1871 ± 144	9.9	42
330	Kamboi	23.67	72.02	1253 ± 97	6.4	41
331	Muthia	23.09	72.69	481 ± 24	0.0	0
332	Paliya	23.18	72.83	1262 ± 52	0.0	0
333	Punsari	23.39	73.10	522 ± 26	0.0	0
334	Dalani Muwadi	23.36	72.88	279 ± 19	13.3	378
335	Rojad	23.35	73.09	281 ± 19	0.0	0
336	Vadrad	23.42	72.89	923 ± 41	1.7	15
337	Tajpur	23.39	72.81	721 ± 36	0.0	0
338	Navalpur	23.60	72.90	245 ± 17	0.0	0
339	Dhanap	23.26	72.75	643 ± 34	0.0	0
340	Indroda Park	23.19	72.65	231 ± 19	0.0	0
341	Rupawati	22.99	72.30	908 ± 41	3.5	30
342	Sokali	23.10	72.11	657 ± 31	0.7	8
343	Dudapur	23.02	71.58	2595 ± 110	44.5	136
355	Salajada	22.80	72.39	480 ± 28	0.9	15
356	Salajada	22.79	72.39	379 ± 25	0.9	18
357	Salajada	22.79	72.39	426 ± 30	0.3	5
358	Gundi	22.55	72.23	301 ± 18	175.3	4624
359	Shiyal	22.68	72.16	262 ± 17	230.1	6958
360	Padgol	22.59	72.84	468 ± 24	1.3	23
361	Morad	22.54	72.86	322 ± 19	0.0	0
362	Gumadia	22.76	73.23	442 ± 22	0.0	0
363	Tuwa	22.80	73.46	62,571 ± 2405	405.0	51
364	Tuwa	22.80	73.46	32,538 ± 1272	277.0	68
366	Tuwa	22.80	73.46	36,394 ± 1413	253.0	55
367	Dholera	22.25	72.19	362 ± 17	465.0	10,189

Calculations are based on: Th/U=7.1 ± 4.3; $\Lambda_{Rn}/\Lambda_{He}$=0.4; ρ=2.6 g cm^{-3}; n=20%.

its short half-life ($t_{1/2}$=3.825 d) is indicative of local mobilisation only whereas ^{4}He, being stable, might have been mobilized from the entire flow-path. For ground waters having high 'excess He' from sources external to the aquifer, the resulting $^{4}He/^{222}Rn$ ages might be over estimated.

4. Experimental

Groundwater samples used in this study were collected from tubewells/hand pumps/dug wells and thermal springs ranging in depth from 3 to 350 m. The sampling locations and other relevant details are given in Tables 1–3 and Figs. 3–6. Prior to sampling, the tubewells were purged long enough (>3 well volumes) to flush out stagnant water. Temperature, pH and electrical conductivity (EC) were measured in the field during sampling.

For ^{14}C dating, ~100 l of groundwater samples from 27 locations spread across the study area as shown in Fig. 3 were collected. The groundwater at each location was piped directly into a collapsible high density PVC bag through a narrow opening. A few pellets of NaOH (~10 g) were added to the PVC bag before piping the groundwater to raise the solution pH>10 for immobilising the dissolved CO_2. Depending upon the alkalinity and sulphate concentration of groundwater samples (measured in the field), a calculated amount of barium chloride ($BaCl_2$) was then added to the 'groundwater–NaOH' solution to ensure complete precipitation of dissolved carbonates (Clark and Fritz, 1997). Following vigorous stirring, the mixture was left undisturbed for precipitates to settle in the conical base of the PVC bag. After discarding the supernatant liquid, precipitates were transferred to glass bottles and sealed by capping the bottle with a bromobutyl synthetic rubber stopper

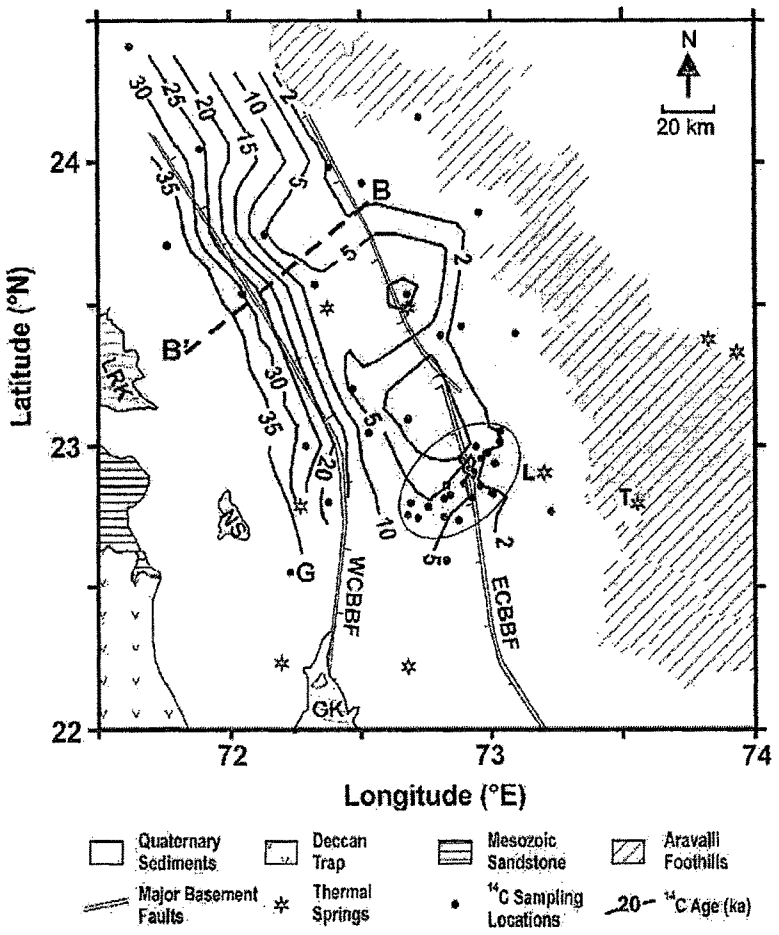

Fig. 3. Radiocarbon groundwater ages (ka) along with sampling locations. Sampling locations of an earlier study (Borole et al., 1979) are enclosed by an ellipse. Within the CB the groundwater ^{14}C ages increase progressively towards the WCBBF, beyond which a limiting age of >40 ka is reached. Dots indicate sampling locations. L, T and G respectively indicate the locations of thermal springs at Lasundra, Tuwa and the free flowing thermal artesian well at Gundi. The groundwater age gradient along BB' is shown in Fig. 9.

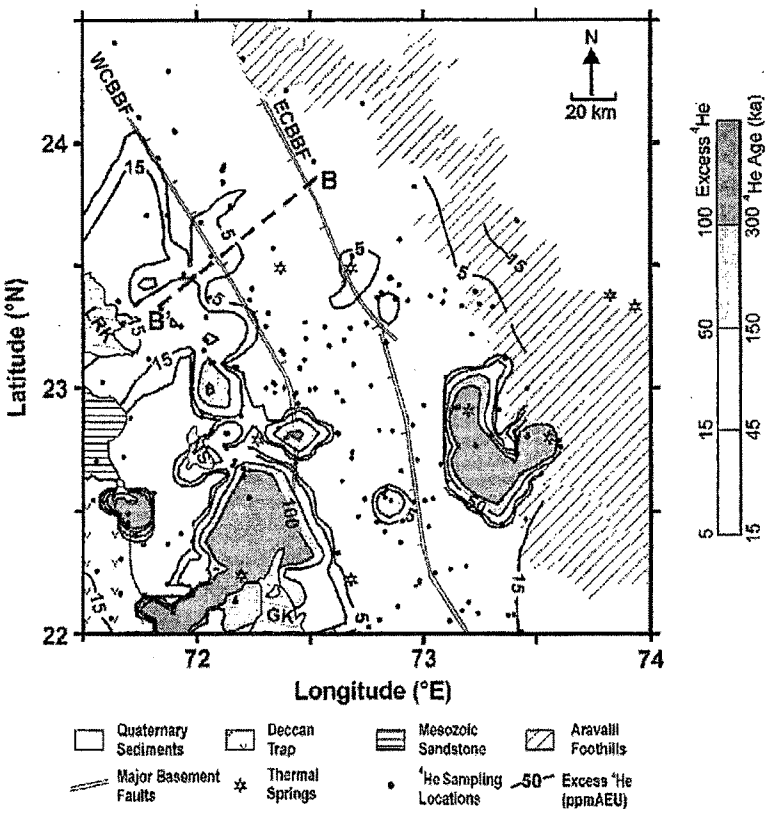

Fig. 4. Iso-distribution map of 'excess He' concentration in groundwater of the North Gujarat–Cambay region. The contour line of 5 ppm AEU runs almost along the WCBBF. For U=1.07 ppm, Th=7.54 ppm, ρ=2.6 g cm^{-3} and n=20%, 5 ppm AEU 'excess He' corresponds to a ^{4}He groundwater age of ~15 ka for a helium release factor, Λ_{He}=1. In contrast, for Λ_{He}=0.4, it corresponds to ~37 ka. Pockets of 'excess He' > 50 ppm AEU overlap pockets of high (>40 °C) temperature. Dots indicate sampling locations. The groundwater age gradient along BB' is shown in Fig. 9.

and triple aluminium protective cover using a hand held crimping tool. Care was taken to prevent/minimise sample exchange with atmospheric CO_2 during the entire field procedure. The ^{14}C analyses were made on the CO_2 liberated from the precipitated barium carbonate by reaction with ortho-phosphoric acid. The liberated CO_2 was first converted to acetylene and then trimerised into benzene and counted by liquid scintillation spectroscopy (Gupta and Polach, 1985). A small aliquot of the sample CO_2 was sealed in glass ampoules for $\delta^{13}C$ measurement (PDZ Europa Model GEO 20-20).

For ^{4}He measurements, water samples from 243 locations (Table 1, Fig. 4) were filled in 3 mm thick, 1.2-l capacity soda-lime glass bottles using standardized procedures reported by Gupta and Deshpande (2003a,b). The water samples were analysed for dissolved ^{4}He within 48 h after collection using a helium sniffer probe (ALCATEL Model ASM 100 HDS). The helium probe is a leak detector consisting of a mass spectrometer tuned for ^{4}He ions (m/e=4). ^{4}He concentration results are expressed in air equilibration units (AEU). Total uncertainty of helium measurements is estimated to be <5%. Reference is made to Gupta and Deshpande (2003a,b) for details of sample collection and helium analysis procedures.

For ^{222}Rn measurements, water samples from 43 locations were drawn directly in 630-ml PVC bottles (Brand Tarson) filled completely after overflowing >3 bottle volumes and sealed to prevent escape of gases. ^{222}Rn was measured, within 5 d of sample collection, by counting 609 keV gamma rays produced by the decay of its short-lived daughter ^{214}Bi using a high purity germanium (HPGe) gamma ray spectrometer. The background in the ^{214}Bi peak was 0.062 ± 0.001 cpm. The counting efficiency of ^{214}Bi determined using a ^{226}Ra source of known activity (107.4 ± 0.4 dpm) in the same configuration as the sample bottle was 0.31 ± 0.01%. Repeated counting for some samples after more than three weeks confirmed that ^{222}Rn was unsupported by ^{226}Ra in the groundwater. Activity values were decay corrected to the time of collection, with quoted errors as one standard deviation based on counting statistics. Total uncertainty of ^{222}Rn measure-

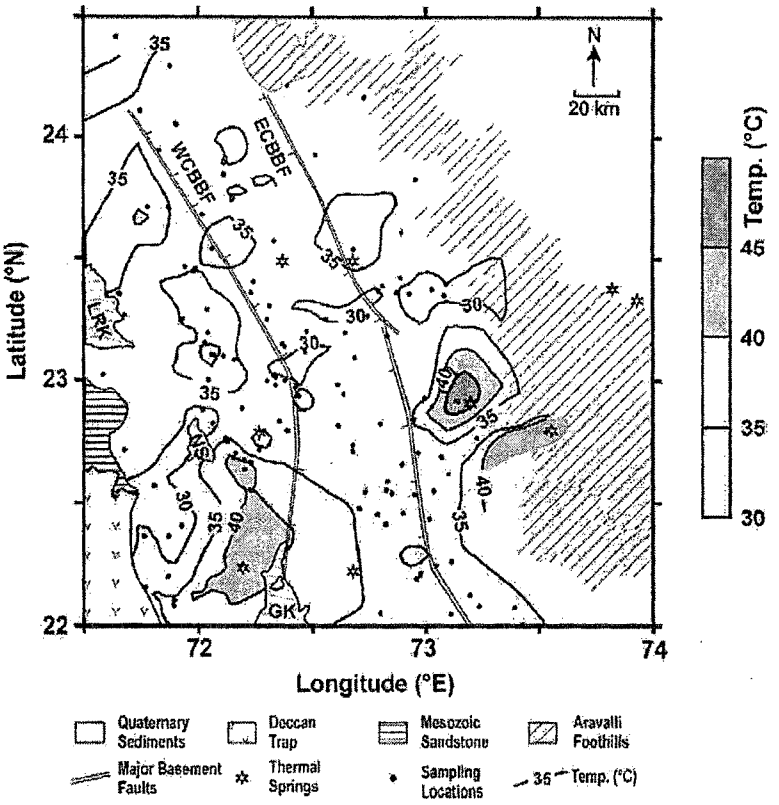

Fig. 5. Contours of groundwater temperature in the North Gujarat–Cambay region. Large areas on both east and west flanks of the CB show temperatures >35 °C, whereas within the CB the temperatures are lower. Temperatures >40 °C are seen around thermal springs. Dots indicate sampling locations.

ments, based on repeat analyses and counting statistics, is <10%.

In addition to groundwater samples, sediments from drill cuttings of a tubewell from Dela village (23.61°N; 72.42°E) in the Cambay Basin were also analysed by γ-spectrometry for uranium and thorium. For this, 22 sediment samples were taken from all the litho-layers encountered in the tubewell between 0–302 m. The samples were dried at 110 °C for 24 h after which they were crushed and packed in pre-weighed plastic containers and then sealed with epoxy resin to prevent escape of gases. Equilibration time of >15 d was given to the sediments in the containers to allow growth of daughter nuclides for steady state achievement. The concentration of U and Th was measured by counting 609 and 583 keV gamma rays using the HPGe gamma ray spectrometer and a common standard sediment sample of known concentration (i.e., 5.69 ppm U and 14.5 ppm Th) with the same configuration as the other samples. Measured U and Th concentrations in the sediments were used to estimate the production of ^{4}He and ^{222}Rn in the groundwater for the subsequent groundwater age determination using Eqs. (8)–(11).

5. Results

The geographical coordinates of well locations, measured values of basic water quality parameters, 'excess He' concentrations and calculated groundwater ^{4}He ages are given in Table 1. The δ^{13}C of TDIC, ^{14}C pmc and calculated radiocarbon groundwater ages are given in Table 2. The contours of radiocarbon dates are shown in Fig. 3. The groundwater sampling locations for ^{4}He measurements and the contours of 'excess He' are shown in Fig. 4. The contours of groundwater temperature are plotted in Fig. 5. The ^{4}He/^{222}Rn ages of the selected samples for which both ^{4}He concentration and ^{222}Rn activity was measured, are given in Table 3. The contours of ^{222}Rn activity in groundwater are given in Fig. 6. The results are summarised as follows:

1. The average groundwater pH for the samples analysed was 7.3 ± 0.4. Only for free flowing artesian thermal wells at Gundi (G), Shiyal (S) and Dholera (D) on the West Flank (see Fig. 6 for locations), pH was >7.9. The redox potential of

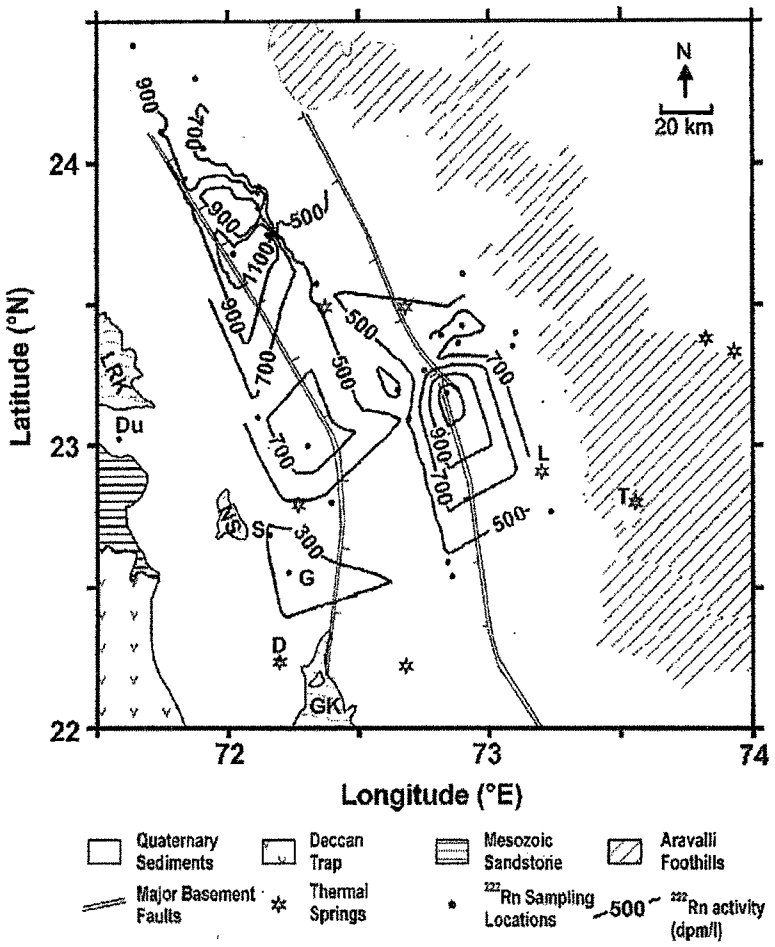

Fig. 6. Iso-distribution map of groundwater ^{222}Rn (dpm/l) in the North Gujarat–Cambay region. Low ^{222}Rn activity was seen in the free flowing artesian wells of Gundi (G), Shiyal (S) and Dholera (D). These wells, however, showed high temperature and helium concentrations (Figs. 4 and 5). Two sampling locations, namely, Tuwa (T) and Dudapur (Du) having very high ^{222}Rn activity (>2500 dpm/l) were excluded during contouring. Dots indicate sampling locations.

groundwater from these wells suggested reducing conditions.

2. The δ^{13}C of TDIC for all groundwater samples varied within a narrow range, with an average of -9.6 ± 1.2 ‰ except for one sample from an artesian thermal well at Gundi with $\delta^{13}C = -21.4$‰ (Table 2).
3. The ^{14}C age contours are nearly parallel to each other and to the WCBBF. The ages increase progressively in the general groundwater flow direction away from the Aravalli foothills (Fig. 3) and reach a value of >35 ka beyond WCBBF (Table 2).
4. The EC of groundwater was lowest (<1 mS) in the foothills of the Aravallis and increased gradually towards the WCBBF running parallel to the Aravalli foothills. Highest EC values were encountered in the south-western part of the study area. A detailed discussion on EC variation in the study area has been presented by Gupta and Deshpande (2003a,b).
5. The groundwater temperatures ranged from 28 to 61 °C (Fig. 5). Within the Cambay Basin which has a thick sedimentary cover, the average groundwater temperature was ~30 °C. Along the WCBBF and on the West Flank a large area showed high groundwater temperatures (≥35 °C). On the East Flank, high groundwater temperatures were observed in and around the thermal springs tapping the Precambrian granitic basement. The highest groundwater temperature (61 °C) was measured in one of the eight sampled vents of the thermal springs at Tuwa (T).
6. Different vents of the Tuwa thermal springs showed different temperature (28–61 °C) and ^{4}He concentrations (137–475 ppm AEU), with

no apparent correlation between these two parameters.

7. Areas of high 'excess He' (>15 ppm AEU; Fig. 4) are generally associated with areas of high temperature (>35 °C), and such samples are mostly found to lie along the major basement faults (i.e., East and West Cambay Basin Boundary Faults) and several criss-cross faults (Fig. 4). On the East Flank, the highest value of 'excess He' (~1100 ppm AEU) was obtained from a hand pump near the thermal spring at Tuwa very close to the Aravalli foothills. On the West Flank, the highest value was from a tubewell in the Zinzawadar village (>2000 ppm AEU).
8. In all samples, except for the thermal springs at Tuwa, the measured ^{222}Rn activity was found unsupported by ^{226}Ra in groundwater. The average ^{222}Rn activity of groundwater within the Cambay Basin was 820 ± 400 dpm/l with lower values in the southern part of the Cambay Basin (Fig. 6). On the East Flank, except for the thermal springs at Tuwa (^{222}Rn ~63,000 dpm/l; ^{226}Ra ~300 dpm/l) the average ^{222}Rn activity of groundwater was 600 ± 300 dpm/l. On the West Flank, samples showed low ^{222}Rn activities (300 ± 100 dpm/l), except for a shallow depth sample at Dudapur (~2600 dpm/l; Table 3; location Du in Fig. 6).
9. High temperatures and high ^{4}He were not necessarily associated with high ^{222}Rn activities. This was particularly apparent from the lowest ^{222}Rn activities (~300 dpm/l) observed at three free flowing thermal wells at Dholka (D), Shiyal (S) and Gundi (G) on the West Flank (Fig. 6). Contrary to this, thermal springs at Tuwa (~50 °C) on the East Flank located in the granitic substrate with ^{4}He concentrations of ~400 ppm AEU showed the highest ^{222}Rn activity (~63,000 dpm/l). In another case, a sample at Dudapur on West Flank exhibited low temperature (~31 °C), high ^{4}He (~50 ppm AEU) and high ^{222}Rn (~2600 dpm/l; Table 3).
10. The average U and Th concentrations of drill cut sediment samples collected from the Dela village (23.61°N; 72.42°E) in the study area were 1.07 ± 0.41 and 7.54 ± 3.5 ppm, respectively, with Th (ppm)/U (ppm) = 7.1 ± 4.3 (Fig. 7). Ten surface sediment samples up to 8.4 m depth from

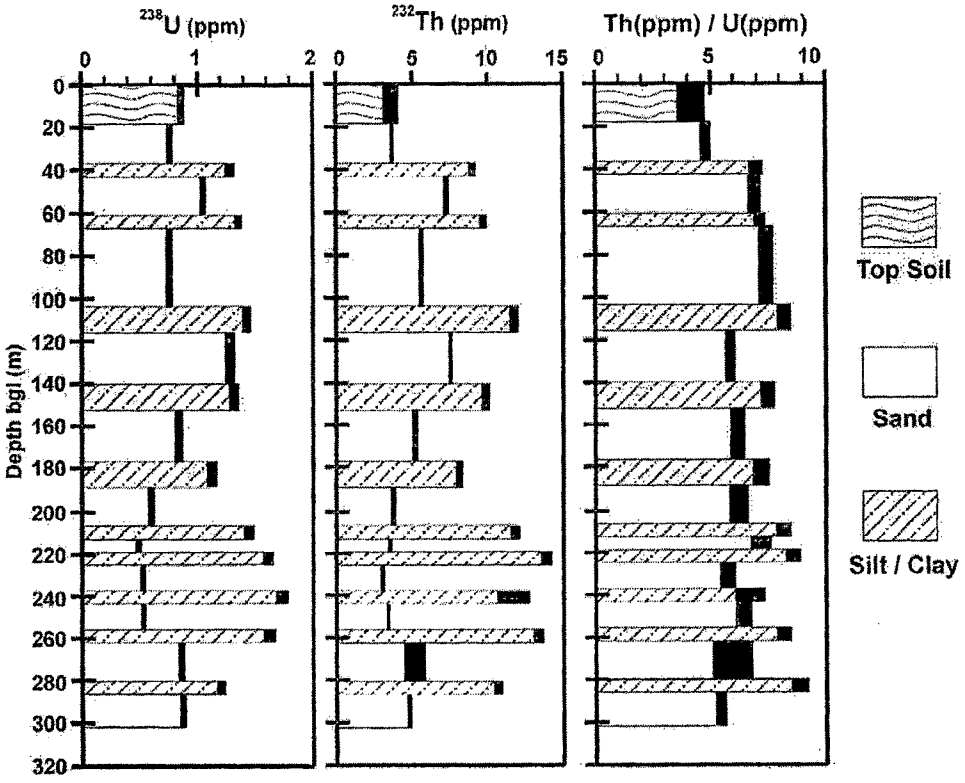

Fig. 7. Plot of U, Th concentration and Th/U ratio in the sediment of drill core samples from Dela village (23.61°N; 72.42°E) in CB. Width of the black vertical bars represents standard counting errors.

the Cambay Basin yielded an average value of U=1.7±0.7 ppm and Th=8.0±3.7 ppm (Srivastava et al., 2001) with Th/U=4.85±2.2.

6. Discussion

6.1. Groundwater radiocarbon age

The estimated groundwater radiocarbon ages are seen to increase roughly westwards from the Aravalli foothills up to the LRK–NS–GK corridor. Further west, lower groundwater ^{14}C ages are encountered (CBGW-344, -351; Table 2). The LRK–NS–GK corridor with the lowest elevation (Fig. 1) in the study area is the zone of convergence for surface drainage (Prasad et al., 1998). Existence of free flowing artesian wells found in the LRK–NS–GK region, and the continuity of their aquifers with those of the Cambay Basin region confirm their recharge area in the foothill region of the Aravalli Mountains. It may also be noted from the subsurface cross-section (Fig. 2) that layers of sand/ silty-clay are roughly inclined parallel to the ground surface and the sampled tubewells tap nearly the same set of water bearing formations across the Cambay Basin. Because the available tubewells tap all the horizons that yield water up to their maximum depth, these are treated as pumping a single aquifer unit, within which the radiocarbon ages progressively increase in the flow direction. The very narrow range of $\delta^{13}C$ values of the TDIC of groundwater (Table 2) indicates that the dead carbon dilution factor for the various samples is not significantly different. As a result the relative age differences between the samples can be relied upon. The only sample (from Gundi) with much depleted $\delta^{13}C$ (−21.4 ‰) is derived from a very deep (>400 m) aquifer and gave an age beyond the ^{14}C dating limit. The low redox potential value (10 mV) of this sample suggested possible CO_2 contribution from anaerobic oxidation.

Further, based on hydro-geological considerations (Fig. 2) the confinement of the regional aquifer in the Cambay Basin appears to become effective near the ECBBF around the ^{14}C age contour of ~2 ka. Within the Cambay Basin, age contours are nearly parallel to each other and the horizontal distance between successive 5 ka contours is nearly constant giving a regional flow velocity in the range 2.5–3.5 m a^{-1} for a natural hydrostatic gradient of 1 in 2000 (GWRDC, Unpublished data), which is comparable to an earlier estimate of ~6 m a^{-1} (Borole et al., 1979) for the small part of the Vatrak–Shedi sub-basin marked in Fig. 3. The Vatrak–Shedi sub-basin (enclosed by an ellipse in Fig. 3) is closer to the recharge area, so both permeability and hydraulic gradient are expected to be relatively higher than the regional estimates of flow velocity (2.5–3.5 m a^{-1}) as given above.

6.2. Groundwater helium ages

It is seen from Fig. 4 that the contour of 5 ppm AEU 'excess He' runs close to the WCBBF. Considering [U] (1.07±0.41 ppm), [Th] (7.5±3.5 ppm), porosity (n)=20%; helium release factor (Λ_{He})=1 and grain density (ρ)=2.6 g cm^{-3} the accumulation time for 'excess He' of 5 ppm AEU will be ~15 ka (Eq. (6)). These ^{4}He ages are in close agreement with the ^{14}C ages, (Fig. 3), when no crustal flux is considered. This is supported by the findings of other workers that relatively young groundwater are dominated by in situ production. Torgersen and Clarke (1985) found good concordance between ^{14}C and ^{4}He ages in the Great Artesian Basin up to ~50 ka. Kulongoski et al. (2003) have found a good match between ^{14}C and ^{4}He ages up to ~25 ka in the Mojave River Basin, California. They have explained the phenomenon by the existence of wells in the basins at shallow depth and hence, above crustal influence. This probably might be the case in the North Gujarat Cambay Basin Region up to the WCBBF. In the Cambay Basin, the fluvial deposits grade from coarse grain sizes near the Aravalli foothills (major recharge region) to fine grain sizes near the LRK–NS–GK (discharge) region. This is indicated by a rapid decrease in aquifer transmissivity from ~1000 m^2 d^{-1} east of the ECBBF to <200 m^2 d^{-1} west of the WCBBF (GWRDC, Unpublished data). Thus, greater transmissivity of the aquifer up to WCBBF of the North Gujarat Region, may result in groundwater flow that entrains insignificant or no basal crustal flux, thereby leaving groundwater ^{4}He ages almost unaffected by the deep crustal ^{4}He flux.

Further, as mentioned earlier, there is some uncertainty on the calculated 'excess ^{4}He' that depends upon (1) 'excess air', and (2) dissolved helium at solubility equilibrium with the atmosphere. It is a common knowledge that the presence of 'excess air' in groundwater leads to ^{4}He concentrations higher than expected from solubility equilibrium (Heaton and Vogel, 1981; Stute and Schlosser, 1993; Aeschbach-Hertig et al., 2000). In this study we are unable to correct for the 'excess air' contribution, as neon concentrations have not been measured. According to laboratory column experiments on the formation of 'excess air' in quasi saturated porous media (Holocher et al., 2002), the amount of 'excess air' can range between 1% to 16%

of the equilibrium solubility concentration. In field studies, higher Ne excesses have also been found (e.g., Heaton and Vogel, 1981; Aeschbach-Hertig et al., 2002).

Since the solubility of He is relatively insensitive to temperature (Ozima and Podosek, 1983); the recharge temperature has a small effect on $^4He_{eq}$, which can be estimated from the regional climate and groundwater temperature measurements. In this study, the mean annual temperature of recently recharged groundwater at the Aravalli foothills was 30 ± 5 °C, as a result $^4He_{eq}$ can decrease by ~10% relative to the groundwater recharged in relatively colder climate.

Thus, both $^4He_{eq}$ and $^4He_{ea}$ would lead a systematic error of ~+10% and ~−20%, respectively on the atmospheric air equilibration value of 5.3 ppm AEU which is subtracted from the measured ^4He in groundwater samples to calculate $^4He_{ex}$ (Section 3.2). While we recognize that such corrections are very important for precise groundwater age estimation, particularly in case of low ^4He concentration samples, the interpretation and conclusion at high ^4He concentrations are not significantly influenced by their absence. Considering this and the accuracy of measurement for low helium concentrations being ~20%, the error on ^4He ages can be as high as 50% for groundwater samples which have <5 ppm AEU 'excess He'. Therefore, only those samples that showed ≥5 ppm AEU 'excess He' are included in the discussion.

It is further seen from Fig. 4 that ^4He concentrations rapidly increase farther west of the 5 ppm AEU 'excess He' contour that almost coincides with WCBBF. This could be due to (i) rapidly increasing residence time of groundwater in response to decreasing transmissivity as a result of a general decrease in grain size away from the sediment source; and/or (ii) increasing effect of the deep crustal flux of helium in the aquifer. The latter possibility is supported by existence of very high helium pockets (>50 ppm AEU) on both East and West Flanks. The East Flank is the major recharge area of aquifers in the Cambay Basin where very high helium pockets are associated with the thermal springs of Lasundra (L) and Tuwa (T). On this flank another small patch of high helium concentration is seen across the ECBBF along the Sabarmati River. Pockets of very high ^4He (>50 ppm AEU) lie outside the Cambay Basin on both flanks (shaded areas in Fig. 4) and considering this helium as in situ production will yield groundwater age $>10^3$ ka, which is not tenable hydro-geologically. The presence of non in situ produced ^4He in these pockets is also indicated by the overlapping pockets of high groundwater temperature (>35 °C) suggesting hydrothermal venting of deep crustal fluids in such pockets. The ^4He method of dating groundwater is not applicable to such pockets.

The deep crustal He flux may also enter the aquifer by diffusion from underlying basement followed by entrainment and upward migration, particularly in the discharge region (Bethke et al., 2000). Thus, more crustal flux may be entrained with increasing distance along flow paths and hence, resulting in a rapid increase in the helium concentration towards the discharge region. For the five samples west of the WCBBF for which ^{14}C groundwater ages were also measured, a ^4He crustal flux of $>1.5\times10^{-8}$ cm^3 STP He cm^{-2} y^{-1} produces a good match between the two dating methods. However, for the Lasundra and Tuwa thermal springs in the East Flank and pockets of very high helium on the West flank (shaded areas in Fig. 4) a crustal flux $>10^{-6}$ cm^3 STP He cm^{-2} y^{-1} is necessary for agreement between ^4He and ^{14}C ages. Takahata and Sano (2000) have reported ^4He crustal flux of 3.0×10^{-8} cm^3 STP He cm^{-2} y^{-1} from a sedimentary basin in Japan. The typical continental ^4He flux is 3×10^{-6} cm^3 STP He cm^{-2} y^{-1} (O'nions and Oxburgh, 1983). It is thus seen that the observed pattern of high helium concentrations in localised pockets can only be explained by invoking 2–3 orders of magnitude variation in crustal diffusion flux which is another way of saying that crustal diffusion occurs along preferred pathways that open where high helium pockets are located.

In the present case, outside the anomalous pockets of helium, the in situ ^4He accumulation (i.e., without crustal flux correction) produces a reasonable correspondence between ^{14}C and ^4He ages within the 50% uncertainty range. For samples to the west of the WCBBF, a low crustal flux of $\sim1.5\times10^{-8}$ cm^3 STP He cm^{-2} y^{-1} cannot be ruled out as invoking it does produce a better match with the few definite ^{14}C groundwater ages. Farther west, ages must be >45 ka, possibly as old as 100 ka.

In the foregoing, the value of Λ_{He} was taken as 1. It is clear from Eqs. (3)–(6) that for lower values of Λ_{He}, the estimate of groundwater ^4He age for the 5 ppm AEU contour (roughly along the WCBBF; Fig. 4) will increase correspondingly. This will result in a better match with the ^{14}C ages (Fig. 3).

6.3. Groundwater helium/radon ages

The measured ^{222}Rn activity within the Cambay Basin and in other parts of the study area (Table 3 and Fig. 6) showed a variation of ±50% around an average

value of ~800 dpm/l (except the thermal spring water at Tuwa) suggesting a similar range of variation in the U concentration of the aquifer material. This range of U variation was also seen in the analysed drill cutting samples (Fig. 7) and on shallow depth sediments from the Cambay Basin (Srivastava et al., 2001).

The distribution of estimated groundwater $^{4}He/^{222}Rn$ ages using Eq. (11) with measured values of ^{222}Rn activity, ^{4}He concentrations and the concentration ratio of [Th]/[U]=7.1±4.3 are shown in Fig. 8. As explained earlier, these ages are independent of porosity, density and U concentration but depend on Th/U of the aquifer material. Additionally, the $^{4}He/^{222}Rn$ ages also depend on the release factor ratio ($\Lambda_{Rn}/\Lambda_{He}$) and accumulation rate ratio ($\Lambda_{Rn}/\Lambda_{He}$) of ^{4}He and ^{222}Rn. As in the case of ^{14}C ages, a gradual age progression from the recharge area towards the WCBBF is observed in the major part of the study area. These ages (Fig. 8) were obtained using $\Lambda_{Rn}/\Lambda_{He}=0.4$ to give the best match with the ^{14}C age gradient (Fig. 3) across the Cambay basin. This gradient matching approach was chosen because the inferred groundwater flow velocities in the confined aquifer by the two methods match when age gradients match. This also ensures that the uncertainties related to, for example the initial activity of ^{14}C in the recharge area or the 'excess He', have as little influence on matching as possible. A Radon release factor (Λ_{Rn}) ranging from 0.01–0.2 has been indicated from laboratory experiments for granites and common rock forming minerals (Krishnaswami and Seidemann, 1988; Rama and Moore, 1984). If measured values of [U]=1.07±0.41 ppm and ^{222}Rn are substituted in Eqs. (9) and (10), Λ_{Rn} is estimated to be 0.15±0.07, which is consistent with the literature. On the other hand for ^{4}He, Torgersen and Clarke (1985), in agreement with numerous other authors have suggested $\Lambda_{He}\approx 1$. For $\Lambda_{Rn}=0.15\pm0.07$ and $\Lambda_{Rn}/\Lambda_{He}=0.4$, $\Lambda_{He}=0.4\pm0.3$ is obtained for best regional matching

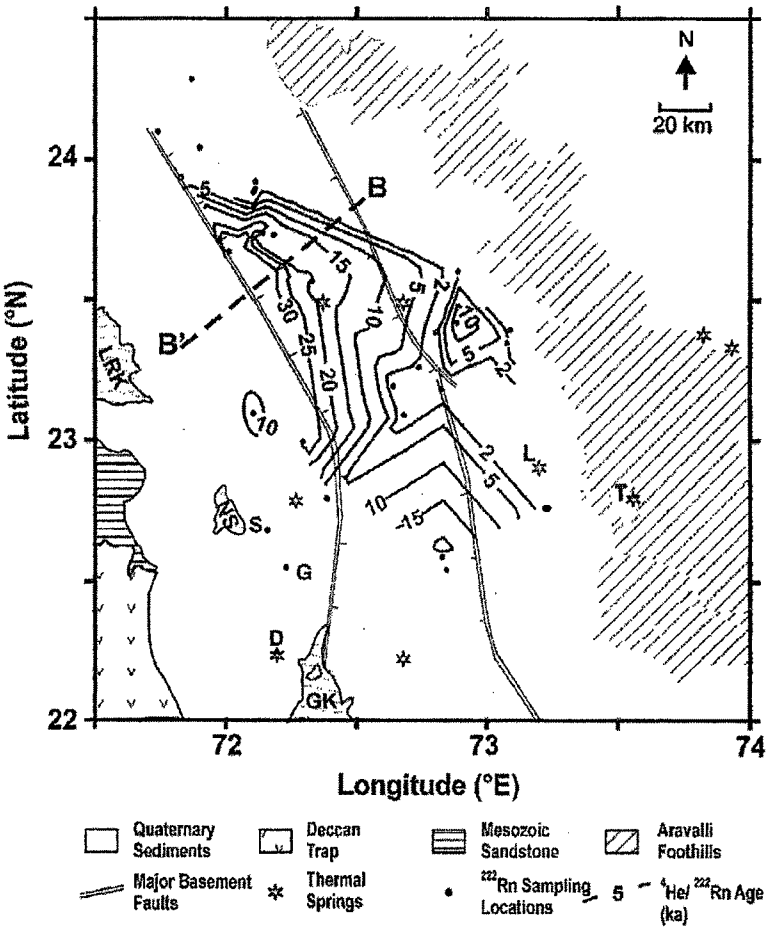

Fig. 8. Iso-distribution map of $^{4}He/^{222}Rn$ groundwater ages in the NGC region for Th/U=7.1; $\Lambda_{Rn}/\Lambda_{He}=0.4$; $\rho=2.6$ g cm^{-3} and $n=20\%$. Samples with >10 ppm AEU 'excess He' and/or >2000 dpm/l ^{222}Rn were excluded during contouring. Dots indicate sampling locations. The groundwater age gradient along BB' is shown in Fig. 9.

between $^4He/^{222}Rn$ and ^{14}C ages, i.e., between Figs. 8 and 3. This is shown in Fig. 9 where age progression along the line BB′ (drawn in Figs. 3, 4 and 8) is plotted. The arrow in the middle of each trapezoid shows the median value of the model age by the respective method. The progressively increasing width of the trapezoid depicts the error at any given median age. The slopes of the respective medians give the age gradients. It is seen that for $\Lambda_{He}=0.4$, the $^4He/^{222}Rn$ age gradient matches the ^{14}C age gradient and, for $\Lambda_{He}=1$, the $^4He/^{222}Rn$ age gradient matches the ^4He age gradient. In view of the various uncertainties that affect the three methods, the ^{14}C method appears most reliable in the present case. Firstly, because the $\delta^{13}C$ values of TDIC show a very narrow range (-9.6 ± 1.2 ‰) and secondly, the ^{14}C age isolines show a nearly parallel distribution, approximately in agreement with the distribution of transmissivity of the aquifers obtained from the pumping test data, progressively decreasing from ~1000 $m^2\ d^{-1}$ east of the ECBBF to <200 $m^2\ d^{-1}$ west of the WCBBF (GWRDC, unpublished data). Therefore, taking ^{14}C age data as reference, the best match for both $^4He/^{222}Rn$ and ^4He ages is obtained for $\Lambda_{He}=0.4$, with the ^4He groundwater age of ~37 ka (instead of ~15 ka) corresponding to the 5 ppm AEU 'excess He' iso-line (Fig. 4). A value of $\Lambda_{He}<1$ in North Gujarat–Cambay region would appear contrary to the apparent $\Lambda_{He}>1$ due to release of geologically stored helium in young sediments derived from old protoliths (Solomon et al., 1996).

The comparatively low estimate of Λ_{He} can either be due to (i) loss of ^4He from the aquifer system, or (ii) incomplete release of radiogenic ^4He from the grains over time scales of ~100 ka. The former possibility is contrary to the basic assumptions of both ^4He and $^4He/^{222}Rn$ dating methods. The latter possibility may not be ruled out because the depositional age of aquifer material in the Cambay Basin is Late Quaternary (Pandarinath et al., 1999; Prasad and Gupta, 1999) and it is possible that all the produced helium has not been released to the interstitial water since deposition. Contrary to Solomon et al. (1996), this would require a mechanism that nearly releases all of the geologically stored helium in the grains due to mechanical/thermal/chemical stress during the process of weathering and transportation and subsequent build up within the grains with a partial release to interstitial water during the quiet post depositional period until steady-state for helium loss is achieved within individual grains. The large grain size (>0.5 mm) of aquifers forming horizons may be a contributory factor to partial helium release in the post depositional period. The present data does not permit giving more definitive arguments concerning the involved mechanisms.

It is interesting to note that the use of groundwater helium for earthquake prediction (Sano et al., 1998) is

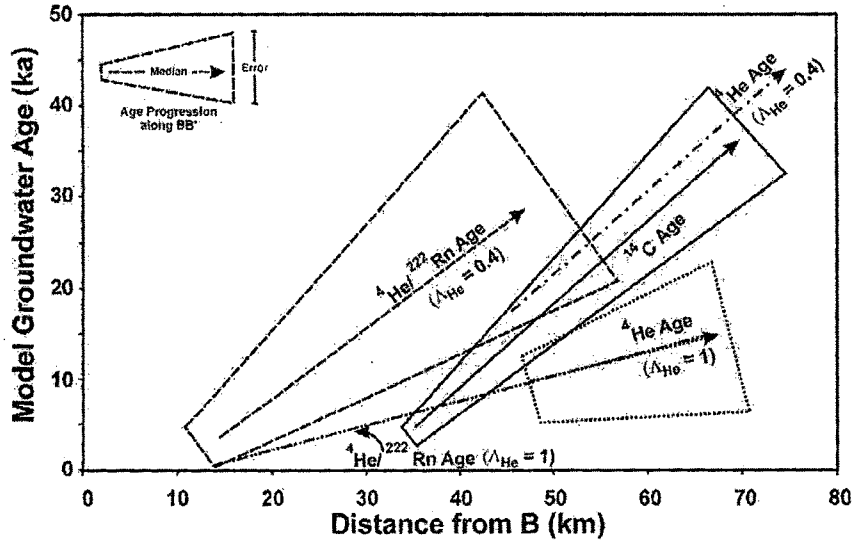

Fig. 9. Plot of groundwater age progression along line BB' (shown in Figs. 3, 4 and 8) for comparing the age gradients for model ^{14}C ages, ^4He ages for $\Lambda_{He}=1$ and $^4He/^{222}Rn$ ages. It is seen that the gradient of $^4He/^{222}Rn$ ages for $\Lambda_{He}=0.4$ matches the gradient for ^{14}C ages. But, the gradient of ^4He ages for $\Lambda_{He}=1$ though matching with the gradient of $^4He/^{222}Rn$ ages for $\Lambda_{He}=1$ is discordant with the ^{14}C age gradient along BB'. Yet for $\Lambda_{He}=0.4$, the gradients of both $^4He/^{222}Rn$ ages and ^4He ages match the ^{14}C age gradient. Only the median values of the age distributions for ^4He ages ($\Lambda_{He}=0.4$) and $^4He/^{222}Rn$ ages ($\Lambda_{He}=1$) are shown.

based on the premise that in the normal course Λ_{He} may be <1.

6.4. Tectonic effects on groundwater helium, radon and temperature

Whatever the Λ_{He} value, high (>50 ppm AEU) ^{4}He concentrations observed in pockets on East Flank (Fig. 4) require residence time >100 ka which is not compatible with the hydrogeology of the region, as this flank forms the recharge area of the regional aquifer system. Association of these high ^{4}He patches with geothermal springs and anomalous (>35 °C) groundwater temperature suggests a role of deep hydrothermal circulation (Gupta and Deshpande, 2003a,b). On this flank, ^{222}Rn measurements do not indicate any unusually high activity suggesting absence of near surface uranium mineralization, except for the thermal water from Tuwa (T). A similar association of helium, geothermal springs and groundwater temperature was observed in the SW part of the study area around 22.5°N and 72.3°E. This region had the highest ^{4}He in groundwater along with the lowest ^{222}Rn activity; clearly suggesting that local near surface uranium mineralization cannot be invoked to explain high groundwater helium. This indicates that, besides the radiogenic component, there is an additional ^{4}He crustal flux with or without physical mixing of groundwater. This area also has a series of criss-cross basement faults and at least two reported thermal springs (Fig. 1) suggesting active deep hydrothermal circulation along these faults. In the majority of groundwater samples, high temperatures (>35 °C) along with very high 'excess He' concentrations (>50 ppm AEU) suggest the possibility of physical mixing of deeper (>500 m) thermal fluids with shallow groundwater. Minissale et al. (2000) have shown, based on ^{3}He/^{4}He ratio and stable isotopic studies on thermal fluids from central-western peninsular India including Tuwa that no signature of mantle derived fluids exists in the thermal waters.

Thus, a few pockets of high helium concentrations overlapping with high temperature pockets located along major basement faults indicate intrusion of deeper crustal fluids to shallow groundwater and adjoining areas. Excluding such pockets, in situ radiogenic production of ^{4}He and ^{222}Rn is able to account for their observed concentrations.

7. Summary and conclusions

A regional aquifer system in the North Gujarat–Cambay region in western India has been investigated for ascertaining the groundwater age evolution from the recharge to the discharge area. A suite of natural tracers, namely ^{14}C, ^{4}He and ^{222}Rn has been employed in addition to temperature and electrical conductivity. The field and laboratory measurements indicated the range of variation for the different parameters as follows: temperature: 28 to 61 °C; EC: 0.5 to 7.6 mS; pH: 6.9 to 8.2; ^{14}C: 0 to 115 pmc; δ^{13}C: −7.26‰ to −21.36‰; ^{4}He: 5.3 to 2850 ppm AEU; and ^{222}Rn: 260 to 62600 dpm/l. The anomalous values of the various parameters were found generally in association with thermal groundwater.

The groundwater age estimates by the three methods (^{14}C, ^{4}He and ^{4}He/^{222}Rn) indicated present to <2 ka ages in the recharge area along the Aravalli foothills. The ages progressively increased in the general flow direction of groundwater, approximately westward in the Cambay Basin, reaching a limiting value of ~35 ka for ^{14}C near the West Cambay Basin Boundary Fault. The ^{4}He method also indicated further west-southwards progression of groundwater ages up to ~100 ka. In the entire study area, there was correspondence in age estimates by the three dating methods within ~50% uncertainty for both ^{4}He and ^{4}He/^{222}Rn methods. In spite of such a large uncertainty in age estimates, the best match of groundwater age distributions by the three methods is obtained for a helium release factor (Λ_{He}) value of 0.4 ± 0.3, significantly less than the conventionally used value of 1. These investigations have validated the hydrological model of the study area as comprising of a regional confined aquifer system with recharge area in the Aravalli foothills and subsurface discharge area in the Gulf of Khambhat.

In addition to the progressive increase of groundwater age in the flow direction, some pockets of anomalously high ^{4}He concentrations, not accompanied by high ^{222}Rn activities (except at Tuwa thermal spring) have been observed along some deep-seated faults in the study area. These anomalously high ^{4}He concentrations were geographically associated with anomalously high groundwater temperatures (Figs. 4 and 5). Considering the positive geographic correlation between ^{4}He and temperature, an active hydrothermal circulation involving deep crustal layers, as suggested earlier (Gupta and Deshpande, 2003a,b), is reaffirmed.

This multi-parameter groundwater study also indicated that release of radiogenic radon from the solid to the liquid phase in the study area was $15 \pm 7\%$ for alluvial sedimentary formations in agreement with previous estimates. Radiogenic helium release from the solid to the liquid phase was, however, estimated as only ($40 \pm 30\%$) instead of literature value of ~100%.

The lower helium release over long time scale (~100 ka) is probably consistent with several known instances of anomalous ^{4}He release during rock dilation and fracturing in association with earthquakes and enhanced release of geologically stored radiogenic helium in relatively young fine grained sediments derived from old protoliths.

Acknowledgements

This study forms part of a research project entitled "Estimation of Natural and Artificial Groundwater Recharge Using Environmental, Chemical and Isotopic Tracers and Development of Mathematical Models of Regional Aquifer Systems in North Gujarat". We thank the Gujarat Water Resources Development Corporation Ltd., Gandhinagar (GWRDC) for sponsoring this project and for sharing the unpublished hydrogeology data from the study area. We are grateful to Prof. N. Bhandari for providing us the HPGe detector for U, Th and ^{222}Rn activity measurements using gamma spectrometry. Help of Mr. M.H. Patel and Mr. N.B Vaghela is gratefully acknowledged for ^{14}C and δ^{13}C analyses. Shri B.R. Raval is thanked for help in fieldwork. We also thank the two referees (Drs. A. Minissale and W. Aeschbach-Hertig) for their valuable suggestions towards improving the manuscript. [SG]

References

Aeschbach-Hertig, W., Peeters, F., Beyerle, U., Kipfer, R., 2000. Palaeotemperature reconstruction from noble gases in ground water taking into account equilibration with entrapped air. Nature 405, 1040–1044.

Aeschbach-Hertig, W., Stute, M., Clark, J.F., Reuter, R.F., Schlosser, P., 2002. A palaeotemperature record derived from dissolved noble gases in groundwater of the Aquia aquifer (Maryland, USA). Geochim. Cosmochim. Acta 66 (5), 797–817.

Andrews, J.N., 1977. Radiogenic and inert gases in groundwater. In: Paquet, H., Tardy, Y. (Eds.), Proc. of the Sec. Int. Symp. On Water–Rock Interaction, Strassbourg, pp. 334–342.

Andrews, J.N., Lee, D.J., 1979. Inert gases in groundwater from the Bunter Sandstone of England as indicators of age and paleoclimatic trends. J. Hydrol. 41, 233–252.

Andrews, J.N., Fontes, J. Ch., 1992. Importance of the in situ production of ^{36}Cl, ^{36}Ar and ^{14}C in hydrology and hydrogeochemistry. Isotopes Techniques in Water Resources Development. IAEA, Vienna, pp. 245–269.

Andrews, J.N., Giles, I.S., Kay, R.L.F., Lee, D.J., Osmond, J.K., Cowart, J.B., Fritz, P., Barker, J.F., Gale, J., 1982. Radioelements, radiogenic helium and age relationships for groundwaters from the granites at Stripa, Sweden. Geochim. Cosmochim. Acta 46, 1533–1543.

Andrews, J.N., Davis, S.N., Fabryka-Martin, J., Fontes, J.Ch., Lehmann, B.E., Loosli, H.H., Michelot, J.L., Moser, H., Smith, B., Wolf, M., 1989. The in situ production of radioisotopes in rock matrices with particular reference to the Stripa granite. Geochim. Cosmochim. Acta 53, 1803–1815.

Ballentine, C.J., Burnard, P.G., 2002. Production, release and transport of noble gases in the continental crust. In: Porcelli, D., Ballentine, C.J., Wieler, R. (Eds.), Noble Gases in Geochemistry and Cosmochemistry, Rev. Mineral. Geochem., vol. 47. pp. 481–538.

Bethke, C.M., Torgersen, T., Park, J., 2000. The "age" of very old groundwater: insights from reactive transport models. J. Geochem. Explor. 69–70, 1–4.

Borole, D.V., Gupta, S.K., Krishnaswami, S., Datta, P.S., Desai, B.I., 1979. Uranium isotopic investigations and radiocarbon measurement of river–groundwater systems, Sabarmati Basin, Gujarat, India. Isotopic Hydrology, vol. 1. IAEA, Vienna, pp. 181–201.

Castro, M.C., Stute, M., Schlosser, P., 2000. Comparison of ^{4}He ages and ^{14}C ages in simple aquifer systems: implications for groundwater flow and chronologies. Appl. Geochem. 15, 1137–1167.

Clark, I.D., Fritz, P., 1997. Environmental Isotopes in Hydrogeology, Lewis Publisher, CRC Press. 328 pp.

Clark, J.F., Davisson, M.L., Hudson, G.B., Macfarlane, P.A., 1998. Noble gases, stable isotopes, and radiocarbon as traces of flow in the Dakota aquifer, Colorado and Kansas. J. Hydrol. 211, 151–167.

Cserepes, L., Lenkey, L., 1999. Modelling of helium transport in groundwater along a section in the Pannonian basin. J. Hydrol. 225, 185–195.

Fontes, J.C., Garnier, J.M., 1979. Determination of the initial ^{14}C activity of the total dissolved carbon: a review of the existing models and new approach. Water Resour. Res. 15 (2), 399–413.

Fröhlich, K., Gellermann, R., 1987. On the potential use of uranium isotopes for groundwater dating. Chem. Geol. 65, 67–77.

Gazetteer, 1975. In: Rajyagor, S.B. (Ed.), Gujarat State Gazetteers. 862 pp.

Geyh, M.A., 1990. Absolute Age Determination: Physical and Chemical Dating Methods and their Applications. Springer Verlag, Germany. 503 pp.

GSI, 2000. Seismotectonic atlas of India and its environs. Geological Survey of India, Calcutta, India. 87 pp.

Gupta, S.K., Polach, H.A., 1985. Radiocarbon Practices at ANU, Handbook, Radiocarbon Laboratory, Research School of Pacific Studies. ANU, Canberra. 173 pp.

Gupta, S.K., Deshpande, R.D., 2003a. Origin of groundwater helium and temperature anomalies in the Cambay region of Gujarat, India. Chem. Geol. 198, 33–46.

Gupta, S.K., Deshpande, R.D., 2003b. High fluoride in groundwater of North Gujarat–Cambay region: origin, community perception and remediation. In: Singh, V.P., Yadava, R.N. (Eds.), Proc. Int. Conf. on Water and Environment 2003, Ground Water Pollution. pp. 368–388.

Gupta, S.K., Bhandari, N., Thakkar, P.S., Rengarajan, R., 2002. On the origin of the artesian groundwater and escaping gas at Narveri after the 2001 Bhuj earthquake. Curr. Sci. 82 (4), 463–468.

Heaton, T.H.E., Vogel, J.C., 1981. "Excess air" in groundwater. J. Hydrol. 50, 201–216.

Holocher, J., Peeters, F., Aeschbach-Hertig, W., Hofer, M., Brennwald, M., Kinzelbach, W., Kipfer, R., 2002. Experimental investigations on the formation of excess air in quasi-saturated porous media. Geochim. Cosmochim. Acta 66 (23), 4103–4117.

Imbach, T., 1997. Deep groundwater circulation in the tectonically active area of Bursa, northwest Anatolia, Turkey. Geothermics 26 (2), 251–278.

Ivanovich, M., 1992. Uranium Series Disequilibrium: Applications to Earth Marine and Environmental Sciences. Claderon Press, Oxford. 910 pp.

Krishnaswami, S., Seidemann, D.E., 1988. Comparative study of ^{222}Rn, ^{40}Ar, ^{39}Ar and ^{37}Ar leakage from rocks and minerals: implications to the role of nanopores in gas transport through natural silicates. Geochim. Cosmochim. Acta 52, 655–658.

Kulongoski, J.T., Hilton, D.R., Izbicki, J.A., 2003. Helium isotope studies in the Mojave Desert, California: implications for groundwater chronology and regional seismicity. Chem. Geol. 202, 95–113.

Lehmann, B.E., Loosli, H.H., Rauber, D., Thonnard, N., Willis, R.D., 1991. ^{81}Kr and ^{85}Kr in groundwater, Milk River Aquifer, Alberta, Canada. Appl. Geochem. 6, 419–424.

Maurya, D.M., Malik, J.N., Raj, R., Chamyal, L.S., 1997. Soft sediment deformation in the Quaternary sediments of the Lower Mahi river basin, Western India. Curr. Sci. 72 (7), 519–522.

Mazor, E., Bosch, A., 1992. Helium as semi-quantitative tool for groundwater dating in the range of 104–108 years. Isotopes of Noble Gases as Tracers in Environmental Studies. IAEA, Vienna, pp. 163–178.

Merh, S.S., 1995. Geology of Gujarat. Geological Society of India. 222 pp.

Minissale, A., Vaselli, O., Chandrasekharan, D., Magro, G., Tassi, F., Casiglia, A., 2000. Origin and evolution of 'intracratonic' thermal fluids from central-western peninsular India. Earth Planet. Sci. Lett. 181, 377–397.

Mook, W.G., 1976. The dissolution-exchange model for dating groundwater with ^{14}C. Interpretation of Environmental Isotopes and Hydrochemical Data in Groundwater Hydrology. IAEA, Vienna, pp. 213–225.

Münnich, K.O., 1957. Messung des ^{14}C—Gehaltes von hartem Grundwasser. Naturwissenschaften 34, 32–33.

Münnich, K.O., 1968. Isotopen-Datierung von Grundwasser. Naturwissenschaften 55, 158–163.

Nazaroff, W.W., Moed, B.A., Sextro, R.G., 1988. Soil as a source of indoor radon: generation, migration and entry. In: Nazaroff, W.W., Nero Jr., A.V. (Eds.), Radon and its Decay Products in Indoor Air. John Wiley and Sons, NY.

O'nions, R.K., Oxburgh, E.R., 1983. Heat and helium in the earth. Nature 306, 429–431.

Ozima, M., Podosek, F.A., 1983. Noble Gas Geochemistry. Cambridge University Press, NY.

Pandarinath, K., Prasad, S., Deshpande, R.D., Gupta, S.K., 1999. Late Quaternary sediments from Nal Sarovar, Gujarat, India: distribution and provenance. Proc. Indian Acad. Sci. (Earth Planet. Sci.) 108 (2), 107–116.

Prasad, S., Gupta, S.K., 1999. Role of eustasy, climate and tectonics in Late Quaternary evolution of Nal–Cambay region, NW India. Z. Geomorph. N.F. 43, 483–504.

Prasad, S., Pandarinath, K., Gupta, S.K., 1998. Geomorphology, tectonism and sedimentation in the Nal Region, western India. Z. Geomorph. N.F. 25, 207–223.

Rama, Moore, W.S., 1984. Mechanism of transport of U–Th series radioisotopes from solids into groundwater. Geochim. Cosmochim. Acta 48, 395–399.

Sano, Y., Takahata, N., Igarashi, G., Koizumi, N., Sturchio, N.C., 1998. Helium degassing related to the Kobe earthquake. Chem. Geol. 150, 171–179.

Solomon, D.K., Hunt, A., Poreda, R.J., 1996. Source of radiogenic helium-4 in shallow aquifers: implications for dating young groundwater. Water Resour. Res. 32, 1805–1813.

Srivastava, P., Juyal, N., Singhvi, A.K., Wasson, R.J., Bateman, M.D., 2001. Luminescence chronology of river adjustment and incision of Quaternary sediments in the alluvial plain of the Sabarmati River, North Gujarat, India. Geomorphology 36, 217–229.

Stute, M., Schlosser, P., 1993. Principles and applications of the noble gas palaeothermometer. In: Swart, P.K., Lohmann, K.C., McKenzie, J., Savin, S. (Eds.), Climate Change in Continental Isotopic Records, Geophysical Monograph Series, vol. 78. American Geophysical Union, Washington, DC, pp. 89–100.

Stute, M., Sonntag, C., Deak, J., Schlosser, P., 1992. Helium in deep circulating groundwater in the Great Hungarian Plain: flow dynamics and crustal and mantle helium fluxes. Geochim. Cosmochim. Acta 56, 2051–2067.

Takahata, N., Sano, Y., 2000. Helium flux from a sedimentary basin. Appl. Radiat. Isotopes 52, 985–992.

Torgersen, T., 1980. Controls on pore-fluid concentration of ^{4}He and ^{222}Rn and the calculation of $^{4}He/^{222}Rn$ ages. J. Geochem. Explor. 13, 57–75.

Torgersen, T., 1992. Helium-4 model ages for pore fluids from fractured lithologies, discussion and application. Isotopes of Noble Gases as Tracers in Environmental Studies. IAEA, Vienna, pp. 179–201.

Torgersen, T., Clarke, W.B., 1985. Helium accumulation in groundwater. I. An evaluation of sources and the continental flux of crustal ^{4}He in the Great Artesian Basin, Australia. Geochim. Cosmochim. Acta 49, 1211–1218.

Torgensen, T., Ivey, G.N., 1985. Helium accumulation in groundwaters: II. A model for the accumulation of the crustal ^{4}He degassing flux. Geochim. Cosmochim. Acta 49, 2445–2452.

Vogel, J.C., 1967. Investigation of groundwater flow with radiocarbon. Isotopes in Hydrology. IAEA, Vienna, pp. 355–368.

Vogel, J.C., 1970. Carbon-14 dating of groundwater. Isotope Hydrology. IAEA, Vienna, pp. 225–237.

Weiss, R.F., 1971. Solubility of helium and neon in water and seawater. J. Chem. Eng. Data 16, 235–241.

Origin of high fluoride in groundwater in the North Gujarat-Cambay region, India

S. K. Gupta · R. D. Deshpande · Meetu Agarwal · B. R. Raval

Abstract This paper reports on the origin of high fluoride in a regional alluvial aquifer system under water stress in the North Gujarat-Cambay (NGC) region in western India. This region is severely affected by endemic fluorosis due to ingestion of groundwater containing excessive fluoride. With an objective to understand factors controlling high fluoride concentration in groundwater of this region, 225 groundwater samples have been analysed for various chemical parameters. Samples were collected from different depth zones tapping shallow dug wells, geothermal springs, hand-pumps and tubewells, including free flowing artesian wells up to 450 m depth from the aquifers in the Quaternary alluvial formation covering most of the study area. No relation was found between fluoride concentration and depth of sampled groundwater. However, certain sub-aquifer zones have been identified within the Cambay Basin where groundwater contains relatively high fluoride concentration. In general, areas of high fluoride overlap areas with high electrical conductivity (EC). On the west flank of the Cambay Basin in the low lying belt linking Little Rann of Kachchh-Nalsarovar-Gulf of Khambhat (LRK-NS-GK), high fluoride and EC in shallow aquifers originate from evaporative enrichment. On the east flank of Cambay Basin, some high fluoride pockets are observed which are probably due to preferential dissolution of high fluoride bearing minerals. On this flank high fluoride is also associated with thermal springs. Within the Cambay Basin, alternating belts of low and high fluoride concentrations are ascribed to groundwater recharge during the past wet and arid climatic phases, respectively. This is based on groundwater radiocarbon age contours of ~20 ka overlapping the high fluoride belt.

Résumé Cet article étudie l'origine des teneurs élevées en Fluorure dans un système aquifère alluvial régional, soumis à un stress hydrique dans le Nord Gujarat–région Cambay (NGC) à l'Ouest de l'Inde. Cette région est sévèrement affectée par une fluorose endémique, due à l'ingestion d'eau souterraine très riche en fluor. Avec pour objectif de comprendre les paramètres contrôlant les fortes teneurs en fluor, 225 échantillons d'eau souterraine ont été analysés sur différents paramètres. Les échantillons ont été pris à différentes profondeurs : puits de surface, sources géothermiques, pompes à main, forages artésiens jaillissant dont la profondeur avoisine les 450 m dans les formations alluviales quaternaire recouvrant la plus grande partie de la région étudiée. Il n'y a pas de relation entre la profondeur et les teneurs en fluorure. Néanmoins, certaines zones sub-aquifères ont été identifiées dans le Basin de Cambay où l'eau souterraine présentait des concentrations relativement élevées en fluorure. En général les zones de hautes concentrations en fluorure recouvrent les zones à fortes conductivité électrique (abréviation en anglais: EC). Sur le flanc Ouest du bassin de Cambay dans le mince lit reliant Little Ran de Kachchh-Nalsarovar au golfe de Khambhat (LRK-NS-GK), les fortes teneurs en fluorure et les EC dans la nappe phréatique proviennent de l'enrichissement par les évaporites. Sur le flanc Est du bassin, des poches de teneurs élevées en fluorures ont été observées, probablement dues à des dissolutions préférentielles de minéraux fluorés. Sur ce flanc des teneurs sont également associées à la présence de sources géothermales. Dans le bassin de Cambay, les alternances de couches lits à fortes teneurs et de lits à faibles teneurs sont expliquées par la recharge durant les périodes climatiques humides et les périodes climatiques plus sèches. Ceci est corroboré par les datations au radiocarbone (environ 20.000 an) au dessus du lit riche en fluorure.

Resumen Este artículo reporta sobre el origen de altas concentraciones de flúor en un sistema regional de acuíferos bajo presión hídrica en la región del norte de Gujarat-Cambay (NGC) del occidente de India. Esta región está afectada severamente por fluorosis endémica debido a la ingestión de agua subterránea que contiene exceso de flúor. Se tomaron 225 muestras de agua subterránea las cuales fueron analizadas por varios parámetros químicos con el objetivo de entender los factores que controlan las elevadas concentraciones de flúor en esta región. Las muestras se colectaron a diferentes profun-

Received: 8 May 2003 / Accepted: 18 August 2004
Published online: 7 October 2004

S. K. Gupta (✉) · R. D. Deshpande · M. Agarwal · B. R. Raval
Physical Research Laboratory (PRL),
PO Box 4218, 380 009 Navrangpura, Ahmedabad, India
e-mail: skgupta@prl.ernet.in

DOI 10.1007/s10040-004-0389-2

didades en pozos someros, manantiales geotermales, pozos con bom-bas de mano, y pozos entubados incluyendo pozos artesianos de flujo libre de hasta 450 m de profundidad emplazados en los acuíferos de la formación aluvial Cuaternaria que cubre la mayor parte del área de estudio. No se encontró ninguna relación entre la concentración de flúor y la profundidad de las muestras de agua subterránea. Sin embargo, se identificaron dentro de la cuenca Cambay algunas zonas sub-acuíferas donde el agua subterránea contiene concentraciones relativamente altas de flúor. En general, las áreas con elevada concentración de flúor están sobrepuestas a áreas de alta conductividad eléctrica (CE). Sobre el flanco occidental de la cuenca Cambay, en la faja baja que une Little Rann con Kachchh-Nalsarovar-Golfo de Khamhat (LRK-NS-GK), las altas concentraciones de flúor y altas CE en acuíferos someros se derivan de enriquecimiento por evaporitas. Sobre el flanco orien-tal de la cuenca Cambay se observaron algunos cuerpos con alta concentración de flúor los cuales se deben probablemente a la disolución preferencial de minerales con alto contenido de flúor. En este flanco el alto contenido de flúor también se asocia con manantiales termales. Dentro de la cuenca Cambay existen fajas alternantes, con concentraciones altas y bajas de flúor, las cuales se atribuyen a recarga de agua subterránea durante las fases climáticas pasadas, húmedas y áridas, respectivamente. Este planteamiento se basa en contornos de edades de ~20 ka de radiocarbono que están sobrepuestos a la faja alta en flúor.

Keywords Groundwater · Fluoride · North Gujarat · Cambay Basin

Introduction

The effects of fluoride on human health have been extensively studied (WHO 1970, 1984). The occurrence and development of endemic fluorosis has its roots in the high fluoride content in water, air and soil, of which water is perhaps the major contributor. Bureau of Indian Standards (BIS 1990) has suggested the permissible limit of fluoride in drinking water to be 1 ppm, which is lower then the WHO (1984) drinking water limit of 1.5 ppm.

Almost the entire population of the NGC region in western India uses groundwater for drinking and other purposes. Evidences of dental and skeletal fluorosis in many areas of this region have been noticed (Gupta and Deshpande 1998). Although knowledge concerning fluoride-affected parts of Gujarat is available (Vasavada 1998; Gujarat Water Supply and Sewerage Board, 1997, unpubl. data), very little is understood about the origin of high fluoride in affected areas. It is only during the last 3–4 decades that high concentrations of fluoride in groundwater have been noticed in North Gujarat and assigned to health problems. During this period, areas irrigated by groundwater increased three times and the water table declined by as much as 100–150 m, particularly in the Mehsana district. This has lead to a general belief that excessive exploitation of groundwater is in some way responsible for the increase of fluoride in groundwater. The most common hypothesis suggests that deep groundwater in the area contains high concentrations of fluoride (Patel, 1986, personal communication). This could be due to its high residence time in the aquifer system thereby having longer contact time for dissolution of fluoride bearing minerals present (Ramakrishnan 1998). Another hypothesis suggests higher concentrations of fluoride bearing minerals in the deeper aquifers. Handa (1975) has linked high fluoride to high evapo-transpiration in arid regions of India.

Since clays are known to be generally rich in fluoride concentration (Agrawal et al. 1997), it is possible that pore water in clay-rich aquitards has relatively higher fluoride concentrations. As a result of decline in piezometric level during the last few decades, increase in flow across the aquitards could provide increased fluoride to the aquifers and be pumped with the groundwater. However, these hypotheses are essentially conjectures, not based on any detailed investigation of the distribution of fluoride and its association with other hydro-geological parameters in the NGC region.

The objective of this study was to understand factors controlling the high fluoride concentration in groundwater of the NGC region. In addition to purely academic inquiry, the understanding of the origin and distribution of fluoride may be useful in devising water exploitation and management strategies.

Various groundwater quality parameters have been measured in samples from various depth zones ranging from shallow dug wells, geothermal springs, hand-pumps and tubewells to artesian wells up to 450 m depth.

Geohydrology of the North Gujarat-Cambay region

North Gujarat—Cambay region (Fig. 1) comprise ~500-m thick multilayered sedimentary sequence of fluvially transported Quaternary alluvium deposited in the Cambay Graben and on its flanks (Merh 1995). This forms the regional aquifer system of NGC region with several sub-aquifers at different depths (Fig. 2).

A geological cross-section from Chadotar to Nayaka across the Cambay Basin (along the line AA' in Fig. 1) is shown in Fig. 2. The sandy layers forming aquifer horizons are seen to be laterally continuous and vertically interspersed with thin semi-permeable clay/silt layers that may not have lateral continuity over a large area. Since the tubewells tap all the horizons that yield water up to their maximum depth, all the pumped horizons have been treated as a single regional aquifer unit and the individual sand layers as sub-aquifers. It is also seen that various sub-aquifers are roughly inclined parallel to the ground surface; so that at different locations, a given depth below ground level (bgl) reaches approximately the same sub-aquifer within the Cambay Basin.

Major rivers traversing the region, namely, Banas, Rupen, Saraswati, Sabarmati and Mahi have eroded the igneous and metamorphic rocks associated with the Delhi

 DOI 10.1007/s10040-004-0389-2

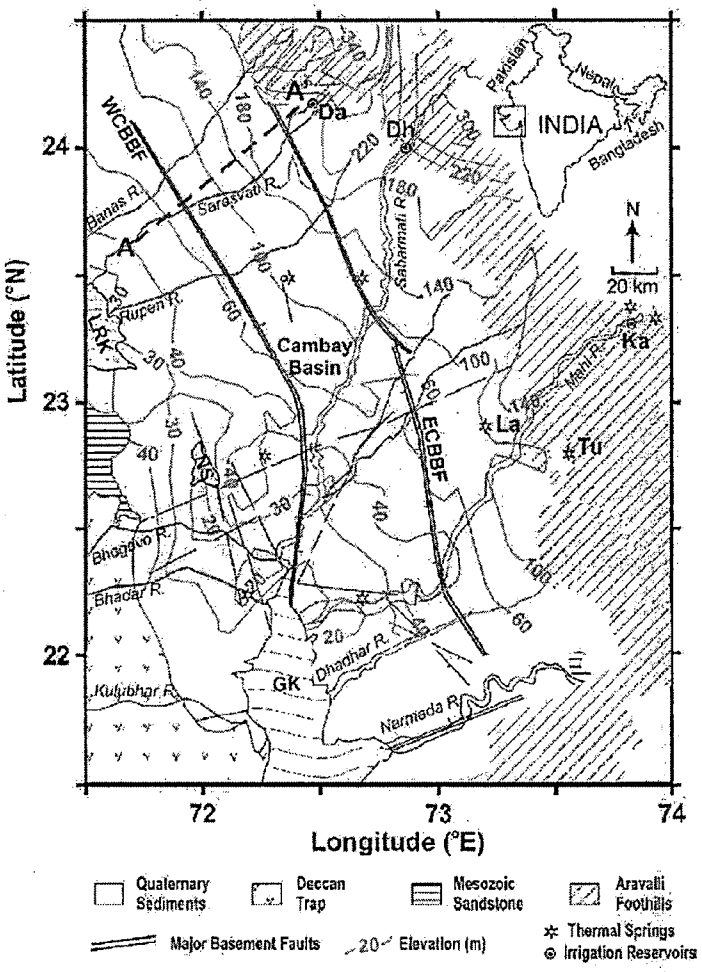

Fig. 1 Map of NGC region showing geological formations, surface elevation (m), drainage pattern and tectonic features. Proterozoic rocks of Delhi super group are exposed in the Aravalli foothills, which is the highest elevation in the study area. The lowest elevations are seen in the tract linking Little Rann of Kachchh, NS and GK. This is also the zone of convergence of rivers originating from Aravallis in the east and Saurashtra in the west. The major faults bounding Cambay Basin, namely, East and West Cambay Basin Boundary Faults (ECBBF and WCBBF) along with sympathetic faults parallel or orthogonal are also shown. A lithological cross section along line AA' is shown in Fig. 2. Acronyms for locations are: *Da* Dantiwada; *Dh* Dharoi; *Ka* Kadana; *La* Lasundra; *Tu* Tuwa

super group from the Aravalli hills in the northeastern part of the study area (Fig. 1). Of these, Banas, Saraswati and Rupen originate from granitic terrain associated with Erinpura and Ambaji granite. In their upper reaches, Sabarmati and its major tributaries traverse across quartzites, phyllites, slates and schists associated with Kumbalgarh, Gogunda, Jharol and Lunawada group of rocks (Merh 1995).

On the west flank of the Cambay Basin, fluvial sediments were also deposited by minor rivers, namely, Bhogavo and Bhadar that traverse the basaltic terrain of the Deccan Trap. Shallow marine sediments were also deposited in the low-lying tract between the Gulf of Khambhat and Little Rann of Kachchh during Late Quaternary. A model of late quaternary deposition related to westward migration of a depositional front caused by marine regression and/or tectonic uplift of the east flank was presented by Prasad et al. (1997), Prasad and Gupta (1999) and Pandarinath et al. (1999a).

From the contours of surface elevation in Fig. 1, it is seen that the low-lying tract linking Gulf of Khambhat and Little Rann of Kachchh has the lowest elevation and forms a zone of convergence wherein both east and west flowing rivers tend to reach.

Due to scanty rainfall (<600 mm a^{-1}), and an ephemeral river system, the entire study area depends heavily on groundwater for its domestic, agriculture and industrial requirements. An acute shortage of water is exacerbated by the inferior water quality in terms of salinity and excessive fluoride.

Experimental

Tubewells and handpumps were purged long enough to flush out the stagnant residual water from the pipes and obtain groundwater samples with in situ chemical composition. In most cases, samples were collected from tubewells that were pumped for several hours prior to sampling. A total of 225 samples were collected and analysed for various parameters. Sample details, including geographical coordinates, groundwater source type, depth below ground level (bgl) along with results of fluoride and EC analyses can be downloaded from (http://www.prl.res.in/%7Ewebprl/web/announce/hydrogeol.pdf)

DOI 10.1007/s10040-004-0389-2

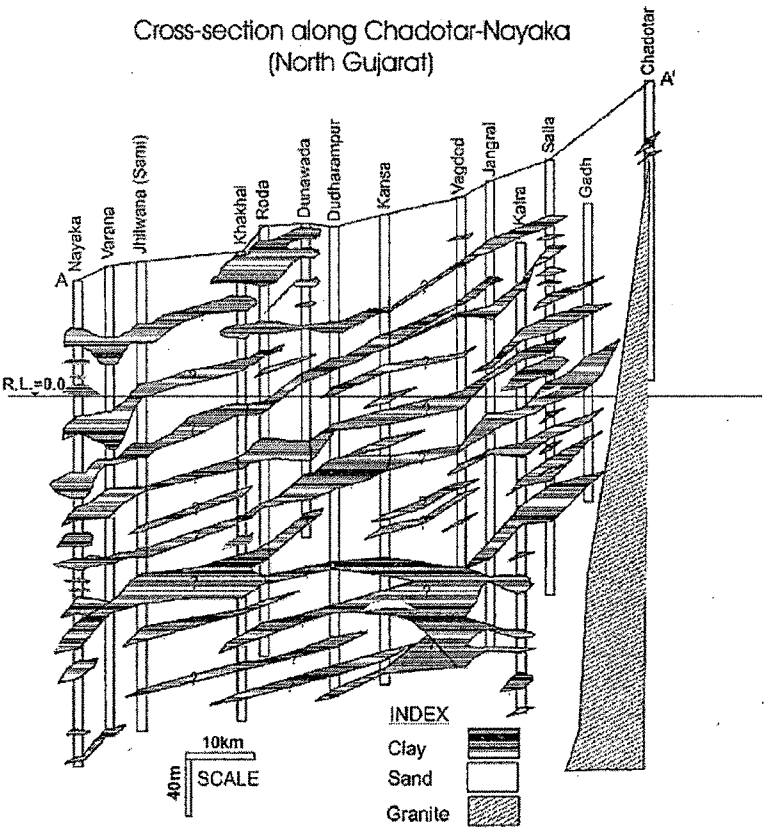

Fig. 2 A typical subsurface litho-section across Cambay Basin along line AA' of Fig. 1. The sandy layers forming sub-aquifers are seen laterally continuous and vertically interspersed with thin semi-permeable clay/silt layers that may not have lateral continuity over a large area. Since the tubewells tap all the horizons that yield water up to their maximum depth, the pumped horizons are treated as forming a single regional aquifer system

The groundwater samples were collected in soda-lime glass bottles after rinsing with the sample water. Sample bottles were immediately sealed using Bromobutyl rubber stoppers and triple aluminium protective caps crimped by a hand-held crimping device. To ensure the integrity of stored water for fluoride addition from the sampling bottles, de-ionised water was stored in several bottles over a period of one year. No measurable fluoride was detected in the stored water.

The standard parameters like temperature, pH, alkalinity, oxidation-reduction potential (ORP) and EC were measured in the field and fluoride concentrations were measured in the laboratory within a few days of the sample collection. Samples were also analysed for their dissolved helium concentration. The results of helium analyses have been separately published (Gupta and Deshpande 2003). Samples were also collected and analysed for radiocarbon dating from some selected wells. These results are being separately reported in detail (Agarwal et al. submitted).

The standard parameters were measured using the μ-processor based water analysis kit (Century: model CMK-731) and fluoride concentrations were measured colorimetrically using 580-nm-tuned colorimeter (Model: Hach) using SPADNS reagent method. The precision of fluoride measurements is <0.1 ppm.

Results

Spatial distribution of fluoride in groundwater from the Cambay Basin area is shown in Fig. 3. It is seen that starting from the 71.5°E, there is a major high fluoride concentration (4–8 ppm) belt (PP') linking LRK-NS-GK roughly in the north–south direction on the west flank of the Cambay Basin. Towards the east, another high fluoride (1.5–4 ppm) belt (QQ') within the Cambay Basin can also be seen. Farther east, there are several small patches with fluoride concentrations greater than 1.5 ppm aligned linearly in a belt (RR') roughly parallel to the Aravallis. Another belt of high fluoride concentration is in E–W direction linking Nalsarovar region to thermal springs of Lasundra (La) and Tuwa (Tu). The fluoride concentrations are high (4–8 ppm) in this belt also.

A plot of fluoride concentration in groundwater samples vs. depth (bgl) of the sampled wells in the NGC region is shown in Fig. 4a. It is seen that in the LRK-NS-GK low lying tract, groundwater at shallow depths indeed have very high fluoride concentrations. Elsewhere in the region, no apparent relationship between the fluoride concentration and depth (bgl) can be discerned. In several cases high fluoride concentrations are found in the shallow dug wells and low fluoride concentrations in deep tubewells and vice versa. This observation is contrary to the conventional understanding that deeper, confined groundwater has high fluoride due to longer residence

DOI 10.1007/s10040-004-0389-2

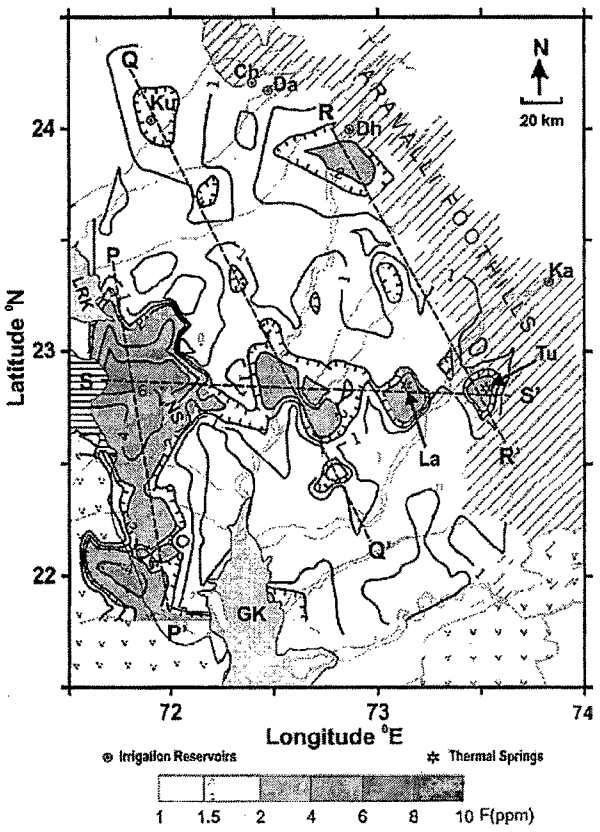

Fig. 3 Contour plot of fluoride concentration in groundwater from NGC region. Patches of high fluoride concentration (>1.5 ppm) appear aligned along four linear belts (PP', QQ', RR', SS') separated by low fluoride areas. Acronyms for locations are: *Ch* Chadotar; *Ku* Kuwarva; *Da* Dantiwada; *Dh* Dharoi; *Ka* Kadana; *La* Lasundra; *Tu* Tuwa

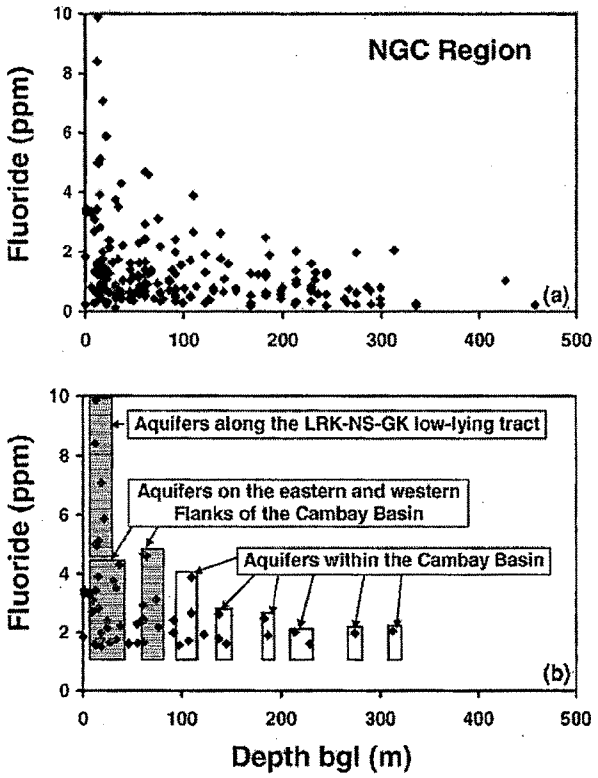

Fig. 4 a Groundwater fluoride concentration versus depth 'bgl' of tubewells in the NGC region. **b** Samples with fluoride concentration <1.5 ppm are filtered out from (*a*). Fluoride rich aquifers can be identified at certain depth zones within Cambay Basin

Table 1 Sub-aquifer zones with depth having excessive fluoride in the Cambay Basin

Zone	Depth range (m)	Zone	Depth range (m)
I	<40	V	180–190
II	50–75	VI	210–230
III	90–110	VII	~275
IV	135–145	VIII	~310

time, hence longer reaction time with the aquifer material to dissolve fluoride (Ramakrishnan 1998). A similar plot, but only for the samples with >1.5 ppm of fluoride from the same dataset, is shown in Fig. 4b. This leads to identification of fluoride rich sub-aquifers with certain depth zones (Table 1) in the Cambay Basin. This follows from Fig. 2, wherein it was shown that by measuring depths bgl, nearly the same sub-aquifer is encountered at different locations within the Cambay Basin.

Most fluoride rich handpumps and tubewells up to the depth of 40 m are located on the west flank of Cambay Basin where aquifers are comprised either of fluvio-marine sediments deposited in the low-lying tract linking LRK-NS-GK or further west in the Mesozoic sandstones. Tubewells shallower than ~40 m and with fluoride concentration <1.5 ppm are mainly located on the east flank of Cambay Basin. Tubewells tapping the depth zones of 53–76 m and yielding groundwater with >1.5 ppm fluoride are located on both east flank and west flank of the Cambay Basin.

All fluoride rich tubewells ranging in depth from 90–300 m are located within the Cambay Basin, limited only to certain depth zones as above. It is hypothesised that if these sub-aquifers are tapped by a particular tubewell, which also taps other sub-aquifers, the fluoride concentration in groundwater exploited from the tubewell is likely to be relatively higher.

To verify this hypothesis, a tubewell (A) in Chadotar village (Ch) and four other tubewells (B, C, D, E) in the vicinity of each other in Kuwarva village (Ku) ~50 km from the village of Chadotar (Fig. 3) were examined for their fluoride content and the depth (bgl) of aquifers tapped (Fig. 5). It is seen that the shallowest (63 m). tubewell-A with fluoride content of 0.9 ppm, taps the fluoride rich zone-II. Tubewell-B taps fluoride rich zones-III and -IV and has the highest fluoride concentration of 2.2 ppm. Tubewell-C taps only one fluoride rich zone-III and its fluoride content is 1.9 ppm. Tubewell-D taps three

DOI 10.1007/s10040-004-0389-2

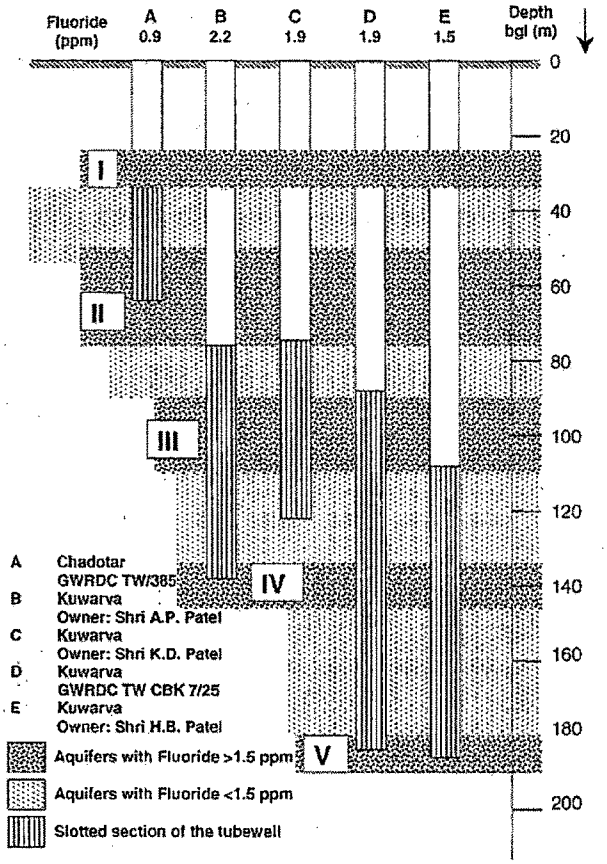

Fig. 5 A comparison of fluoride content of five tubewells with their tapped aquifers. The shallowest tubewell (*A*), taps the fluoride rich Zone II and has the lowest fluoride content. Tubewells *B*, *C* and *D* tap fluoride rich Zone III and have higher fluoride content of ~2 ppm. The deepest tubewell *E*, which taps aquifers from depth zones *IV* and *V*, has comparatively lower fluoride content of 1.5 ppm. It is seen that among these high fluoride zones highest fluoride is contributed by zone *III*

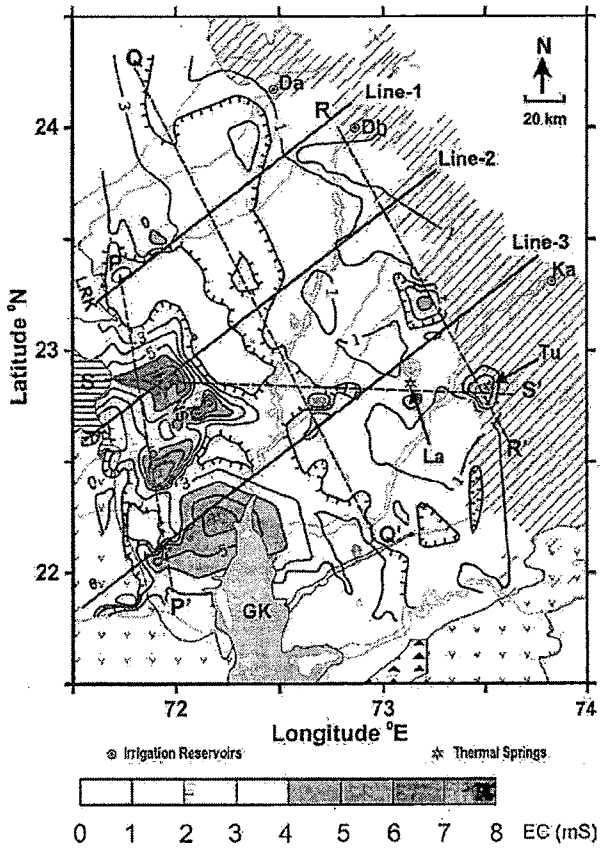

Fig. 6 Contour plot of EC of groundwater from NGC region. Areas of high EC overlap in general with areas of high fluoride shown in Fig. 3. Acronyms for locations are: *Da* Dantiwada; *Dh* Dharoi; *Ka* Kadana; *La* Lasundra; *Tu* Tuwa

fluoride rich zones (III, IV and V) and fluoride concentration of groundwater from it is 1.9 ppm. Tubewell-E is the deepest tubewell (185 m) and taps only two fluoride rich zones (IV and V). Its fluoride content is 1.5 ppm. It is seen that depth zones-III and -IV provide maximum fluoride input to the water pumped from the concerned tubewells. Depth zone-V has relatively low fluoride content and acts as a diluter in case of tubewells-D and -E.

A contour map of EC of groundwater samples is shown in Fig. 6. The EC values range from 0.3–8 mS, with values >5 mS in the LRK-NS-GK belt and lowest values in isolated pockets along the Aravalli foothills. In general, the areas with high EC overlap with the areas having high fluoride concentrations (Fig. 2). However, a patch of >3 mS in the NW corner of the study area has lower fluoride concentration. Another patch of ~1 mS around 24°N along the Aravalli foothills on the other hand has high fluoride concentration. In spite of these differences, it can be seen from Fig. 6 that high EC regions are approximately aligned along the same linear belts PP', QQ', RR', SS' showing high fluoride concentrations. The central (QQ') belt of both high fluoride concentration and EC is flanked on either side by belts of relatively low values. This is also seen in Fig. 7 that shows variation in both EC and Fluoride concentrations along four lines (lines 1–3 approximately NE–SW and SS' approximately E–W). Some westward displacement of the high EC region along line-3 is also noticed.

A contour plot of radiocarbon ages from Agarwal et al. (personal communication) is reproduced in Fig. 8. The radiocarbon ages are based on total dissolved carbonate precipitated from groundwater pumped from all the subaquifers tapped by the sampled tubewells. These, therefore represent the composite ages of groundwater in the regional aquifer system. The groundwater ages are seen to progressively increase in a W-SW direction from a recharge zone in the Aravalli foothills. This implies that the composite residence time of groundwater increases progressively in a W-SW direction.

DOI 10.1007/s10040-004-0389-2

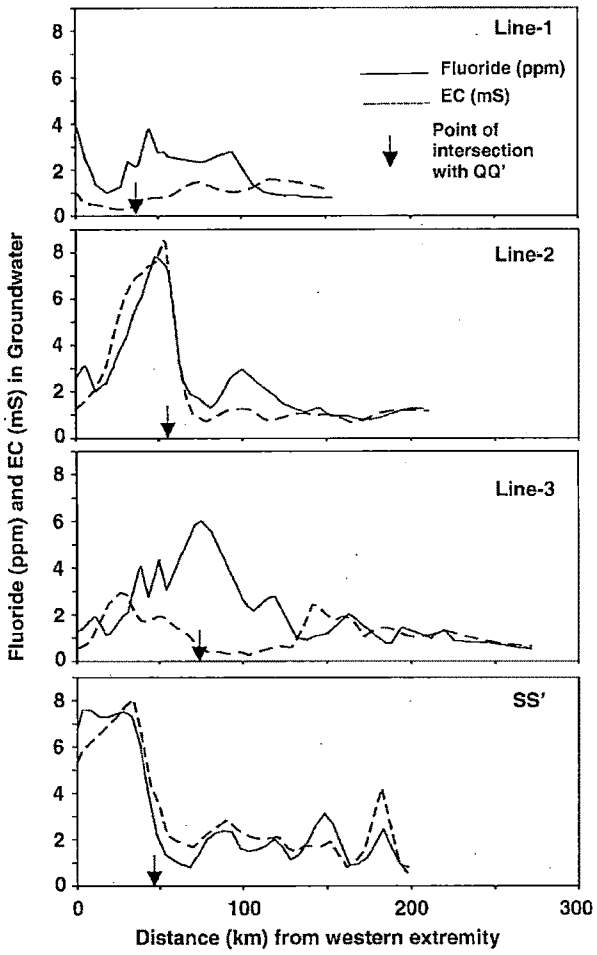

Fig. 7 Variation of fluoride and EC of groundwater along four lines shown in Fig. 6. The distances are from the western extremity of each line and the position of intersection with QQ' is marked by an *arrow*

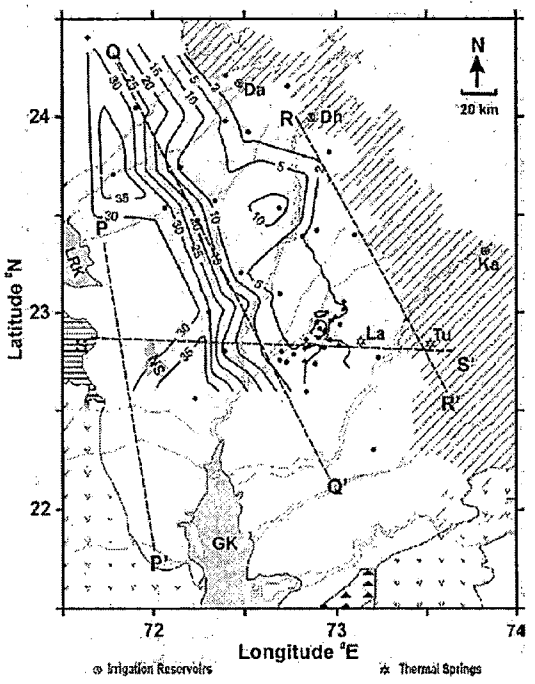

Fig. 8 Contour plot of radiocarbon ages of groundwater in the regional aquifer system from NGC region (reproduced from Agarwal et al., personal communication). The ages are seen to progressively increase away from the recharge zone in Aravalli foothills. The age of the high Fluoride, high EC groundwater belt QQ' is ~20 ka, i.e., around LGM. This is identified as the arid climatic phase in the study area. Acronyms for locations are: *Da* Dantiwada; *Dh* Dharoi; *Ka* Kadana; *La* Lasundra; *Tu* Tuwa

Discussion

From the global map of endemic fluorosis available at UNICEF website (http://www.unicef.org/programme/wes/info/fl_map.gif) it is seen that most of the affected regions have an arid to semiarid climate. Within India, fluoride rich groundwaters are found in the dry parts, especially Rajasthan, Gujarat and interior parts of the southern peninsula characterised by episodic rainfall separated by extended dry periods (Agrawal et al. 1997; Vasavada 1998; Jacks et al. 1993). Fluoride poisoning is also reported from the dry climatic regime (Yong and Hua 1991) in North China.

Although aridity of climate in general seems to be the primary reason for the origin of high fluoride globally, several processes, namely, dissolution of fluoride bearing minerals, ion exchange and evaporative concentration can locally account for high fluoride concentration in groundwater. With this in mind, occurrence of high fluoride in the following three sub-regions of the study area was examined.

1. West flank of Cambay Basin in the low-lying tract
2. East flank of Cambay Basin
3. The Cambay Basin

Groundwaters in the low-lying LRK-NS-GK tract have >5 ppm fluoride (Fig. 3) at a shallow depth of up to 15 m. This area is relatively flat, receives low rainfall (~500 mm a^{-1}) and is the zone of convergence of surface gradients wherein surface flow both from Aravallis (in the NE) and Saurashtra (in the West) accumulates. These factors lead to evaporative enrichment of fluoride and other salts along this tract. The deeper confined aquifers in this belt are at the farthest end of the regional aquifer system of Late Quaternary origin (Prasad and Gupta 1999) and do not necessarily have high fluoride or EC. In terms of fluoride distribution these exhibit similar characteristics as sub-aquifers in the Cambay Basin as described later.

Groundwaters on the east flank of Cambay Basin, in general, have lower fluoride concentrations. However, there are patches of fluoride concentration >1.5 ppm located along the rock-alluvium contact zone (RR') in the Aravalli foothills (Fig. 3). This sub-region, forming a recharge area of the regional aquifer system in the NGC,

DOI 10.1007/s10040-004-0389-2

receives fresh rainwater annually. The presence of high fluoride (with low EC) patches in this sub-region, therefore, suggests preferential dissolution of fluoride bearing minerals. The proterozoic rocks of the Kumbhalgarh group, Ambaji Granites and Gneisses of Delhi super group, Lunawada group and Godhra granite are exposed in the vicinity of the high fluoride-bearing groundwater patches. These rocks are characterized by mineralogical assemblages of quartz, K-feldspar, plagioclase, biotite, amphiboles, fluorite and apatite (Choudhary 1984). These granites are invaded by dykes of pegmatite and also xenoliths of amphibolite. Both pegmatites and amphibolites have high concentrations of fluoride. It is likely that these rocks could be providing higher fluoride to groundwater during weathering. Koritnig (1951) suggested that fluoride is leached in the initial stages of weathering of granite massifs. Deshmukh et al. (1995) suggested that fluoride is particularly leached out rapidly from micas. Preferential dissolution of fluoride can, however, explain high fluoride patches only in the Aravalli foothills and not within the Cambay Basin wherein sediments eroded from diverse rock types in Aravalli have been transported and deposited by several rivers (Prasad et al. 1997).

With the general understanding that groundwater in deeper aquifers contains relatively long resident water; confinement of high fluoride concentrations to certain sub-aquifer zones (Figs. 3, 4b and 5) within the Cambay Basin implies that the contact time of groundwater with the aquifer material is not the principal factor governing the origin of high fluoride in the Cambay Basin. This is also supported by the results of radiocarbon dating of groundwater samples from this region. As seen in Fig. 8, groundwater radiocarbon ages increase progressively in the W-SW direction away from the recharge area in the Aravalli foothills. If the fluoride dissolution were proportional to groundwater residence time, the alternation of high and low fluoride concentration belts as seen in Fig. 3 can not be explained.

Another hypothesis involved leakage of fluoride rich pore water from the intervening clay rich aquitard layers induced by excessive exploitation of groundwater and a resultant decrease in piezometric level. This was examined by comparing the geographical distribution of high fluoride regions with regions of high groundwater withdrawal. It was found that the two do not overlap. The high groundwater withdrawal areas were actually found to overlap the low fluoride concentration areas, i.e., between PP' and QQ', and QQ' and RR'. Roughly, these are also areas of the highest decline in piezometric level during the last few decades. This ruled out leakage of fluoride rich pore-fluid from clay rich horizons as a primary source of high fluoride concentration in the Cambay Basin.

It is thus seen that the various hypothesis on the origin of fluoride—long residence time of groundwater, sediments containing fluoride bearing minerals in the aquifer material and leakage of fluoride from clay rich aquitard horizons in response to excessive pumping—cannot explain the observed geographical distribution of fluoride in the Cambay Basin.

It can be seen by comparing Figs. 3 and 8 that the central belt of high fluoride concentration within Cambay Basin corresponds to a groundwater age of ~20 ka which is globally know to be the maxima of the last glacial period and an arid period in the climatic history of the study area. Prasad and Gupta (1999) have reported the presence of a thick gypsum layer dated by interpolation in luminescence ages to be ~20–30 ka in the Nalsarovar core, which represents periods of extreme aridity. Based on the crystallinity index of illite, Pandarinath et al. (1999b) have also indicated aridity for this layer. Regional evidences of aridity have also been reported in the form of dune building activity which began ~20 ka in N. Gujarat (Wasson et al. 1983). The evidence of increased aridity ~20 ka and the dating of the high fluoride/high EC belt QQ' to this period suggest that the dated groundwater was recharged during a relatively arid climatic phase and has since moved to its present location through subsurface transport.

In the following, combining the explanations given for the three sub regions of the study area, a general hydrologic model to explain the high fluoride concentration (>1.5 ppm) in groundwater of the NGC region is presented. In this model general aridity of the region together with presence of granitic rocks with pegmatites, amphibolites and other minerals susceptible to preferential dissolution of fluoride in the Aravalli Hill ranges and/or sediments derived there from make the region naturally prone to increased fluoride concentration in groundwater. Superposed on to this general hydrologic model, local imprints of increased/decreased aridity and/or other applicable factors can be seen.

During the arid regime, the dry deposition of dust is also expected to increase. The normal fluoride content in the atmospheric air is reported between 0.01–0.4 $\mu g/m^3$ (Bowen 1966). Average fluoride content of precipitation varies from almost nil to 0.089 mg/L (Sugawara 1967). However, fortnightly accumulated precipitation samples from selected irrigation reservoirs (Fig. 3) during the early part (June) of the 1999 rainy season, showed a fluoride content of 0.90 ppm at Dantiwada (Da), 0.60 ppm at Dharoi (Dh) in North Gujarat, 0.34 ppm at Kadana (Ka) in East Gujarat, 0.35 ppm at Bhadar (21.08^0N; 70.77^0E) in Saurashtra, and 0.26 ppm at Ukai (21.29^0N; 72.65^0E) in South Gujarat. The latter two locations are just outside the study area shown in Fig. 3. These values of fluoride in local precipitation matched the general trend of decreasing aridity from Dantiwada to Ukai. Although average fluoride concentration in seasonal precipitation at these locations was ~ 0.1 ppm, high values in June precipitation suggest significant input of fluoride along with the dust. This further suggests that during an arid climate with an intense wind regime, dry precipitation can be a significant source of salts including fluoride. Coupled with high evaporation, both fluoride and EC will tend to be high in the groundwater recharged in the naturally fluoride prone region such as the NGC. This is manifested in the form of

DOI 10.1007/s10040-004-0389-2

a high fluoride and EC in the LRK-NS-GK belt on the west flank of the Cambay Basin, where not only is the rainfall lowest (~500 mm a^{-1}), but due to it's being a regional depression, the runoff from surrounding regions accumulates, evaporates and contributes to shallow groundwater. Corollary to this is that relatively lower aridity on the east flank (rainfall ~900 mm a^{-1}) together with low surface retention time due to high ground slope results in lower EC and fluoride in groundwater except where pockets of fluoride rich rocks exist locally and/or thermal waters are vented. In such regions there will be little correspondence between EC and fluoride concentrations. The aquifers in the main Cambay Basin are largely confined with recharge area in the foothills of Aravallies. These aquifers receive little direct recharge locally except in the recharge area. But, groundwater in these aquifers will reflect the fluoride and EC in the recharged groundwater of the past at different distances from the recharge area. Relatively high EC and fluoride concentrations will be seen in groundwater recharged in relatively arid climatic phases and low EC and fluoride in relatively wet phases. This is actually observed in the Cambay Basin where groundwater recharged in an arid phase ~ 20 ka shows high EC and fluoride concentration (along QQ'). The low fluoride and EC areas on either side represent groundwater recharged during preceding and succeeding wetter phases.

The east–west belt SS' approximately linking the Nalsarovar on west flank with thermal springs (~60 °C) of Lasundra (La) and Tuwa (Tu) on the east flank also showed both high fluoride and EC (Figs. 3, 4). This is possibly due to increased rock-water interaction at elevated temperature (Chandrasekharam and Antu 1995) and/or scavenging from the larger volume during hydrothermal circulation (Minissale et al. 2000; Gupta and Deshpande 2003). Since Nalsarovar is the lowest elevation, it is possible that a constant venting of thermal fluids with high EC and fluoride have always been contributed to the groundwater flow streams linking Lasundra and Tuwa in the recharge area to Nalsarovar. This continuous venting of thermal fluids is superposed on the palaeoclimatic effects to give the SS' belt of high fluoride and EC.

The observation that in Cambay Basin, only certain sub-aquifer zones have high fluoride concentrations still must be explained (Figs. 4b and 5). It is possible to speculate that these layers represent small variations in the sediment mineralogy deposited at different times during the Late Quaternary during which the entire region was receiving sediments from the east and evolving (Prasad and Gupta 1999).

Summary and conclusions

Geographical distribution of fluoride in groundwaters of the Cambay region is presented. Areas with high fluoride have been identified and possible causes of excessive fluoride have been investigated. From the contour map of fluoride (Fig. 3), it is seen that patches of fluoride concentration (>1.5 ppm) are aligned along certain linear belts (PP', QQ', RR', SS'). The areas with high fluoride content in groundwater in general overlap areas of high EC (Fig. 6), although all patches of high fluoride along the Aravalli foothills (RR') are not overlapped by high EC. These are explained by preferential dissolution of fluoride bearing minerals from certain rocks in the Aravallis.

The low lying LRK-NS-GK belt has the highest fluoride concentrations in the study area due to high evaporation of stagnant water converging from both the Saurashtra in the west and Aravallis in the east. Within the Cambay Basin, there are certain depth zones where sub-aquifers contain groundwater with high fluoride (Fig. 4). It is shown that tapping of such aquifers results in groundwater with higher fluoride content (Fig. 5).

It is shown that low fluoride and EC areas separate the high fluoride and EC belts running parallel to the Aravalli foothills. A groundwater radiocarbon age of (~20 ka) for the central (QQ') high fluoride and EC belt is indicated. This suggests the groundwater corresponding to this belt may have been recharged during the global climatic phase of last glacial maxima (LGM). Earlier studies have indicated that this was an arid phase (compared to the present) in this part of the world. Taking a cue from the present day distribution of high fluoride in the arid regions, the high fluoride and EC of water in the Cambay Basin have been hypothesised to have originated during the past climatically arid phases.

In this model, the general aridity of the region together with presence of granitic rocks with pegmatites, amphibolites and other fluoride bearing minerals, susceptible to preferential dissolution (and their sedimentary derivatives), make the region naturally prone to increased fluoride concentrations in groundwater. As a result, enhanced groundwater fluoride concentrations are seen in shallow, relatively young ground waters, in more arid parts and/or those parts of the region where specific local factors such as accumulation and evaporative enrichment of runoff, presence of fluoride bearing minerals and hydrothermal influx operate. In deeper confined aquifers enhanced fluoride is observed where ground waters recharged during past periods of enhanced aridity ~20 ka (last glacial maxima) are being exploited. There may have been other minor periods of aridity but their signatures appear to have been obliterated by dispersion and mixing during regional groundwater flow.

The westward flowing groundwater acquired its fluoride content from the prevailing fluoride content in the recharge area in the past and the model shows the influence of varying past aridity/wet conditions at the time of recharge. The confinement of high fluoride concentrations in specific sub-aquifer intervals within Cambay Basin as shown in Figs. 4b and 5, though apparently convincing, has been verified only in a small area around Chadotar and Kuwarva (Fig. 5). Given the uncertainty in regionally correlating the sub-aquifer zones and the fact that the entire region has evolved during Late Quaternary through sediments from the east, the observed confine-

DOI 10.1007/s10040-004-0389-2

ment is explained within the above general hydrologic model as due to variations in the sediment mineralogy (including clay content) deposited at different times during Late Quaternary.

The enhanced EC and fluoride concentrations in the groundwater flow streams linking thermal springs of Lasundra and Tuwa in the recharge area to the Nalsarovar along the SS' belt, are explained as due to superposition on the above general hydrologic model of the constant venting of thermal fluids into the groundwater of the flow stream.

This study has indicated that exploitation of deeper groundwater per se is not responsible for origin of high fluoride concentration in groundwater of the NGC region. Although, the problem of high fluoride cropped up within the last few decades, its origin involved prevalence of a more arid climate approximately 20 ka before present, a period globally known as the last glacial maxima. Apparently recent appearance of high fluoride in groundwater in parts of the study area is linked to recent exploitation of groundwater recharged during the past arid climatic phases. This study has helped in identifying certain fluoride rich sub-aquifer zones and the geographical area where they exist, indicating thereby that if during construction of tubewells, these zones are sealed, it should be possible to avoid high fluoride groundwater.

Acknowledgement This study forms a part of a research project entitled "Estimation of Natural and Artificial Groundwater Recharge Using Environmental, Chemical and Isotopic Tracers and Development of Mathematical Models of Regional Aquifer Systems in North Gujarat". We thank Gujarat Water Resources Development Corporation Ltd., Gandhinagar (GWRDC) for sponsoring this project and sharing important dataset of elevation and groundwater withdrawal for NGC region. Several colleagues from PRL have helped us in this study. Dr. M. G. Yadava provided the radiocarbon ages for groundwater samples. Mrs. Vasanti Somayajulu analysed the fluoride concentration and EC of groundwater samples. Their contribution is acknowledged with thanks. Mr. M.H Patel helped in field and various laboratory operations.

References

Agrawal V, Vaish AK, Vaish P (1997) Groundwater quality: focus on fluoride and fluorosis in Rajasthan. Curr Sci 73(9):743–746

BIS (1990) Drinking water specifications, IS:10500. Bureau of Indian Standards, New Delhi

Bowen HJM (1966) Trace elements in biochemistry. Academic Press, New York

Chandrasekharam D, Antu MC (1995) Geochemistry of Tattapani thermal springs, Madhyapradesh, India: field and experimental investigations. Geothermics 24(4):553–559

Choudhary AK (1984) Pre-Cambrian geochronology of Rajasthan, western India. PhD Thesis, Physical Research Laboratory, Ahmedabad, India

Deshmukh AN, Wadaskar PM, Malpe DB (1995) Fluorine in environment: a review. Gondwana Geol Mag 9:1–20

Gupta SK, Deshpande, RD (1998) Depleting groundwater levels and increasing fluoride concentration in villages of Mehsana District, Gujarat, India: cost to economy and health. Water Resources Research Foundation (WRRF), PRL, Ahmedabad, 74 pp

Gupta SK, Deshpande RD (2003) Origin of groundwater helium and temperature anomalies in the Cambay region of Gujarat, India. Chem Geol 198:33–46

Handa BK (1975) Geochemistry and genesis of fluoride containing groundwaters in India. Ground Water 13:275–281

Jacks G, Rajagopalan K, Alveteg T, Jonsson M (1993) Genesis of high F groundwaters, southern India. Appl Geochem 2:241–244

Koritnig S (1951) Ein Beitrag zur Geochemie des Fluor (A contribution to the geochemisty of fluorine). Geochim Cosmochim Acta 1:89

Merh SS (1995) Geology of Gujarat. Geol Soc India, Bangaore, 220 pp

Minissale A, Vaselli O, Chandrasekharam D, Magro G, Tassi F, Casiglia A (2000) Origin and evolution of 'intracratonic' thermal fluids from central-western peninsular India. Earth Planet Sci Lett 181:377–397

Pandarinath K, Prasad S, Deshpande RD, Gupta SK (1999a) Late Quaternary sediments from Nal Sarovar, Gujarat, India: distribution and provenance. Earth Planet Sci 108(2):107–116

Pandarinath K, Prasad S, Gupta SK (1999b) A 75 ka record of Palaeoclimatic changes inferred from crystallinity of Illite from Nal Sarovar, western India. J Geol Soc India 54:515–522

Prasad S, Kusumgar S, Gupta SK (1997) A mid-late Holocene record of palaeoclimatic changes from Nal Sarovar: a palaeodesert margin lake in western India. J Quat Sci 12:153–159

Prasad S, Gupta SK (1999) Role of eustasy, climate and tectonics in late Quaternary evolution of Nal-Cambay region, NW India. Z Geomorph N F 43:483–504

Ramakrishnan S (1998) Groundwater. Ramakrishnan, Chennai 761 pp

Sugawara K (1967) Migration of elements through phases of the hydrosphere and atmosphere. In: AP Vinogradov (ed) Chemistry of the earth's crust, vol 2, Israel Program for Scientific Translations, Jerusalem, 501 pp

Vasavada BJ (1998) Excessive fluoride in Gujarat. a perspective plan of solution. J Indian Water Works Assoc 1998:191–198

Wasson RJ, Rajguru SN, Misra VN, Agrawal DP, Dhir RP, Singhvi AK (1983) Geomorphology, Late Quaternary stratigraphy and palaeoclimatology of the Thar dune field. Z Geomorph NF 45:117–151

WHO (1970) Fluorides and human health. World Health Organisation, Geneva

WHO (1984) Fluorine and fluorides. Environmental health Criteria 36, World Health Organisation, Geneva

Yong L, Hua ZW (1991) Environmental characteristics of regional groundwater in relation to fluoride poisoning in North China. Environ Geol Water Sci 18:3–10

DOI 10.1007/s10040-004-0389-2

ELSEVIER

Chemical Geology 198 (2003) 33–46

CHEMICAL GEOLOGY
INCLUDING
ISOTOPE GEOSCIENCE

www.elsevier.com/locate/chemgeo

Origin of groundwater helium and temperature anomalies in the Cambay region of Gujarat, India

S.K. Gupta*, R.D. Deshpande

Earth Science Division, Physical Research Laboratory, Post Box No. 4218, Navrangpura, Ahmedabad 380 009, India

Received 12 March 2002; accepted 13 November 2002

Abstract

A survey of natural helium in soil-gas and groundwater was undertaken in the Cambay region of Gujarat, India. The Cambay basin, known for high heat flow, is a graben characterised by NNW–SSE trending major fault system and successive down faulting along sympathetic faults parallel to major trendline and orthogonal faults cutting across. Several wells indicated higher than atmospheric equilibration concentration of helium, referred to as anomalous helium concentration. These wells generally had high groundwater temperature and appear to be located along basement faults in the study area, particularly on both eastern and western flanks of the Cambay basin.

Groundwater helium anomalies are explained through a conceptual model as originating largely from within the crystalline basement, through radioactive decay in the form of plumes localised by the major faults and fractures. Groundwater temperature anomalies originate due to setting up of a shallow (~ 1–2 km) depth convective circulation, again along major faults and fractures, which facilitate both upward and downward migration of groundwater. The sedimentary cover acts as a dispersive medium. Therefore, no significant helium anomalies are seen within the Cambay graben that has more than 3-km-thick sedimentary cover. It is thus seen that even though helium and groundwater have different origins, the faults and fractures in the crust can associate anomalous concentrations of helium and groundwater temperatures along themselves in a longitudinally distributed manner by providing preferred pathways for migration of helium and by facilitating establishment of convective hydrothermal circulation of groundwater.

Keywords: Groundwater; Soil-gas; Helium anomalies; Groundwater temperature; Hydrothermal circulation; Cambay basin; Gujarat; India

1. Introduction

Following the Bhuj earthquake of January 26, 2001, there has been a renewed interest in identifying active faults in western India. Most of the recent work in this direction is based on re-evaluation of seismic data combined with remote sensing and geomorphological investigations of a few selected localities. These studies in the state of Gujarat have delineated four major linear tectonic structures (Fig. 1) that converge in this region: the 'Kachchh rift zone', the 'Cambay tectonic zone', the 'Narmada Tapti tectonic zone' and the 'Kukdi–Ghod lineament zone' (Misra, 2001). Earlier, Burke and Dewey (1973) had identified the region of this convergence as a 'triple junction' comprising of the 'Cambay graben' (CG),

* Corresponding author. Tel.: +91-79-6302129; fax: +91-79-6301502.
E-mail address: skgupta@prl.ernet.in (S.K. Gupta).

0009-2541/03/$ - see front matter © 2003 Elsevier Science B.V. All rights reserved.
doi:10.1016/S0009-2541(02)00422-9

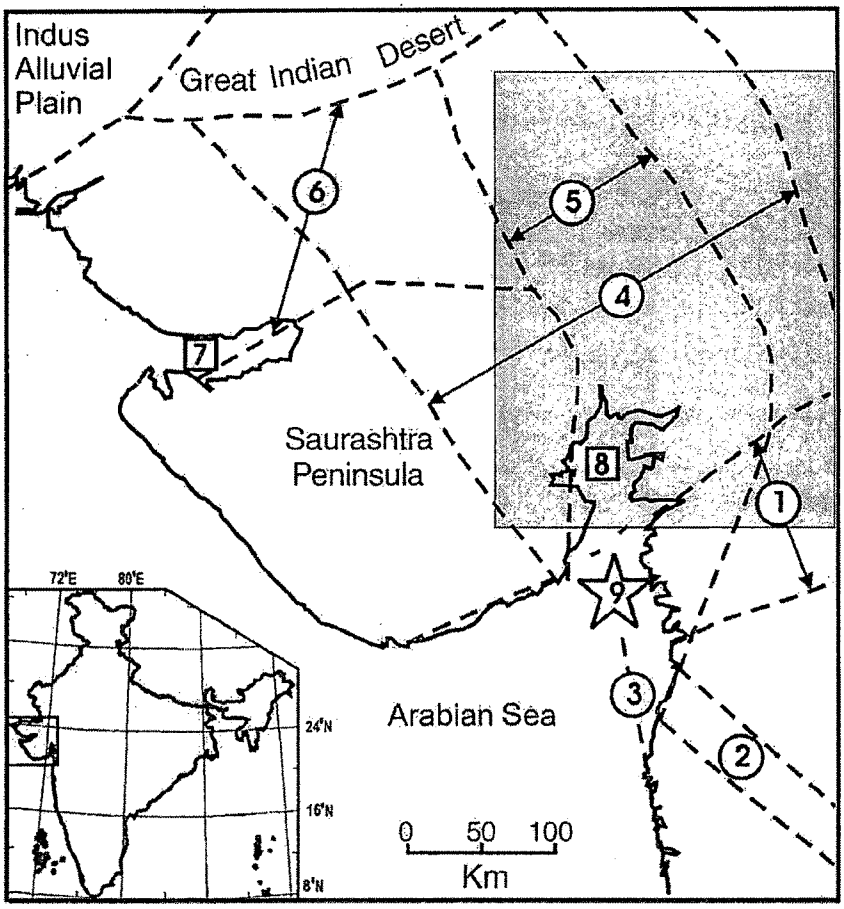

Fig. 1. Tectonic framework of the Gujarat State in western India showing major linear tectonic structures based on Burke and Dewey (1973), Biswas (1987) and Misra (1981, 2001). The names of various structural elements are as follows: (1) Narmada Tapti tectonic zone; (2) Kukdi–Ghod lineament zone; (3) West Coast fault; (4) Cambay structure; (5) Cambay graben; (6) Kachchh rift; (7) Gulf of Kachchh; (8) Gulf of Khambhat; and (9) triple junction of 1, 2 and 5. The study area is marked in grey shade.

the 'Narmada Tapti (NT) rift system' and the 'West Coast (WC) fault' in the Gulf of Cambay (also known as Gulf of Khambhat). Repeated block faulting along these tectonic structures has broken the lithosphere into several blocks separated by major or minor faults running parallel and orthogonal to each other. The intersecting network of faults has given rise to such a tectonic configuration that movement of any lithospheric block along a particular fault is propagated along other faults. Many of these faults and fissures within these major structures seem to extend to the lower lithosphere (Ravi Shankar, 1991; 1995) and several hot springs lie along them indicating hydrothermal circulation. It has long been recognised (Golubev et al., 1975; Dikum et al., 1975) that helium and radon produced by radioactive decay of U and Th in rocks and minerals get liberated during convective circulation, rock dilation and fracturing. Since the Cambay region is known to be tectonically active, anomalously high amounts of these gases may be escaping the crust from above the active faults.

The gases, before escaping to the atmosphere, must pass through the omnipresent groundwater zone. Hence, a survey of helium and radon in groundwater can potentially help to identify regions of active fault zones, hydrothermal circulation and fluid transfer through the crust, in addition to zones of radioactive mineral accumulation. Because of its short half-life (3.84 days), radon may not be so useful in identifying deep structures. Helium, on the other hand, through

its characteristic of having higher isotopic ratio of $^3He/^4He$ in mantle fluids ($\sim 10^{-6}$) in comparison to $<10^{-7}$ in crust, can also help to identify regions of mantle fluid transfer.

With the above perspective, a programme of groundwater and soil-gas helium survey in parts of the Cambay basin was initiated. Results of this investigation are presented in this paper.

As part of the investigations, a simple standardised procedure was also developed for sample collection, storage and measurement of helium concentrations in soil-gas and groundwater samples using commercially available helium leak detector.

2. Sample collection procedure

2.1. Soil-gas samples

Soil-gas samples are collected from 1 m below the ground level. A 1.2-m-long copper tube ($\Phi = 5$ mm) with 15-cm-long perforated wall at its lower end is inserted into the soil. The ground near the upper end of the copper tube is then hammered and watered to effectively seal the hole from direct contact with atmosphere. The upper end of the copper tube is connected to a hand-operated suction pump by a Tygon tube. The pump is operated sufficiently long to ensure removal of atmosphere/soil-gas mixture from the copper tube and the surrounding soil-gas. The upper end of Tygon tube is then closed using a three-way stopcock for accumulating soil-gas inside the tubes. After about 12 h, the hypodermic needle fitted to the third end of the stopcock is made to pierce the rubber stopper of a 1.2-l pre-evacuated soda-lime glass bottle for soil-gas sample collection. Withdrawal of the hypodermic needle from rubber stopper effectively seals the soil-gas sample.

2.2. Groundwater samples

Groundwater samples are collected directly from the pump outlet (that has been pumping for some time prior to sampling) using PVC tubing ($\Phi = 8$ mm) to divert the water flow and to transfer the same to the bottom of a 1.2-l soda-lime glass sample bottle. After allowing the sample bottle to overflow for a while and when no bubbles are visually seen, the PVC tube is withdrawn and the sample volume is reduced to a pre-marked position leaving 98 ml of air in the bottle above water surface. The bottle is then sealed within few seconds with rubber stopper and triple aluminium protection cap using hand-operated crimping tool. Wherever pumping facility does not exist (e.g. a dug well), the sample is collected by immersing an inverted (mouth at lower end) empty 2-l glass bottle inside the water with the help of a rope and weight attached to it. After the bottle reaches the required sampling depth, it is reverted for water sampling. The collected sample is then transferred to a 1.2-l soda-lime bottle and sealed as above. The bottles with water sample are stored in inverted position to minimise any loss of helium from the stopper. The air in the bottle is equilibrated with water by shaking for sometime before measurement of helium concentration following the procedure outlined subsequently.

3. Sample storage

Helium permeates readily through many materials, and for this reason, it is important to carefully choose the containers in which the soil-gas and groundwater samples intended for later helium analysis are to be stored. The optimal material for such containers is oxygen-free high conductivity (OFHC) copper tubing in which samples for helium analyses are sealed by crimping at either ends (Craig and Lupton, 1976; Lupton et al., 1977). Gupta et al. (1990) showed that loss of dissolved helium from thick-walled soda-lime glass bottles with conventional laboratory rubber stopper was less than 3% during a storage period of 24 h. This storage method, however, is not suited for soil-gas and for equilibration measurement techniques of helium. Therefore, thick (3 mm)-walled soda-lime glass bottles with bromobutyl synthetic rubber stopper manufactured according to guidelines of U.S. Pharmacopoeia standard II (USP Std-II) and secured by additional triple aluminium cap fixed by hand-held crimping tool in the field are used for sample collection and storage. The synthetic rubber stopper is easily pierced by hypodermic needle and seals effectively when the needle is withdrawn. Each bottle used for sampling is pre-checked for vacuum retention by evacuating the same and measuring air pressure inside after 10 days. Bottles showing pressure >2 Torr are

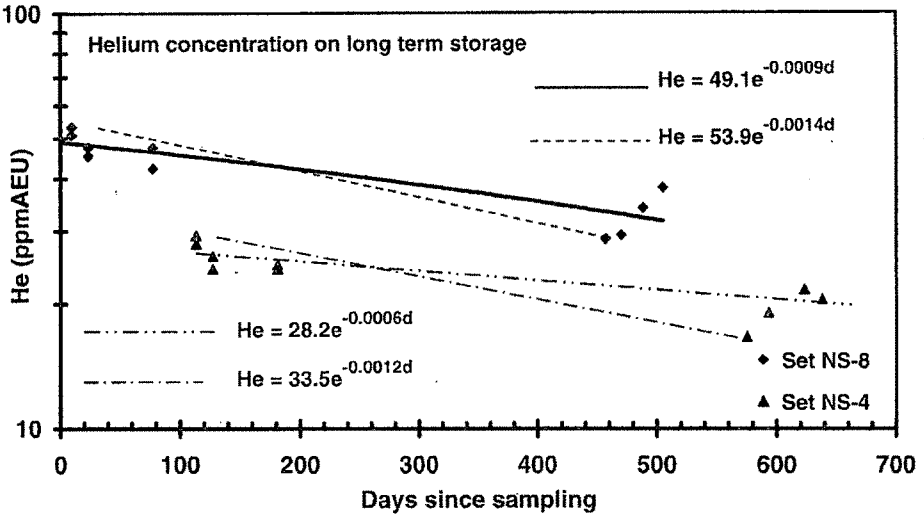

Fig. 2. Residual helium concentrations on long-term storage in soda-lime glass sampling bottles with bromobutyl rubber stopper and triple aluminium protection seal. Two separate sets of multiple samples were collected from two different sources. Individual samples were analysed subsequently at different times up to 20 months after the collection. The maximum observed loss of helium is given by the steepest line on this log-linear plot which corresponds to a loss of <0.15% per day. The average loss obtained by averaging the rates from the two best-fit lines is, however, 0.075% per day.

rejected. To test the preservation of samples against leakage and diffusion of helium, two sets of 10 water samples each were simultaneously collected from the same source following the procedure described previously. Helium concentrations in these sets of sample bottles were measured over a period of 20 months. The measured concentrations are then plotted on a log-linear plot (Fig. 2). It is assumed that the loss during storage is a first-order process, like radioactive decay, depending on the concentration. The slope of the steepest line through any particular set of data points corresponds to the highest loss rate and the best-fit line corresponds to the average loss rate. It is seen from Fig. 2 that the maximum loss of helium during storage is given by the line ($He = 53.94e^{-0.0014\ day}$ for NS-8). Applying the concept of half life; a value of 495 days is obtained corresponding to 50% loss using this equation. This corresponds to a loss of <0.15% per day.

4. Measurement procedure

A helium leak detector (ALCATEL Model ASM 100 HDS) comprising of a tuned mass spectrometer for helium ions ($m/e = 4$) was used for helium measurements by connecting an inlet port to its sniffer probe. This system is in many ways similar to the one used by Friedman and Denton (1975) and Reimer (1984). Equilibrated air samples (Fig. 3a) are drawn from the head space of the bottles by piercing their rubber seal using a 20-ml syringe (Syringe-1). As the sample is drawn, an equal amount of air from another syringe (Syringe-2) enters the bottle and mixes with the sample gas. Test sample drawn in Syringe-1 is injected first into a pre-evacuated Syringe-3 by piercing the rubber septum on the inlet port and then allowed to be sucked into the leak detector through a moisture trap connected to sniffer probe (Fig. 3b). The system response, directly proportional to the helium partial pressure in the air/gas flowing through the analyser, is recorded as voltage output on a data logger and chart recorder. The measured helium concentrations are corrected for (i) volume of headspace, (ii) water volume, (iii) volume of air drawn in during analysis and (iv) duration of storage (obtained by averaging the values given by the two solid lines in Fig. 2).

Since the helium measurements were actually made on equilibrated headspace air samples, the

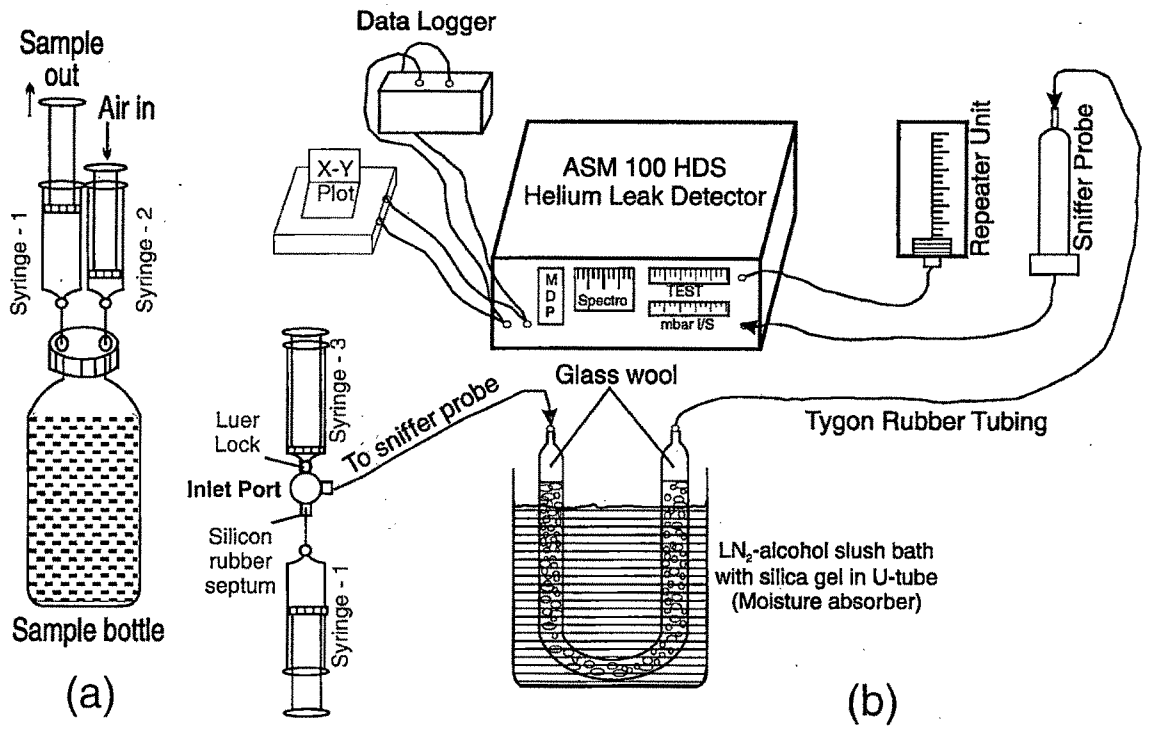

Fig. 3. Schematic diagram showing layout of (a) drawing of equilibrated air sample and (b) helium measurement through helium leak detector for water/air/gas samples.

groundwater helium concentrations can be calculated using Henry's law and the respective volumes of water and air in the sampling bottles. Dimensionless Henry's Law constant is defined as [H_x=(mass of helium in gas phase/gas phase volume)/(mass of dissolved helium/water volume), i.e. = C_g/C_w]. Using H_x=94.5 at 25 °C (Fry et al., 1995), the concentration of dissolved helium in equilibrium with air containing 5.3 ppmv helium is given by (5.6×10^{-2} ppmv). For the sake of convenience, dissolved helium concentrations are expressed in terms of Air Equilibration Units (AEU). This unit expresses helium concentration in air in equilibrium with water sample at 1 atm. Thus dissolved helium concentration of 5.6×10^{-2} ppmv is equal to 5.3 ppm AEU.

5. Calibration

The helium leak detector is calibrated using atmospheric air with He concentration of 5.3 ppmv. The standard calibration curve for the chart recorder reading (set at 10 V range) is given by the mathematical expression:

$$\mathrm{He} = \mathrm{Const}_1 \times \exp(\mathrm{Const}_2 \times D_s) \quad (1)$$

where D_s is the number of chart recorder divisions at the 10-V full-scale setting and He is the concentration of helium in ppmv.

If the chart recorder divisions are measured as deviation/difference from the atmospheric background reading, the calibration equation can be rewritten as;

$$\mathrm{He} = 5.3\exp(\mathrm{Const}_2 \times (D_s - D_{bkg})) \quad (2)$$

where $D_s - D_{bkg}$ is the difference in the chart recorder reading between the sample and the atmospheric background.

The calibration checks carried out in the study were designed to verify the combination of factory calibration and modification made in the input port and to verify the robustness of procedure specified in the previous section for helium assay in air/gas

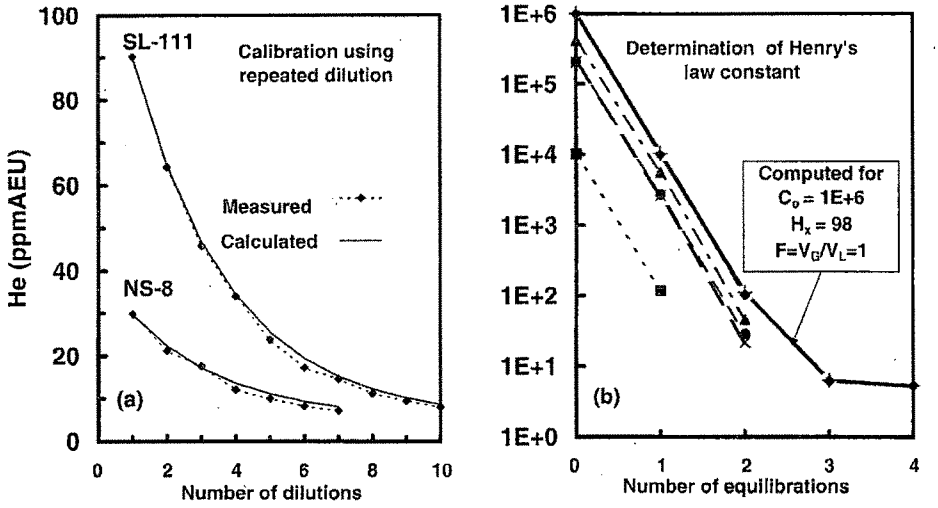

Fig. 4. (a) Comparison of measured and calculated dilution curves); (b) the results of a set of six experiments undertaken for estimation of Henry's law constant for water–helium system. The experimental values are similar to the known value of 94.5 at 20 °C (Fry et al., 1995). These experiments verify the calibration of the helium measurements and the robustness of the analytical procedure.

samples. For this purpose, we used (i) repeated dilution of an arbitrary helium concentration sample with fixed volume of atmospheric air and (ii) determination of Henry's law constant for helium.

5.1. Repeated dilution by atmospheric air

A fixed volume ($=V_A$) is drawn from the head space (volume $=V_0$) of storage bottle using a hypodermic syringe. As the sample is drawn, equal volume of atmospheric air is allowed to enter the sampling bottle through another hypodermic syringe (Fig. 3a). As a result, helium concentration in the sample being drawn varies continuously in response to dilution by atmospheric air and mixing with remaining 'mixed' sample in the bottle. If drawing of sample and dilution is repeated several times, a recursive equation as below can be obtained:

$$C_{Mn} = \frac{C_0 e^{-(n-1)f}}{f}(1 - e^{-f}) - \frac{C_A e^{-(n-1)f}}{f}(1 - e^{-f}) + C_A$$

where C_{Mn} is the measured helium concentration drawn by the hypodermic syringe after nth dilution, C_0 is the original helium concentration in volume V_0, and C_A is the helium concentration of incoming atmospheric air; $f = V_A/V_0$.

$$\text{For } C_A \ll C_0,\ C_{Mn} = \frac{C_0 e^{-(n-1)f}}{f}(1 - e^{-f})$$

Therefore,

$$\frac{C_{Mn}}{C_{M(n-1)}} = e^{-f} \quad (3)$$

Thus, the measured concentration will decrease by a factor of e^{-f} after every dilution. In our standard experiments, $V_A = 20$ ml, $V_0 = 56$ ml.

Eq. (3) can be used to experimentally check the calibration of the instrument and the entire analytical procedure, starting with air/gas sample with any arbitrary helium concentration. A graph of two separate experiments showing measured and calculated

Table 1
Reproducibility of measured helium concentration in groundwater samples

Sample location	Helium concentration (ppm AEU)		Variability (%)
	Sample-1	Sample-2	
Ranip	6.17	6.20	1
Bagodra	339.7	339.7	0
Roika	24.3	24.8	2
Tilaknagar	5.3	5.3	0

helium concentration variation involving repeated dilution with atmospheric air is given in Fig. 4a. The close matching between the measured and calculated values not only confirm the calibration of the instrument but also the correctness of the experimental procedures.

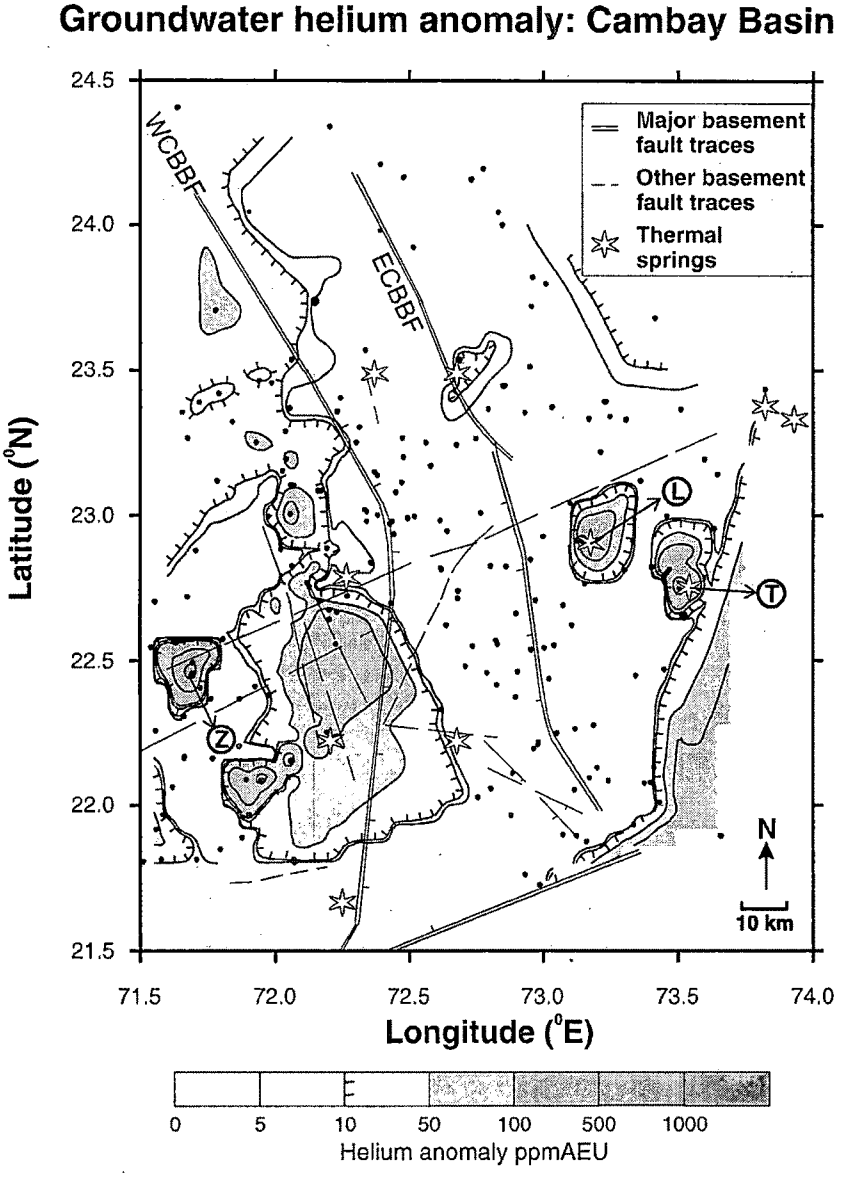

Fig. 5. The study area in the Cambay basin showing (i) contours of anomalous groundwater helium concentrations along with sampling locations; (ii) traces of major basement faults (after Mathur et al., 1968; Merh, 1995); and (iii) locations of thermal springs (after GSI, 2000). The helium anomaly contours of 510 ppm AEU run approximately along the WCBBF and almost equidistant from the groundwater recharge area along the Aravalli foothills in the NE (see Fig. 6). Very high groundwater helium anomalies are seen west of WCBBF in the SW corner where a set of intersecting orthogonal basement faults are located. These fault traces are shown by broken lines. The highest helium anomaly was observed at Zinzawadar (Z) located close to the western extremity of the longest orthogonal fault trace cutting across the Cambay basin. High groundwater helium anomalies are also seen at a few locations on the eastern flank of the Cambay basin, mostly in association with thermal springs of Lasundra (L) and Tuwa (T).

5.2. Estimation of Henry's law constant

The next step in calibration test was to estimate the Henry's law constant following the standardised measurement procedure. For nth equilibration, the relation derived for determination of Henry's law constant by repeated equilibration of atmospheric air with water containing dissolved helium is:

$$\log C_{Gn} = \log C_{G0} - n\log(1 + FH_x) \quad (4)$$

where C_{Gn} = concentration of helium in gas phase after nth equilibration; C_{G0} = original concentration of helium in gas phase; $F = V_G/V_L$ = volume of gas phase/volume of liquid phase; and H_x = Henry's law constant.

Plot of log C_{Gn} vs. n (equilibration number) would be a straight line with intercept = log C_{G0} and slope = $-\log(1 + FH_x)$.

In our experiments, while the values of C_0 were arbitrarily varied, the values of V_G and V_L were 50 ml each. Fig. 4b is a plot showing measured helium concentration in equilibrated air against the number of equilibration in several experiments involving different initial helium concentrations. The estimated average value of Henry's law constant for six sets of similar experiments is 98 against the known value of 94.5 at 25 °C (Weiss, 1971; Perry, 1984). Close matching between the different experiments and between estimated and standard value once again confirm the calibration of the total set up and the robustness of the standardised procedure for helium concentration estimation in air/water sample.

Reproducibility of helium measurements was checked by repeated analyses on a set of four samples collected at the same time in two different bottles in the concentration range of 5.3–340 ppm AEU. The results of these experiments (Table 1) show that the analytical precision is better than 5%.

6. Results of field survey

A field survey of helium in groundwater and soil-gas was undertaken in the Cambay basin (Fig. 5). The geographical coordinates of the sampling locations were determined using hand-held Geographical Positioning System (GPS) receiver (Trimble Scout GPS). Temperature of water was also measured at the time of collection.

Of the 12 soil-gas samples analysed, only 1 sample, ~ 100 m away from the thermal springs of Tuwa, showed helium concentration (7.0 ppmv) higher than the atmospheric background (5.3 ppmv). All other soil-gas samples had helium concentrations close to atmospheric value. However, many groundwater samples from the 246 analysed from the study area showed dissolved helium concentrations significantly higher (up to >200 times) than the atmospheric equilibration concentration (5.3 ppm AEU). It may be noted that reproducibility of measurements of dissolved helium concentration is better than 5% (Table 1).

Table 2
Variation of groundwater temperature and anomalous helium concentration in different emergences of thermal springs at the locations of Lasundra and Tuwa on eastern flank and some free-flowing artesian wells on the western flank of the Cambay basin

Sample no.	Temperature (°C)	Depth below ground level of the spring/well (m)	Dissolved helium anomalous concentration (ppm AEU)
On eastern flank of Cambay basin			
Location: Lasundra (22.914°N; 73.145°E)			
CBDW/8/98	51.5	6.1	186
CBDW/9/98	33.0	6.1	55
Location: Lasundra (22.918°N; 73.153°E)			
CBT/15/98	33.0	85.4	221
Location: Tuwa (22.800°N; 73.461°E)			
CBDW/18/98	61.0	0.9	137
CBDW/19/98	46.5	0.9	96
CBDW/20/98	27.5	0.9	475
Location: Tuwa (22.798°N; 73.461°E)			
CBHP/21/98	51.0	12.2	1163
On western flank of Cambay basin			
Location: Dholera (22.249°N; 72.192°E)			
CBTA/45/98	42.5	167.6	109
Location: Gundi (22.553°N; 72.227°E)			
CBTA/55/98	40.0	289.6	235
Location: Shiyala (22.702°N; 72.164°E)			
CBTA/65/98	38	274.3	73
Location: Ruhika (22.663°N; 72.231°E)			
CBTA/66/98	41	457.2	157
Location: Sarala (22.671°N; 72.201°E)			
CBTA/67/98	40	274.3	90
Location: Zinzawadar (22.452°N; 71.694°E)[a]			
CBTW/120/99	34	285.0	2843

[a] This is not a free-flowing tubewell but is included in this table because the highest dissolved groundwater helium anomaly was observed at this location.

Interpretation of groundwater helium data on regional scale may, at times, be difficult because of local scale variability, as, for example, noticed at the location of the thermal springs of Tuwa and Lasundra. At both these locations, even within a distance of 20 m, springs show different temperature and helium concentrations (Table 2).

Fig. 5 shows the contour lines of anomalous helium concentration (i.e. in excess of 5.3 ppm AEU) in groundwater samples. Traces of major basement faults

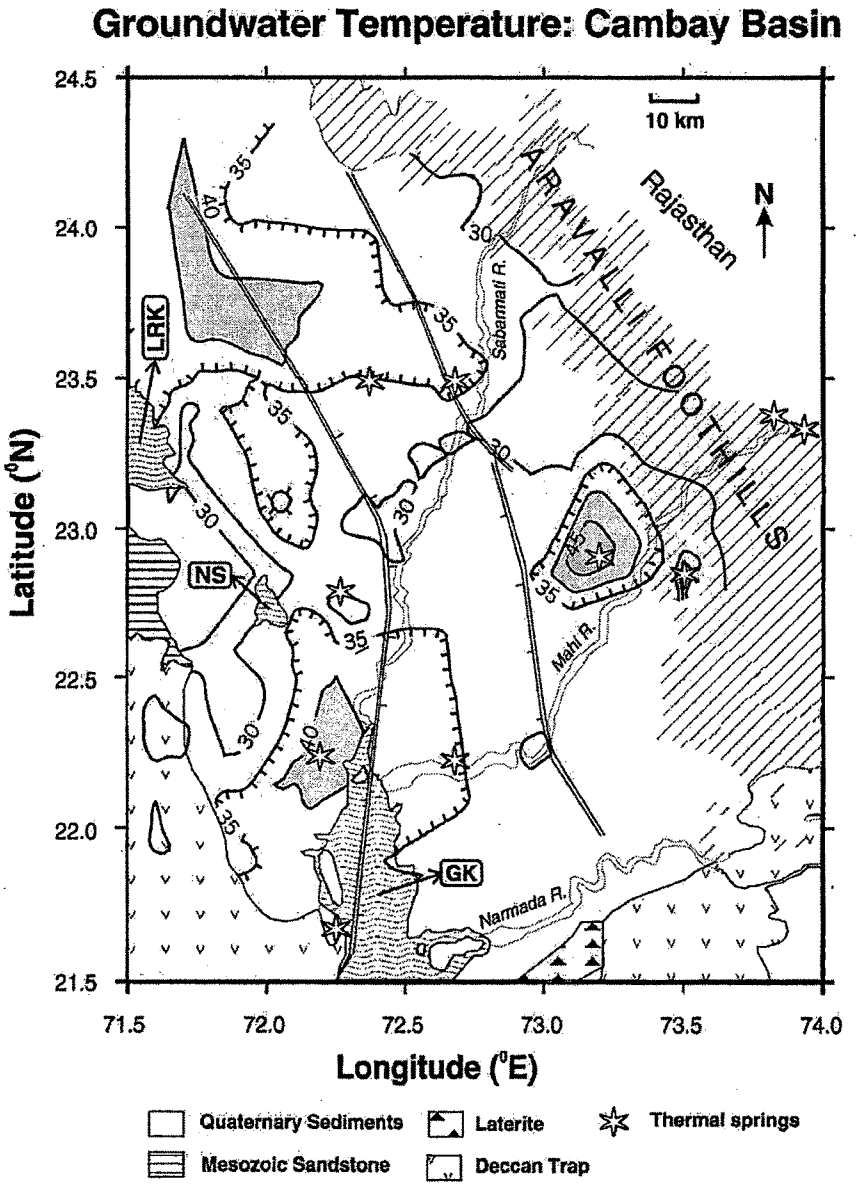

Fig. 6. Contours of groundwater temperature and locations of thermal springs (after GSI, 2000) superposed on geological map (after Merh, 1995) of the study area in the Cambay basin. The sampling locations are shown in Fig. 5. The areas with enhanced groundwater temperature (>35 °C) are associated with (a) locations of thermal springs, (b) enhanced groundwater helium (Fig. 5) except within the Cambay graben with >3 km thick sedimentary cover, and (c) the major basement faults. The region linking Little Rann of Kachchh (LRK)–Nalsarovar (NS)–Gulf of Khambhat (GK) forms the lowest elevation in the study area.

(Merh, 1995; Misra, 1981; Biswas, 1982, 1987) in the region are superposed on the contour map. As one moves eastwards from 71.5°E, a series of N–S trending step faults roughly parallel to West Cambay Basin Boundary Fault (WCBBF) have caused a progressive lowering of the Deccan Basalt, where the basaltic layer is abruptly downthrown by >3 km. The highest helium anomalies in this region are seen between 22° and 23°N (Fig. 5) on the faults running transverse to the fault traces linking the Little Rann of Kachchh–Nalsarovar–Gulf of Khambhat (LRK–NS–GK) corridor. Further north, several pockets of high helium concentration can be identified up to 24°N. Datta et al. (1980) had also noted that some artesian wells on the western flank of Cambay basin in the vicinity of the Nalsarovar (22°48′ N; 72°E) had enhanced groundwater temperature and helium. Within the CG, between WCBBF and the East Cambay Basin Boundary Fault (ECBBF), the thickness of Cenozoic sedimentary cover is >3 km (Mathur et al., 1968). The groundwater in this region is almost completely devoid of anomalous helium.

On the eastern flank of CG, highest helium anomalies are associated with the thermal springs of Lasundra and Tuwa. On this flank, another small patch of high helium concentration is seen across ECBBF along the Sabarmati River. Major concentration of anomalous helium is also seen in southern part at the extension of ECBBF along the Narmada-Son-Geofracture that confines the flow of Narmada River.

Fig. 6 shows the contours of groundwater temperature, superposed by traces of regional basement fault and geology (after Merh, 1995). Average groundwater temperature in the study area is about 30 °C. Temperatures >35 °C are generally seen associated with high helium anomalies particularly along the two flanks of the CG. Geographically, the areas with anomalous helium >5 ppm AEU tend to lie within the contours with groundwater temperature >35 °C. It is also noticed from Figs. 5 and 6 that areas of helium and temperature anomalies surround the locations of known thermal springs in this region. In fact, all three appear to be geographically related to the known positions of the basement faults in the study area. However, major areas of high groundwater temperature, not associated with groundwater helium anomalies, are seen across the CG between 23.5–24°N and 22–22.5°N. However, an association with geothermal springs is clearly seen.

7. Discussion

Minissale et al. (2000) have ascribed the high concentration of helium in the gas phase of thermal springs along the arms of the triple junction to long residence time. Within the Cambay basin, 10 samples of fluvial deposits gave average concentration of 1.7 ± 0.8 ppm for uranium and 8.0 ± 3.3 ppm for thorium (Srivastava et al., 2001). Since there are no known deposits of uranium/thorium mineralisation in the entire study area, we assume a uniform mineralogy with an average of the above reported concentrations and porosity $\approx$ 20%. A residence time of the order of $\sim 10^4$ years is required for growth of $\sim$ 10 ppm AEU anomalous helium under the assumption of complete acquisition of radiogenic helium by groundwater. This is in conformity with the radiocarbon ages in the area having helium anomaly of the order of $\sim$ 10 ppm AEU (PRL ^{14}C Laboratory, M.G. Yadav, personal communication). Further, the 10 ppm AEU contour is roughly parallel and equidistant from the trend of Aravalli foothills which is the recharge area of aquifers in this region (Fig. 5). It therefore seems that, for groundwater on the western flank of Cambay basin, a helium anomaly of the order of 10 ppm AEU may be attributable to the groundwater residence time. However, the high anomaly contours of 50–100 ppm AEU do not form a continuous patch parallel to Aravalli foothills but encircle the location of thermal springs on either flanks of Cambay basin. On the western flank, anomaly contours of 50–100 ppm AEU overlie the crisscrossing basement faults. The highest values of helium anomaly ($\sim$ 1000 ppm AEU) were obtained at Tuwa, on the eastern flank very close to foot hills and (>2000 ppm AEU) from the Zinzawadar village on the western flank. The residence time of $\sim 10^6$ years required to explain the high groundwater helium is not compatible with the hydrogeology of the region. Therefore, additional source for anomalous helium is required. Alternatively, in the absence of any report of high U–Th concentrations in the alluvial sediments of Cambay basin, the additional helium must be derived from a rock/sediment/soil volume many times larger than the one that groundwater comes in contact with.

As mentioned earlier, the study area of Cambay basin is part of a larger tectonic structure in the

western part of India (Fig. 1). The Narmada Tapti (NT) rift system and the CG cross each other in the Gulf of Cambay (also known as Gulf of Khambhat). Together with West Coast (WC) fault, the area has been identified as a triple junction (Burke and Dewey, 1973). These structures are considered to reach the mantle in the NT and Cambay areas (~ 40 km in depth; Kaila et al., 1989). Based on deep seismic soundings (Kaila et al., 1981, 1989; Kaila and Krishna, 1992) and gravity surveys (Singh and Meissner, 1995; Singh, 1998), it has been hypothesised that a thick high density (3.02 g cm^{-3}) igneous layer lies at the base of the crust in this region. Underlying the accreted igneous layer, a low velocity zone of hot mantle and/or a zone of intense lower crust and upper mantle interaction has been identified beneath the area of triple junction (Arora and Reddy, 1991). This configuration is compatible with high geothermal regime (heat flow 55–90 mW m^{-2}; temperature gradient 36–58 °C km^{-1}) in the region (Gupta, 1981; Panda, 1985; Ravi Shankar, 1988; Negi et al., 1992). Therefore, the lithosphere beneath the triple junction and the three arms, namely the CG, NT rift zone and WC fault, is now much warmer, thinner relatively ductile and less viscous compared to the margins (Pandey and Agrawal, 2000).

A large number of thermal springs dot the three arms of the triple junction. From a tectonic perspective, these thermal springs along geologically, well-defined structures, with frequent earthquakes of moderate intensity, suggest that these structures are active. This is also implied by the observed neotectonic movements recorded in the Quaternary sediments and from the geomorphic studies of the region (Sridhar et al., 1994; Maurya et al., 1995, 1997; Tandon et al., 1997; Srivastava et al., 2001). However, no active volcanism in any of the three arms has been observed. A recent study (Minissale et al., 2000) employing chemical and isotopic signatures on a large number of thermal springs and the associated gas phase from the three arms of the triple junction has concluded that water emerging from these thermal springs is meteoric in origin with low equilibration temperatures (90–150 °C). No evidence of mantle-derived ^3He in the gas phase otherwise rich in N_2, He and Ar could be detected. These convectively circulating spring waters were therefore termed 'intracratonic thermal waters' (Minissale et al., 2000).

With this background, it is possible to construct a conceptual model that explains the observed features in the abundance of helium and groundwater temperature in the study area.

8. A tectono-hydrothermal model of the Cambay basin

At the micro-scale, helium is visualised to be released from the rocks and grains by diffusion, α-recoil and the weathering processes that include etching, dissolution and fracturing. The released helium migrates upwards due to concentration gradient (with lowest concentration in the atmosphere) by diffusion and temperature variations facilitated by micro- and macro-cracks, pores, fractures and fissures that act as collectors and conduits of helium from the underlying formations. The upward migration of helium can be further facilitated by mass flow of crustal liquids (e.g. groundwater and petroleum) which may also be present in these conduits.

On a regional scale, therefore, higher concentration of helium in soil-gas and groundwater are expected over regions where such preferred pathways lie close to the surface.

Near surface helium distribution is, however, modulated by inherent differences in the migratory pathways between the crystalline and sedimentary formations. Sedimentary formations are generally characterised by uniform and high density of pores that cause almost omnidirectional migration of helium. This is in contrast to crystalline rocks where a relatively small density of interconnected fractures and fissures dictate the migration. As a result, sedimentary formations cause dispersion of the upward migratory helium plume whereas the crystalline formations tend to act as sources of helium plumes.

The presence of deep-seated faults and fractures also facilitates percolation of groundwater to deeper layers which, in a high heat flow regime, establishes a convective circulation with thermal waters of meteoric origin emerging as springs. Often, this convective circulation of meteoric water will not emerge as springs but discharge the thermal waters back into the groundwater thereby giving rise to temperature anomalies. Thus, it is seen that though helium and groundwater have different sources, the faults and

fractures in the crust can associate anomalous concentrations of helium and groundwater temperatures thereby providing an overall coupling between them. As the sources of the two anomalies are different, one may not expect a quantitative relationship between the two parameters. Geographical correlation is, however, expected because localisation of both anomalies is facilitated by fissures, fractures and faults at shallow (within 1–2 km) depth.

This conceptual model is depicted in Fig. 7 where a block diagram from western margin of the study area to the middle of the CG is schematically drawn. Two sets of braided fractures either joining into or emanating out from the major fault traces are shown. Those joining into are indicative of migration of helium from micro-cracks into macro-fractures, eventually joining the conduits provided by the major fractures and faults. Those emanating out are indicative of the pathways that upwardly migrating helium takes through the overlying sedimentary cover. In case of shallow depth of the basaltic layers, some of these pathways reach the surface and cause anomalous helium concentration in groundwater and soil-gas as seen on both flanks of the CG. In case of large thickness of the sedimentary cover, helium emanating from the fractures within or below the basaltic layer gets dispersed and diluted before reaching the surface. This explains the low concentration of groundwater helium as seen within the CG where the thickness of sedimentary cover is >3 km. It was, however, noted earlier that two areas of high groundwater temperature associated with geothermal springs but not associated

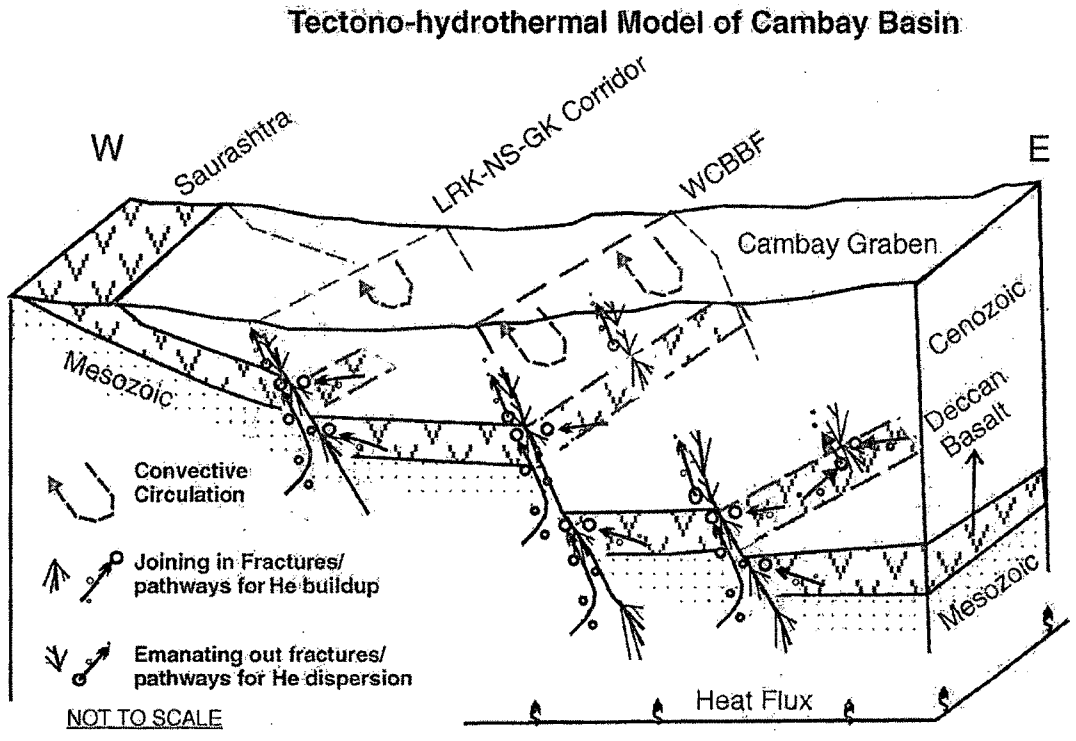

Fig. 7. A conceptual tectono-hydrothermal model for the origin of groundwater helium and temperature anomalies in the Cambay basin, Gujarat, India, is depicted schematically in an E–W block diagram across the Cambay graben. The set of braided fractures joining the major fault traces is indicative of migration of helium from micro-cracks into macro-fractures, eventually joining the conduits provided by the major fractures and faults. The joining in fractures thus acts as the pathway for helium build-up. Another set of braided fractures emanating out from the major fault traces is indicative of the pathway that the upwardly migrating helium takes through the overlying sedimentary cover leading to dispersion/ diffusion. In both cases, the size of open circles schematically depicts the changing helium concentration during upward migration. The continuous arrows leading to major faults depict the preferred migration pathway of radiogenic helium derived from a large area. The broken arrows depict the shallow depth (~ 1–2 km) hydrothermal circulation facilitated by high heat flux and the ongoing tectonic movements along major fractures and faults.

with groundwater helium anomalies are seen across the CG between 23.5–24°N and 22–22.5°N. This is the most direct evidence that the localisation of helium anomaly is controlled not only by the presence of faults and fractures but also by the depth to the crystalline basement. The temperature anomalies, on the other hand, are localised by the existence of faults and fractures that may facilitate setting up of convective groundwater circulation.

Alternatively, the data could have also been explained by using a model wherein both helium and hydrothermal fluids had a common deep-seated origin possibly at the base of the crust (only ~ 40 km deep) and the faults/fractures were acting as conduits for the migration of the two towards the surface. However, this model is not tenable in view of the low equilibration temperature (90–150 °C) of the thermal spring waters and the absence of any ^{3}He signatures of mantle origin in the associated gas bubbles (Minissale et al., 2000).

9. Summary and conclusion

A commercially available portable helium leak detector has been converted into a sensitive soil-gas/water helium analyser by modifying the input port. A simple and cost-effective sample collection and storage system using commercially available soda-lime glass bottles with bromobutyl rubber stopper and triple protection aluminium cap has been shown to retain the vacuum and stored helium for reasonably long period with little loss for a groundwater helium survey. Calibration checks involving repeated dilution and water–helium equilibration testify the correctness and robustness of the standardised procedure for helium assays.

A survey of natural helium in groundwater and soil-gas was undertaken in the Cambay basin region. Several wells investigated in this study indicated higher than atmospheric equilibration concentration, referred to as anomalous helium concentration.

In most parts of the study area, high groundwater helium anomalies are seen to be associated with the enhanced groundwater temperatures except within the Cambay graben. The areas of high helium concentration and enhanced groundwater temperatures are seen to overlie some of the basement faults. This association of high helium anomaly, enhanced groundwater temperature and some of the basement faults is explained through a conceptual model wherein the fractures and fissures in the crystalline basement act as sources of helium plumes and the sedimentary cover as a dispersive media. The high heat flow in the region facilitates convective hydrothermal circulation of groundwater along the major faults and fractures within 1–2 km depth. The faults and fractures thus act to localise the helium and thermal emergences both on the western and eastern flanks of the CG. Within the CG, the presence of thick sedimentary cover disperses the helium plumes originating from deeper basement layers.

Acknowledgements

Dr. D.N. Yadav is thanked for his contribution during initial calibration experiments. We also thank the referee, Dr. Nilgun Gulec, and another unknown referee for suggestions on improvement of the final manuscript. **[SG]**

References

Arora, B.R., Reddy, C.D., 1991. Magnetovariational study over a seismically active area in the Deccan trap province of western India. Phys. Earth Planet. Inter. 17, 21–28.

Biswas, S.K., 1982. Rift basins in Western margin of India and their hydrocarbon prospects with special reference to Kutch basin. Am. Assoc. Pet. Geol. Bull. 66 (10), 1497–1513.

Biswas, S.K., 1987. Regional tectonic framework, structure and evolution of the western marginal basins of India. Tectonophysics 135, 307–327.

Burke, K., Dewey, J.F., 1973. Plume generated triple junctions: key indicators in applying plate tectonics to old rocks. J. Geol. 81, 406–433.

Craig, H., Lupton, J.E., 1976. Primordial neon, helium and hydrogen in oceanic basalts. Earth Planet. Sci. Lett. 31, 369–385.

Datta, P.S., Gupta, S.K., Jaisurya, A., Nizampurkar, V.N., Sharma, P., Plusnin, M.I., 1980. A survey of helium in groundwater in parts of Sabarmati basin in Gujarat state and in Jaisalmer district, Rajasthan. Hydrol. Sci. Bull. 26, 183–193.

Dikum, A.V., Korobeynik, V.M., Yanitskiy, I.N., 1975. Some indications of existence of transcrustal gas flow. Geochem. Int. 12 (6), 73–78.

Friedman, I., Denton, E.H., 1975. A portable helium sniffer. US Geological Survey, Open File Report 75-532.

Fry, V.A., Istok, J.D., Semprini, L., O'Reilly, L.T., Buscheak, T.E.,

1995. Retardation of dissolved oxygen due to a trapped gas phase in porous media. Groundwater 333, 391–398.

Golubev, V.S., Yeremeyev, A.N., Yanitskiy, I.N., 1975. Analysis of some models of helium migration in the lithosphere. Geochem. Int. 11 (4), 734–742.

GSI, 2000. Seismotectonic Atlas of India and its environs. Geological Survey of India, Calcutta, India. 87 pp.

Gupta, M.L., 1981. Surface heat flow and igneous intrusion in the Cambay basin, India. J. Volcanol. Geotherm. Res. 10, 279–292.

Gupta, S.K., Lau, L.S., Moravcik, P.S., El-Kadi, A., 1990. Injected Helium: A New Hydrological Tracer. Special Report 06.01:90 Water Resources Research Center, University of Hawaii at Manoa, Honolulu.

Kaila, K.L., Krishna, V.G., 1992. Deep seismic sounding studies in India and major discoveries. Curr. Sci. 62, 117–154.

Kaila, K.L., Krishna, V.G., Mall, D.M., 1981. Crustal structure along Mehmedabad–Billimora profile in the Cambay basin, India from deep seismic soundings. Tectonophysics 76, 99–130.

Kaila, K.L., Rao, I.B.P., Rao, P.K., Rao, N.M., Krishna, V.G., Sridhar, A.R., 1989. D.S.S. studies over Deccan traps along the Thuadara–Sendhawa–Sindad profile, across Narmada-Son lineament, India. In: Mereu, R.F., Mueller, S., Fauntain, D.M. (Eds.), Properties and Processes of Earth's Lower Crust. AGU Geophys. Monogr., vol. 51, pp. 127–141. IUGG6.

Lupton, J.E., Weiss, R.F., Craig, H., 1977. Mantle helium in the Red Sea. Nature 266, 244–246.

Mathur, L.P., Rao, K.L.N., Chaube, A.N., 1968. Tectonic framework of Cambay basin, India. Bull. ONGC 5 (1), 7–28.

Maurya, D.M., Chamyal, L.S., Merh, S.S., 1995. Tectonic evolution of the central Gujarat plain, western India. Curr. Sci. 69 (7), 610–613.

Maurya, D.M., Malik, J.N., Raj, R., Chamyal, L.S., 1997. Soft sediment deformation in the Quaternary sediments of the Lower Mahi river basin, Western India. Curr. Sci. 72 (7), 519–522.

Merh, S.E., 1995. Geology of Gujarat, Geological Society of India. 222 pp.

Minissale, A., Vaselli, O., Chandrasekharan, D., Magro, G., Tassi, F., Casiglia, A., 2000. Origin and evolution of 'intracratonic' thermal fluids from central-western peninsular India. Earth Planet. Sci. Lett. 181, 377–397.

Misra, K.S., 1981. The tectonic setting of Deccan Volcanism in southern Saurashtra and northern Gujarat. Deccan Volcanism and Related Basalt Provinces in Other Parts of the World. Geol. Surv. India Memoir, vol. 3, pp. 81–86.

Misra, K.S., 2001. Lineament fabric and its relation to the eruption of Deccan volcanics and seismicity of west-central India. Geol. Surv. India, Spec. Publ. 64, 209–221.

Negi, J.G., Agrawal, P.K., Singh, A.P., Pandey, O.P., 1992. Bombay gravity high and eruption of Deccan flood basalts India from a shallow secondary plume. Tectonophysics 206, 341–350.

Panda, P.K., 1985. Geothermal maps of India and their significance in resources assessments. Petrol. Asia J. VIII 2, 202–210.

Pandey, O.P., Agrawal, P.K., 2000. Thermal regime, hydrocarbon maturation and geodynamic events along the western margin of India since late Cretaceous. J. Geodyn. 30, 439–459.

Perry, J.H., 1984. Chemical Engineers' Handbook. McGraw-Hill, New York.

Ravi Shankar, J.H., 1988. Heat flow map of India and discussions on its geological and economic significance. Ind. Min. 42, 89–110.

Ravi Shankar, J.H., 1991. Thermal and crustal structure of "SONATA". A zone of mid-continental lifting in Indian shield. J. Geol. Soc. India 37, 211–220.

Ravi Shankar, J.H., 1995. Fragmented Indian shield and recent earthquakes. Geol. Surv. India, Spec. Publ. 27, 41–48.

Reimer, G.M., 1984. Prediction of central California earthquakes from soil-gas helium. PAGEOPH 122, 369–375.

Singh, A.P., 1998. 3-D structure and geodynamics evolution of accreted igneous layer in the Narmada-Tapti region. J. Geodyn. 252, 129–141.

Singh, A.P., Meissner, R., 1995. Crustal configuration of the Narmada-Tapti region India from gravity studies. J. Geodyn. 20, 111–127.

Sridhar, V., Chamyal, L.S., Merh, S.S., 1994. North Gujarat Rivers: remnants of super fluvial system. J. Geol. Soc. India 44, 427–434.

Srivastava, P., Juyal, N., Singhvi, A.K., Wasson, R.J., Bateman, M.D., 2001. Luminescence chronology of river adjustment and incision of Quaternary sediments in the alluvial plain of the Sabarmati river, north Gujarat, India. Geomorphology 36, 217–229.

Tandon, S.K., Sareen, B.K., Rao, M.S., Singhvi, A.K., 1997. Aggradation history and luminescence chronology of late Quaternary semi-arid sequences of the Sabarmati basin, Gujarat, Western India. Palaeogeogr. Palaeoclimatol. Palaeoecol. 128, 133–357.

Weiss, R.F., 1971. Solubility of helium and neon in seawater. J. Chem. Eng. Data 167, 235–241.

Dissolved helium and TDS in groundwater from Bhavnagar in Gujarat: Unrelated to seismic events between August 2000 and January 2001

S K GUPTA* and R D DESHPANDE

Physical Research Laboratory, P.O. Box 4218, Navrangpura, Ahmedabad 380 009, India

Temporal variations have been observed in both dissolved helium and TDS in the form of increase in basaltic and decrease in alluvial aquifers. The increase in basaltic aquifers has been explained by enhanced pumping of old groundwater with relatively higher concentration of dissolved helium and salt, whereas the decrease in alluvial aquifers has been explained by dilution from the post monsoon groundwater recharge. Therefore, the observed temporal variations cannot be ascribed to the contemporary enhanced seismic activity in this region since August–September 2000.

1. Introduction

Helium-4 is radiogenic, produced in decay of uranium and thorium series nuclides in soils and rock grains within the Earth. The gas is steadily released from grains by their etching, dissolution, fracturing and alpha recoil during weathering and then exhaled into the atmosphere by diffusion and temperature variations. The Earth's atmosphere has a small concentration of helium since it quickly escapes to the outer space. Since the production of both ^{4}He and radon occurs within the Earth, their concentrations show a gradient decreasing towards the ground-atmosphere interface. Before escaping to the atmosphere through fractures, these gases are intercepted by the omnipresent groundwater zone. Since the diffusivity of helium in water is small ($7.78 \times 10^{-5}\,\mathrm{cm^2 s^{-1}}$ at 25°C; CRC Handbook, 80th edition, 1999–2000), it generally follows groundwater flow.

While a part of the radiogenic helium is released to the atmosphere the remaining fraction continues to accumulate in grains. Episodes of rock dilation and fracturing may occasionally release this fraction. On such occasions, and for a short period of time, this fraction may dominate over steady-state release. Creation of micro-fractures due to slow build-up of strain resulting in escape of radiogenic helium and radon provides the basis of geochemical methods of earthquake prediction (Barsukov *et al* 1985a; Reimer 1985; Virk *et al* 2001). Tremors of significant magnitude can create new fractures in the crust and also unlock some that may already exist. Earthquakes can thus facilitate escape of helium through fractures and suddenly increase its concentration in the overlying groundwater zone. The sensitivity range of the gaseous components of groundwater including helium, radon, carbon dioxide and hydrogen sulphide has been estimated to be 300–500 km or more (Varhall *et al* 1985; Barsukov *et al* 1985b). On the basis of Tashkent precursor study during 1974–1980 an empirical formula (Log $RT = 0.63\,\mathrm{M} \pm 0.15$) relating time T to magnitude M and epicentral distance R had been put forward (Sultankhodzhayev *et al* 1980). Observations in helium content of Yavros flowing well waters in Dushanbe study area during 1977–79 have been useful in revealing that both precursor time and anomaly amplitude increased with magnitude of the following seismic event. The anomaly duration and amplitude decreased with epicentral distance. But in many other areas it is still uncertain if the observed anomalies were truly earthquake related or induced by other environmental

Keywords. Groundwater; Helium; TDS; Bhavnagar; seismicity.

Proc. Indian Acad. Sci. (Earth Planet. Sci.), **112**, No. 1, March 2003, pp. 51–60

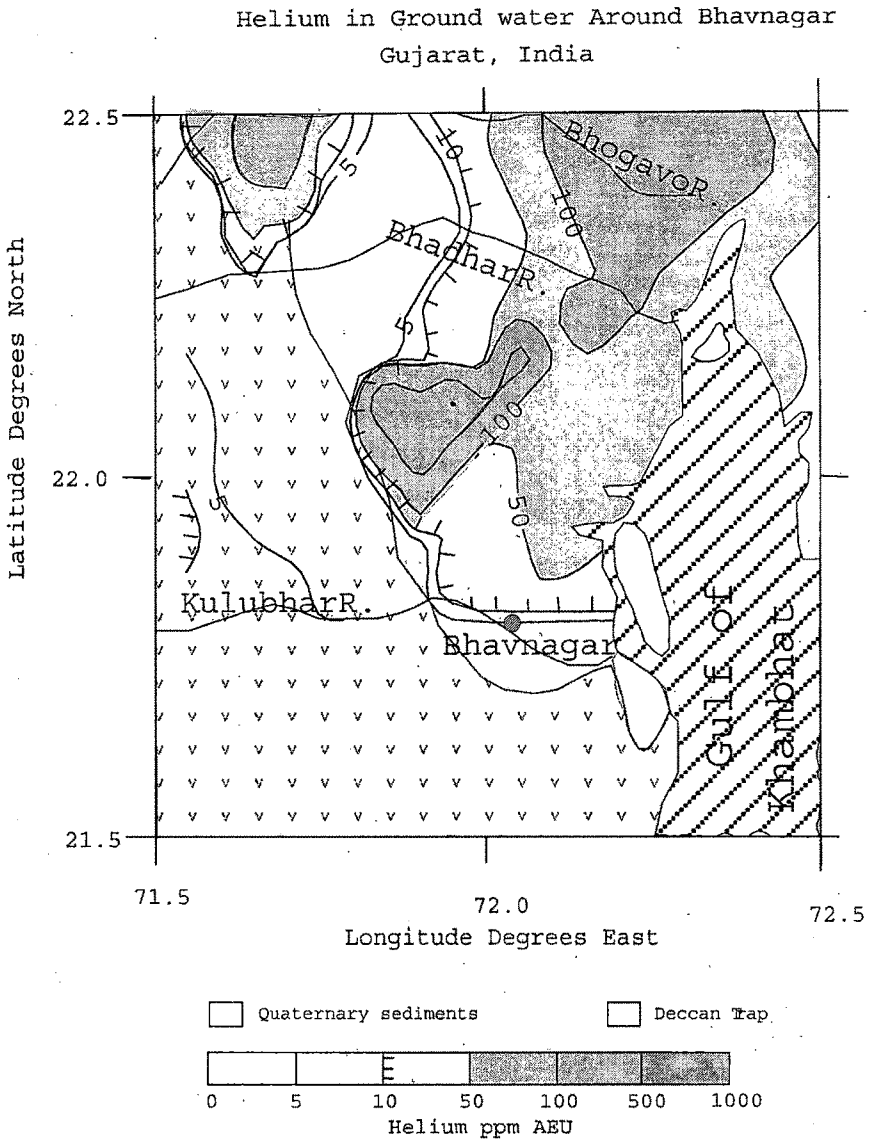

Figure 1. Contours of dissolved helium anomaly in groundwater in the region around Bhavnagar in March 1998, i.e., during a quiet seismic period.

variables such as weather and groundwater pumping (King 1985).

During the last two decades, Bhavnagar city (21.86°N; 72.04°E) in western India has intermittently experienced earthquakes of magnitude > 3 (Srivastava and Rao 1997). The city is located on the southern tip of Saurashtra, which is bound by the extension of Narmada geofracture in the south and western Cambay Basin fault in the east. During 1979 and 1982, several earthquakes with epicentres in Bhavnagar, Chandod, Gulf of Khambhat, Rajpipla etc., located along the Narmada geofracture were experienced. A survey of dissolved helium in groundwater from parts of Cambay Basin during 1999 did indeed show significantly high concentrations (figure 1) around Bhavnagar. During August–September, 2000 the frequency of small tremors around Bhavnagar increased significantly and presented an opportunity to test the earthquake induced helium release model in this part of the world.

Sixteen groundwater samples were collected from tubewells and hand pumps from different parts of the city (figure 2) on 16th and 17th September 2000. Some of the same stations were re-sampled on 22nd January 2001 after a long quiescence period for comparison. After the Bhuj earthquake of 26th January 2001, a repeat survey of these stations was conducted in March 2001. During the two repeat surveys,

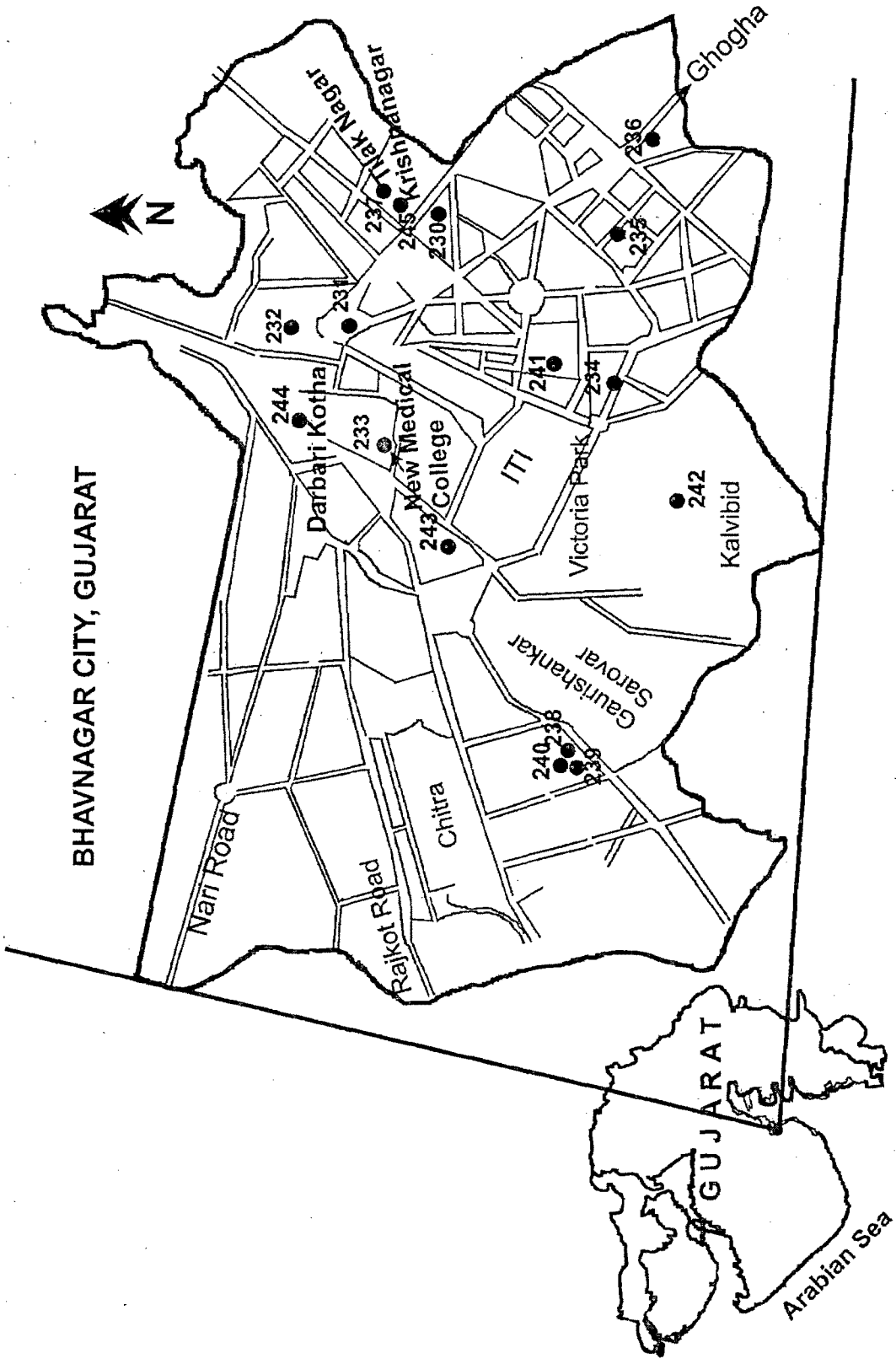

Figure 2. Map of Bhavnagar city with groundwater helium sampling stations.

some of the original wells could not be re-sampled and had to be abandoned because of a decline in the water table and drying up of the wells. In such cases wells in the vicinity were sampled.

2. Experimental

Water samples for analyses of dissolved helium were collected in 3-mm thick, 1.2-litre capacity, soda-lime glass bottles using procedures standardised in our laboratory for these analyses and described earlier (Gupta *et al* 2002). Briefly, after complete purging of air by groundwater, the bottles were filled by the water samples up to the top and then water above a pre-determined level was quickly sucked off, keeping headspace for exsolving gases. The bottles were immediately sealed. The temperature, TDS and pH of groundwater samples were measured at the sampling stations using standard pre-calibrated probes.

The helium analyses were made on the equilibrated air from the headspace of the sampling bottles within a day using a helium sniffer probe (ALCATEL Model ASM 100 HDS) with a modified inlet port to enable quantitative helium analyses (see Gupta *et al* 2002). The measured helium concentrations are corrected for

- volume of headspace,
- water volume,
- volume of air drawn-in during analysis and
- loss during storage.

The equilibrated air helium concentrations can be converted to the groundwater helium concentrations using Henry's Law and the respective volumes of water and air /gas in the sampling bottles. Henry's constant is defined by $H = C_g/C_w = \{$ (concentration of helium in gas phase)/(concentration of helium dissolved in water)$\}$. Using $H = 94.5$ (Fry *et al* 1995) at 25°C, the concentration of dissolved helium in equilibrium with air containing 5.3 ppmv helium is equivalent to 5.6×10^{-2} ppmv. However, for the sake of convenience the dissolved helium concentrations are expressed here in terms of Air Equilibration Units (AEU), i.e., helium concentration in air that was in equilibrium with the water at one atmospheric pressure. Helium anomaly is defined as concentration above the atmospheric equilibration value of 5.3 ppmAEU). The reproducibility of sampling and measured helium concentration variation is $< 5\%$ (table 1).

3. Results

Twelve of the sixteen groundwater samples collected for dissolved helium survey in September 2000 (figure 2) showed helium concentrations more than the air equilibration value of 5.3 ppmAEU (table 2). The values ranged between 11 and 498.2 ppmAEU. The highest value was found in a groundwater sample from a 60-m deep tubewell (#233) followed by 179.5 ppmAEU from a 43-m deep tubewell (#242). These values are much higher than those ($\sim$20ppmAEU) found even in deeper tubewells (#238, #239, #240) on the western outskirts of Bhavnagar. The groundwater temperatures ranged from 30° – 40°C and helium solubility changes due to these (Weiss 1971) cannot account for observed helium excesses.

Although a few studies (Datta *et al* 1980) had suggested that in alluvial aquifers, deeper groundwaters have higher helium concentration, subsequent measurements (Gupta and Deshpande 2003) and the present study indicate that in basaltic aquifers, this may not necessarily be the case. The present study, however, indicates that in the Bhavnagar city, high values of helium in groundwater are generally found in the basaltic aquifers and relatively low helium concentrations in the alluvial aquifer (see table 2). This observation is consistent with the understanding that interconnected pore space and high porosity in alluvial aquifers facilitate quick escape of helium from groundwater and the unconnected pore space and low porosity in basaltic aquifers limit the opportunity for groundwater helium to escape.

4. Discussion

The temporal variations of groundwater helium are plotted in figure 3. Some stations, particularly those with high levels of excess dissolved helium, showed a change by more than a factor of 2. From September 2000 to January 2001, except in case of stations #233 & #244 located in the basaltic aquifers, helium concentrations have either not changed or decreased marginally. Between January and March 2001, five out of seven stations, again located in basaltic aquifers, showed increase in helium concentration. This increase was also accompanied by an increase in TDS (except Stn. #238 & #239). It will also be noticed from figure 3 and table 2 that with respect to the data for September 2000, helium and TDS concentration changes in January and March 2001 have largely been in the same direction (increase/ decrease/ no change) for respective wells.

There also appears a certain pattern in the helium concentration and TDS between the three sets of sampling. It is seen that helium concentration changes (Sept. 2000 – March 2001; figure 4) at different stations are related to changes in (i)

Table 1. *Data of post-earthquake groundwater helium survey in Bhavnagar city, Gujarat, India.*

Sample code	Well type TW/HP	Location name	Near surface lithology AL/BAS	Depth (m)	Temperature (°C)			TDS (ppm)			Helium concentration (ppm AEU)		
					Sept. 2000	Jan. 2001	March 2001	Sept. 2000	Jan. 2001	March 2001	Sept. 2000	Jan. 2001	March 2001
CBGW-230	TW	Ambawadi	BAS	10	32	29	30	2800	2700	3500	5.3	5.3	6.2
CBGW-231	HP	Navapura	AL	21	30	28	28	500	500	500	5.9	5.3	5.9
CBGW-232	HP	Vorawad	AL	24	30	29	29	600	600	500	5.3	5.6	5.3
CBGW-233	TW	Medical College	BAS	61	32	31	32	3300	4100	3900	498.2	518.6	687.3
CBGW-234	TW	Kalvibid D-136	BAS	53	33	31	33	1100	1200	1200	5.3	5.3	5.9
CBGW-235	TW	Siddhipark	AL	18[α]/18[β]	33[α]	30[β]	31[β]	1700[α]	1400[β]	1300[β]	5.9[α]	5.3[β]	5.9[β]
CBGW-236	TW	Malanaka	AL	9	31.5	30	31	2400	2100	2000	5.3	5.3	5.3
CBGW-237	TW[α]/HP[β]	Tilaknagar	AL	20[α]/12[β]	31[α]	29[β]	30[β]	5100[α]	800[β]	1000[β]	10.6[α]	5.3[β]	5.3[β]
CBGW-238	TW	Chitra[γ]	BAS	229	40	–	39	2200		2200	22.9		53.7
CBGW-239	TW	Chitra	BAS	218	40	–	40	1200		1200	18.1		36.6
CBGW-240	TW	Chitra[δ]	BAS	293	39	–	40	1400		1600	26.3		18.8
CBGW-241	TW	Hill Drive	BAS	55	35	31	31	1000	1000	900	11.7	10.1	11.7
CBGW-242	TW	Kalvibid, Shantinagar	AL	43	33	28	31	7100	5900	6400	179.5	112.7	112.6
CBGW-243	TW	Vijayraj Nagar	BAS	21	32	–	30	900		1000	7.8		12.9
CBGW-244	HP	Darbari Kotha	BAS	34	31	30	30	1000	1300	1400	13.0	14.9	17.2
CBGW-245	HP	Krishnanagar	AL	15	31	α	α	2800	α	α	5.9	α	α
September 1998 sampling				Depth (m)	Temperature °C			TDS (ppm)			Helium concentration (ppm AEU)		
CBGW-47	TW	Chitra	BAS	127	–			–			6.6		
CBGW-48	TW	Chitra	BAS	229	39.5			–			100.2		

[α] Dried up and abandoned.
[β] Neighbouring tubewell to the one abandoned.
[γ] Repeat of CBGW-48.
[δ] Repeat of CBGW-47.

Table 2. *Reproducibility of measured helium concentration in groundwater samples.*

Sample location	Helium concentration (ppmAEU)		Variability(%)
	Sample-1	Sample-2	
Ranip	6.17	6.20	1
Bagodra	339.7	339.7	0
Roika[x]	24.3	24.8	2
Tilaknagar	5.3	5.3	0

[x] In this case eight samples in different sampling bottles were collected at the same time and analysed over a period of two years to estimate loss of helium during storage in sampling bottles. This loss has been estimated to be $< 0.15\%$ per day.

TDS of groundwater and, (ii) the lithology of the aquifer.

It is recalled that the sampling dates correspond to three distinct seismic phases at Bhavnagar:

- September 2000 – during this period low magnitude (< 4.2) tremors were repeatedly experienced;
- January 2001 – a long quiescent phase preceded the sampling;
- March 2001 – quiescent period following a major (26th January 2001) earthquake (magnitude: 7.6, IMD; 7.9 USGS) with epicentre > 300 km in NE.

Based on the reports of seismically induced geochemical changes in groundwater and local hydro-geological observations, two possible models to explain the observed variations in helium and TDS are examined.

- Seismically induced release of helium and/or forced injection of deep groundwaters (in general with higher helium and TDS concentrations) to shallow aquifers.
- Pumping of deep groundwaters due to decline in water table leading to progressive increase in helium and TDS.

The first model is based on several reported cases of increase in helium and salts in groundwater in response to earthquakes (Barsukov *et al* 1985a; Reimer 1985; Virk *et al* 2001). Also, in case of the Bhuj earthquake, large-scale liquefaction and resultant oozing of groundwater accompanied by release of gases at many places over a large area extending from Rajasthan to south Gujarat has been reported (Rajendran *et al* 2001). It may be useful to note that at Narveri (23.96°N;69.85°E); in the Great Rann of Kachchh an outflow of groundwater continued more than four months after the Bhuj earthquake (Gupta *et al* 2002). Air or gases bubbling through the freshly oozing water was observed at Narveri. Based on measurements of helium, radon, chloride, sulphate, sodium and temperature it was suggested that the outpouring water and escaping gases at Narveri had a deep confined source with a reservoir age in excess of $\sim 10^4$ years.

If seismically induced release of helium and/or forced injection of deeper groundwater were operative during the seismically active phase in September 2000, a decrease of helium concentration in the samples collected in January 2001 (quiescent phase) was expected. However, the decrease is observed only at three stations in alluvial terrain. In case of basaltic terrain, helium concentrations have either remained unchanged or have increased. This pattern of change in helium concentration has continued even in March 2001 (post Bhuj earthquake quiescent phase). This observed steady increase of helium concentration during quiescent phases in basaltic aquifers accompanied by no or marginal decrease in alluvial aquifers rules out the case of seismically induced injection of deep groundwater.

The second model is based on the observations that groundwater levels during successive sampling periods at Bhavnagar have steadily declined in basaltic terrain indicating pumping of progressively deeper (long resident) groundwater. As before, the deeper groundwater is expected to have higher concentrations of both helium and TDS due to longer residence in contact with aquifer material. This would explain the observed steady increase in both helium concentration and TDS in basaltic terrain. However, concurrent enhancement in helium and TDS concentrations in basaltic terrain and decrease or 'no change' in the alluvial terrain needs to be explained. One also needs to explain the non-linearity of TDS and helium concentration variations (figure 4).

In aquifers comprising of secondary unconnected porosity in the form of fractures and fissures (e.g., the basaltic aquifers) groundwaters exhibit large spatial variability in dissolved constituents reflecting their largely local origin. This is clearly seen from table 2. The old groundwaters in such aquifers too will carry this spatial variability of dissolved constituents but with higher concentrations due to

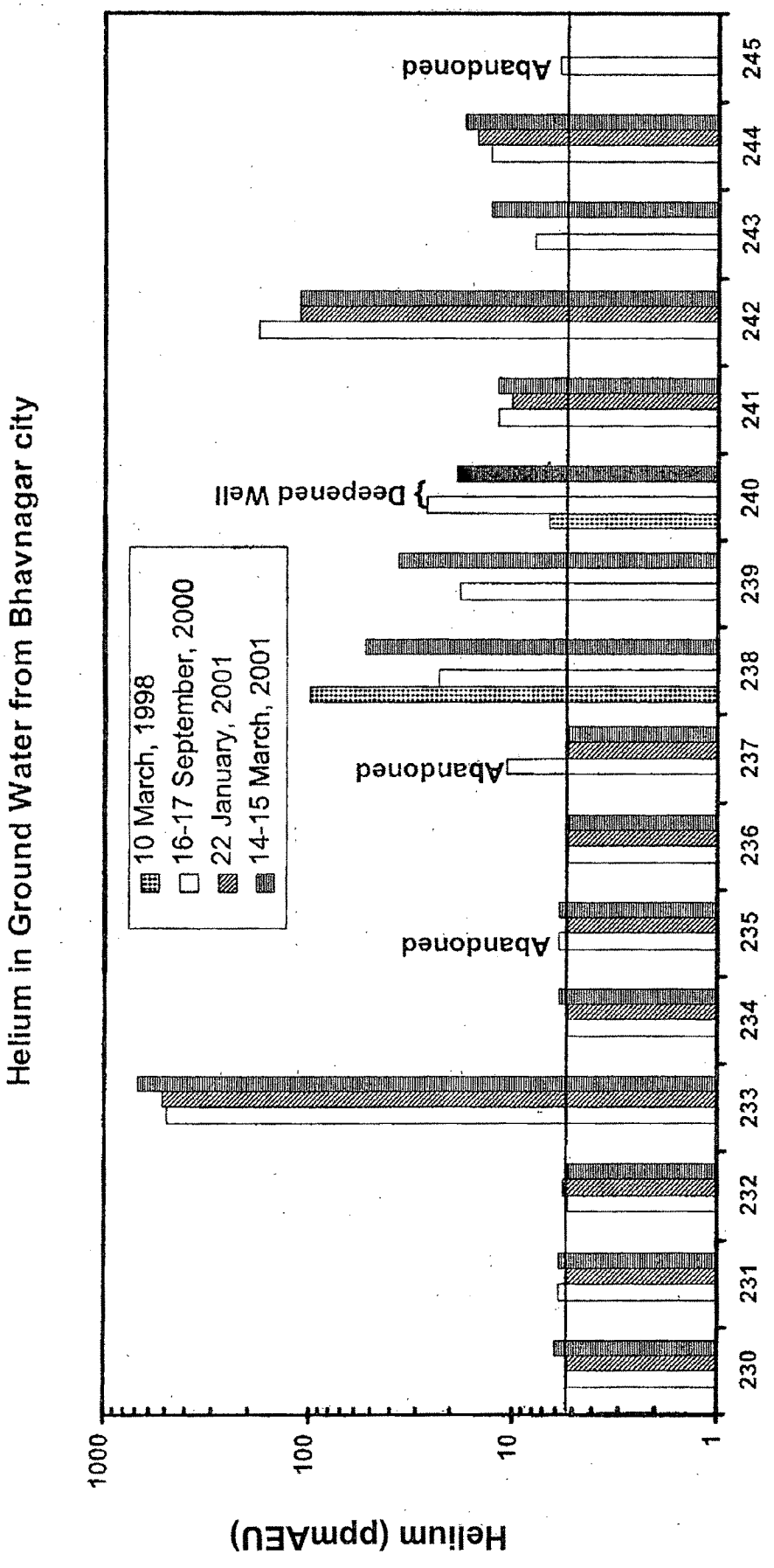

Figure 3. Temporal variation of groundwater helium concentration from Bhavnagar city during September 2000 to March 2001. Two analyses on samples collected in March 1998 are also shown. The horizontal line at 5.3 ppmAEU indicates the helium concentration expected in a water sample in equilibrium with atmosphere. Decline in groundwater level and drying up/ deepening of wells forced abandonment of three observation wells. In their place new wells were selected in the vicinity.

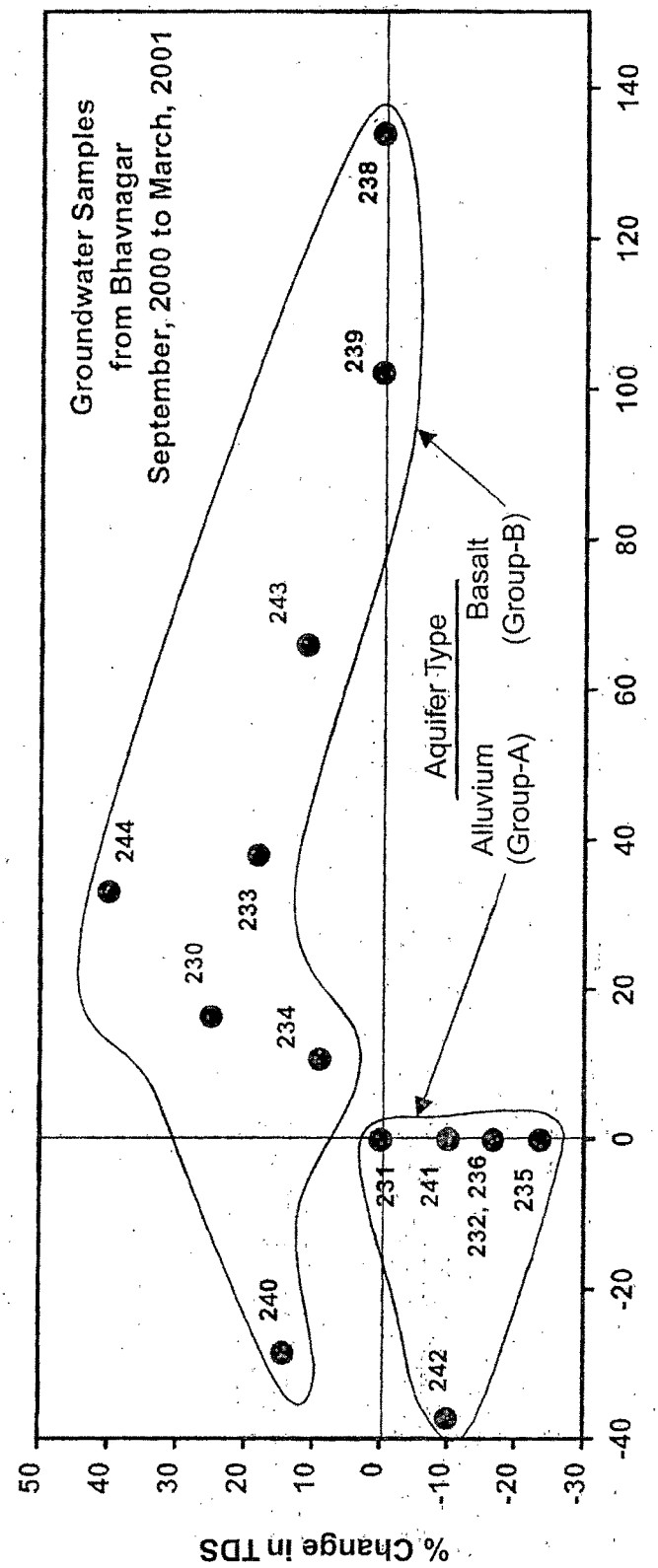

Figure 4. Bivariate plot of groundwater helium and TDS variation for different stations in Bhavnagar city between two sets of sampling. Samples derived from alluvial aquifers (Group-A) show decrease in TDS and/or helium concentration. Samples derived from basaltic aquifers (Group-B) show increase in TDS and/or helium concentration.

longer residence. The fractures and fissures quickly recharge these aquifers after the rain, but the amount is limited by the small availability of pore space. In post rainy season, excessive withdrawal of groundwater (as was indicated by decline in groundwater levels and drying up of some wells leading to their abandonment) results in pumping of old 'long resident' groundwater. This is in contrast to a relatively slow recharge that takes place during post monsoon period due to infiltration over a large area in regions of primary porosity such as alluvial aquifers. This recharge leads to slow but significant dilution of resident groundwater in alluvial aquifers in the post rainy season. Therefore, in a region having aquifers with both primary and secondary porosity correlation between variations of TDS and helium concentration in response to either mixing of old groundwater and/or post monsoon recharge may exhibit considerable variation. The variability of this relationship is due to the inherent spatial variability in dissolved constituents in groundwater, the porosity and the permeability.

It is seen from figure 4 that stations falling in Group-A, showing decrease in TDS and little or no decrease in helium are drawn from aquifers in the alluvial terrain. These stations had relatively lower values (table 2) of both TDS and helium in September 2000. The observed reduction in January and March 2001, therefore, represent dilution with slow post monsoon recharge through the overlying soil. It may be noted that the post monsoon recharge will have a 'fixed' low (= 5.3 pptnAEU) concentration of helium and low (though not necessarily a 'fixed' value) TDS. In contrast, stations falling in Group-B, showing a significant increase (except #240) in helium and moderate increase in TDS (except #238 & 239) are drawn from aquifers in the basaltic terrain. These stations, derived from the basaltic aquifers, had relatively high values of both TDS and helium in September 2000 (table 2). The observed increase in both TDS and helium in January and March 2001 represents pumping of relatively old groundwater with high but locally variable values of both TDS and helium due to the unconnected nature of secondary porosity.

5. Summary and conclusions

Temporal variations have been observed in both the concentration of dissolved helium and TDS of groundwaters at Bhavnagar following a period of locally enhanced seismic activity during August–September 2000. A significant aspect of the observed variation is the enhancement of helium and TDS concentrations in basaltic terrain and reduction in both parameters in alluvial terrain during the subsequent quiescent phases interrupted by a major Bhuj earthquake on 26th January 2001. Because of the large variability, it has not been possible to draw a quantitative relationship between the observed changes in TDS and helium concentration.

The observations have been explained by a model involving addition of deeper (old, long resident) groundwater in response to post-monsoon excessive pumping in the basaltic terrain and a concurrent dilution by slow post monsoon groundwater recharge in the alluvial terrain. The observed large variation is therefore due to the prevailing hydro-geological situation at Bhavnagar.

The steady increase of helium concentration in basaltic aquifers during quiescent phases, accompanied by little or marginal decrease in alluvial aquifers rules out the possibility that the observed variations were seismically induced.

Acknowledgements

The authors are thankful to Mr. G C Srivastava, Mr. P M Joshi, Mr. Y Sharma, Mr. S A Qureshi and Mr. D Dodia of GWRDC for identifying suitable sampling stations and fruitful discussions. We thank Prof. N Bhandari for critically reviewing the manuscript.

References

Barsukov V L, Varshall G M and Zamokina N S 1985a Recent results of hydrogeochemical studies for earthquake predictions in the USSR; *PAGEOPH* **122(2–4)** 143–156

Barsukov V L, Serebrennikov V S, Belaev A A, Bakaldin Yu A and Arsenyeva R V 1985b Some experience in unravelling geochemical earthquake precursors; *PAGEOPH* **122(2–4)** 157–163

Datta P S, Gupta S K, Jayasurya A, Nijampurkar V N, Sharma P and Plusnin M I 1980 A survey of helium in groundwater in parts of Sabarmati basin in Gujarat state and in Jaisalmer district, Rajasthan; *Hydrological Sciences- Bulletin* **25(2)** 183–193

Fry V A, Istok J D, Semprini L, O'Reilly L T and Buscheck T E 1995 Retardation of dissolved oxygen due to a trapped gas phase in porous media; *Groundwater* **33(3)** 391–398

Gupta S K, Bhandari N, Thakkar P S and Rengarajan R 2002 On the origin of the artesian groundwater and escaping gas at Narveri after the Bhuj earthquake in 2001; *Curr. Sci.* **82(4)** 463–468

Gupta S K and Deshpande R D 2003 Origin of groundwater helium and temperature anomalies in the Cambay region of Gujarat, India; *Chem. Geol.* (in press)

King Chi-Yu 1985 Earthquake hydrology and chemistry; *PAGEOPH* **122(2–4)** 141–142

Rajendran K, Rajendran C P, Thakkar M and Tuttle M P 2001 The 2001 Kutch (Bhuj) earthquake: coseismic surface features and their significance; *Curr. Sci.* **80(11)** 1397–1405

Rao G V, Reddy G K, Rao R U M and Gopalan K 1994 Extraordinary helium anomaly over surface rupture of September 1993 Killari earthquake, India; *Curr. Sci.* **66(12)** 933–935

Reddy G K, Rao G V, Rao R U M and Gopalan K 1994 Surface rupture of Latur earthquake: The soil-gas helium signature; *Mem. Geol. Soc. India* **35** 83–99

Reimer G M 1985 Prediction of central California earthquakes from soil-gas helium fluctuations; *PAGEOPH* **122(2–4)** 369–375

Srivastava S and Rao D T 1997 Present status of seismicity of Gujarat; *Vayumandal*, **27** (1–2) 32–39

Sultankhodzhayev A N, Latipov S U, Zarikov T Z, Zigan F G 1980 Dependence of hydrogeoseismological anomalies on the energy and epicentral distance of earthquakes; *Dokl. AN Uzb. SSR* **5** 57–59

Varshall G M, Sobolev G A, Barsukov V L, Kohsov A V, Kostin B I, Kudinova T F, Stakheyev Yu I and Tretyakova S P 1985 Separation of volatile components from rocks under mechanical loading as the source of hydrogeochemical anomalies preceding earthquakes; *PAGEOPH* **122(2–4)** 463–477

Virk H S, Walia V and Kumar N 2001 Helium/Radon precursory anomalies of Chamoli earthquake, Garhwal Himalaya, India; *Journal of Geodynamics* **31** 201–210

Weiss R F 1971 Solubility of helium and neon in seawater; *Journal of Chemical Engineering Data* **167** 235–241

MS received 1 January 2002; revised 30 August 2002